Neural models of learning and visual grouping in the presence of finite conduction velocities

Dissertation

in partial fulfillment
of the requirements for the degree

Doctor of natural sciences
(Dr. rer. nat.)

submitted to the Faculty of Physics,
Philipps University Marburg

by

Mirko Saam

Marburg/Lahn
January 2006

Vom Fachbereich Physik der Philipps-Universität als Dissertation

angenommen am:	29.3.2006
Erstgutachter:	Prof. Dr. R. Eckhorn
Zweitgutachter:	Prof. Dr. F. Rösler
Tag der mündlichen Prüfung:	28.4.2006

To Kristina

Zusammenfassung

Die Hypothese der Objektbindung durch Synchronisation wurde im visuellen Kortex durch neuere Experimente am wachen Affen unterstützt. Diese zeigten das Auftreten kohärenter γ-Aktivität (30–90 Hz) in lokalen Neuronengruppen und deren Modulation in Abhängigkeit von Regeln der Figur-Hintergrund Trennung. Wechselwirkungen innerhalb und zwischen diesen neuronalen Gruppen basieren auf axonaler Fortleitung von Aktionspotentialen mit endlicher Geschwindigkeit. Physiologische Untersuchungen haben gezeigt, dass die zeitliche Verzögerung dieser Fortleitung vergleichbar mit dem Zeitraum ist, der durch die γ-Aktivität (11–33 ms) definiert wird. Wie beeinflussen diese endlichen Geschwindigkeiten die Entwicklung von synaptischen Verbindungen in und zwischen visuellen Arealen? Welche Beziehung besteht zwischen der Reichweite der γ-Kohärenz und der Geschwindigkeit der Signalübertragung? Sind die großen zeitlichen Verzögerungen kompatibel mit dem kürzlich entdeckten Phänomen der laufenden γ-Wellen, die sich über größere Teile des primären visuellen Kortex erstrecken?

Die Anpassung von Verbindungen im sich entwickelnden visuellen Kortex basiert auf zeitlichem Hebb'schen Lernen zur Änderung der synaptischen Effizienz. Die Auswirkung konstanter, endlicher axonaler Geschwindigkeiten auf diesen Prozess wurde mit einer Reihe topographischer Netzwerkmodelle untersucht. Zufällige Aktionspotentiale mit einer begrenzten zeitlichen Korrelationsbreite bildeten die kortikale Aktivität ohne visuelle Erfahrung nach. Nach dem Lernvorgang waren die lateralen Verbindungen innerhalb einer Netzwerkschicht räumlich begrenzt, wobei die Breite der Verbindungsprofile direkt proportional zur lateralen Leitungsgeschwindigkeit war. Weiterhin entwickelte sich eine begrenzte Vorwärtsdivergenz zwischen den Neuronen zweier aufeinanderfolgender Schichten. Die Größe dieser Verbindungsprofile entsprach dabei den lateralen Verbindungsprofilen der Neuronen der unteren Schicht. Der Mechanismus in diesem

Netzwerkmodell ist geeignet, die Entstehung größerer rezeptiver Felder in höheren visuellen Arealen unter Aufrechterhaltung einer retinotopen Abbildung zu beschreiben.

Der Einfluss abstandsabhängiger Verzögerungen auf die lokale Erzeugung von γ-Aktivität und deren räumliche Synchronisation wurde in einem Modell eines entwickelten visuellen Areals untersucht. Anhaltende Stimulation und lokale inhibitorische Rückkopplung waren ausreichend für das Auftreten kohärenter γ-Aktivität, die sich über wenige Millimeter ausdehnte. Die Leitungsgeschwindigkeit hatte einen direkten Einfluss auf die Frequenz der γ-Oszillationen, aber sie beeinflusste weder die γ-Leistung noch die räumliche Ausdehnung der γ-Kohärenz. Das Hinzufügen langreichweitiger Horizontalverbindungen zwischen exzitatorischen Neuronen, ähnlich denen in Schicht 2/3 im primären visuellen Kortex, vergrößerte die räumliche Ausdehnung der γ-Kohärenz. Diese Reichweite war maximal für instantane Fortleitung von Aktionspotentialen und schwächte sich für alle Entfernungen mit endlichen, reduzierten Leitungsgeschwindigkeiten ab. Für Geschwindigkeiten unter 0.5 m/s waren die γ-Leistung und die γ-Kohärenz sogar kleiner als ohne die Existenz dieser Verbindungen, d.h. langsame Horizontalverbindungen desynchronisierten die neuronalen Populationen. Zusammenfassend kann gesagt werden, dass die mögliche Steigerung der γ-Kohärenz durch exzitatorische Horizontalverbindungen kritisch von deren hoher Fortleitungsgeschwindigkeit abhängt.

Kohärente γ-Aktivität im primären visuellen Kortex und in den begleitenden Netzwerkmodellen bedecken nur kleine Regionen des visuellen Feldes. Dies stellt die Rolle der γ-Synchronisation zur Lösung des Bindungsproblems für größere Objektrepräsentationen in Frage. Eine genauere Analyse des bereits beschriebenen Netzwerkmodells zeigte, dass Bereiche mit kohärenter γ-Aktivität (1.8 mm Halbwertsbreite) in eher global auftretende γ-Wellen eingebettet waren, welche über viel größere Entfernungen koppelten (6.3 mm Halbwertsbreite). Die im Modell beobachteten γ-Wellen sind den γ-Wellen im primären visuellen Kortex von wachen Affen sehr ähnlich, was darauf hindeutet, dass lokale rückgekoppelte Inhibition und begrenzte Horizontalverbindungen mit endlichen axonalen Leitungsgeschwindigkeiten für deren Auftreten hinreichend sind. Da das Modell mit der Verbindungsstruktur und den γ-Prozessen im primären visuellen Kortex übereinstimmt, unterstützen die Ergebnisse die Hypothese, dass γ-Wellen ein generalisiertes Konzept zur Objektbindung im visuellen Kortex darstellen.

Abstract

The hypothesis of object binding-by-synchronization in the visual cortex has been supported by recent experiments in awake monkeys. They demonstrated coherence among γ-activities (30–90 Hz) of local neural groups and its perceptual modulation according to the rules of figure-ground segregation. Interactions within and between these neural groups are based on axonal spike conduction with finite velocities. Physiological studies confirmed that the majority of transmission delays is comparable to the temporal scale defined by γ-activity (11–33 ms). How do these finite velocities influence the development of synaptic connections within and between visual areas? What is the relationship between the range of γ-coherence and the velocity of signal transmission? Are these large temporal delays compatible with recently discovered phenomenon of γ-waves traveling across larger parts of the primary visual cortex?

The refinement of connections in the immature visual cortex depends on temporal Hebbian learning to adjust synaptic efficacies between spiking neurons. The impact of constant, finite, axonal spike conduction velocities on this process was investigated using a set of topographic network models. Random spike trains with a confined temporal correlation width mimicked cortical activity before visual experience. After learning, the lateral connectivity within one network layer became spatially restricted, the width of the connection profile being directly proportional to the lateral conduction velocity. Furthermore, restricted feedforward divergence developed between neurons of two successive layers. The size of this connection profile matched the lateral connection profile of the lower layer neuron. The mechanism in this network model is suitable to explain the emergence of larger receptive fields at higher visual areas while preserving a retinotopic mapping.

The influence of finite conduction velocities on the local generation of γ-activities and their spatial synchronization was investigated in a model of a mature visual area. Sustained input and local inhibitory feedback was sufficient for the emergence of coherent γ-activity that extended across few millimeters. Conduction velocities had a direct impact on the frequency of γ-oscillations, but did neither affect γ-power nor the spatial extent of γ-coherence. Adding long-range horizontal connections between excitatory neurons, as found in layer 2/3 of the primary visual cortex, increased the spatial range of γ-coherence. The range was maximal for zero transmission delays, and for all distances attenuated with finite, decreasing lateral conduction velocities. Below a velocity of 0.5 m/s, γ-power and γ-coherence were even smaller than without these connections at all, i.e., slow horizontal connections actively desynchronized neural populations. In conclusion, the enhancement of γ-coherence by horizontal excitatory connections critically depends on fast conduction velocities.

Coherent γ-activity in the primary visual cortex and the accompanying models was found to only cover small regions of the visual field. This challenges the role of γ-synchronization to solve the binding problem for larger object representations. Further analysis of the previous model revealed that the patches of coherent γ-activity (1.8 mm half-height decline) were part of more globally occurring γ-waves, which coupled over much larger distances (6.3 mm half-height decline). The model γ-waves observed here are very similar to those found in the primary visual cortex of awake monkeys, indicating that local recurrent inhibition and restricted horizontal connections with finite axonal velocities are sufficient requirements for their emergence. In conclusion, since the model is in accordance with the connectivity and γ-processes in the primary visual cortex, the results support the hypothesis that γ-waves provide a generalized concept for object binding in the visual cortex.

Statement of Originality

Major parts of this thesis consist of manuscripts already published (Chapter 2) or ready for submission (Chapter 3, 4). Chapter 2 was written in co-authorship with Reinhard Eckhorn. All other parts of this thesis are originally composed by the author unless otherwise indicated explicitly. All models and data analyses were implemented self-dependently, including the simulation kernel for delayed interactions. The wave detection method used in Chapter 4 was kindly provided by Andreas Gabriel. All simulations base in part on elementary routines, that were developed in close cooperation with other members of the Neurophysics Group led by Reinhard Eckhorn.

This thesis has not been submitted, either in whole or part, for a degree at this or any other university or institution.

Contents

List of Figures

1 Introduction

Human perception of the outside world is primarily based on vision. Looking around and recognizing a person or a tree in a natural environment is an accomplishment that no computer can perform at present. The reason for this inability to find adequate algorithms is the extreme complexity of transforming physical stimuli into perceived objects. Light is reflected from a physical object and falls onto the retinae of the left and the right eye. These two-dimensional images can change drastically with an object's position, view and illumination. Nevertheless, the visual system provides a stable object recognition under most conditions. An approaching person will not grow larger, although the retinal image does. A tree remains the same, even when a breeze considerably changes its shape. This stability is remarkable and illustrates, that the brain does not passively record images. Instead, it actively transforms a sequence of two-dimensional retinal images into a stable, reliable, three-dimensional mental world.

1.1 Feature extraction and scene segmentation

The world we perceive around us is composed of whole objects, like chairs, tables, trees or faces. When focusing on one specific object, we also have access to its subordinate, local features like the color, texture, shape or motion. The sequence of this subjective perception could lead to the assumption that local features are not relevant for the coherent perception of objects in the first place. There is, however, considerable evidence from anatomy, neurophysiology and psychology that these local features are essential for defining visual objects. Different local aspects of the visual input are simultaneously processed by specialized maps of local detectors in several visual areas (e.g., Felleman and van Essen, 1991). There is a ventral pathway, mainly processing and representing shape and color, that is separated from the dorsal pathway, representing space and

motion (Ungerleider and Mishkin, 1982; Ungerleider and Haxby, 1994). The distributed computation is further supported by lesion studies, showing e.g., that the ability to perceive motion can be lost independently of other features, resulting in the perception of frozen stills (Zeki, 1991).

So why are we able to perceive the world around us as consisting of whole objects instead of disembodied shapes, colors or motions? If we would only look at scenes containing a single object at one time there would not be a problem at all, because all features would simply belong to that object. Yet, the world around us usually contains numerous objects. The visual system must therefore provide a mechanism to structure and combine distributed, local features into objects. This process of grouping is called *feature binding*. The separation of features belonging to one object from other features is called *segmentation*, in vision: *scene segmentation*.

But what makes up a visual object? While we have a profound implicit knowledge of what visual objects are, a precise and complete definition is hard to formulate, if not impossible at the current state of knowledge. A visual object is a limited region in visual space that exhibits some kind of contrast to its surround, like a change in intensity, color, texture or motion. The spatial arrangement of the object's local features is not arbitrary but has to meet certain correlational requirements. Systematic rules for perceptual grouping were first formulated by Gestalt psychologists (e.g. Koffka, 1935). Some of their elementary and intuitive laws are illustrated in Fig. 1.1. For a more complete view of object definition, they have to be complemented by other factors including previous knowledge, attention and expectation.

A neurophysiological correlate for the extraction of local, basic visual features was found in the primary visual cortex using microelectrode recordings (Hubel and Wiesel, 1962; Hubel, 1982). External stimuli induce specific responses in single cortical neurons. The averaged, linear part of the response function can be captured by the concept of the classical receptive field (cRF), that characterizes how local features of a small visual stimulus affect the average output spike rate of a single neuron. A simulated response of simplified, orientation specific, local feature detectors can be seen in Fig. 1.2. These feature detectors extract local orientations that are in accordance with the observers perception for most parts of the image. An interesting exception, however, is an intersection of two line segments where orientation detection breaks down. These X-junctions as well as the closely related T-junctions often occur in natural vision and usually indicate that one object is partly occluded by another object. At this point,

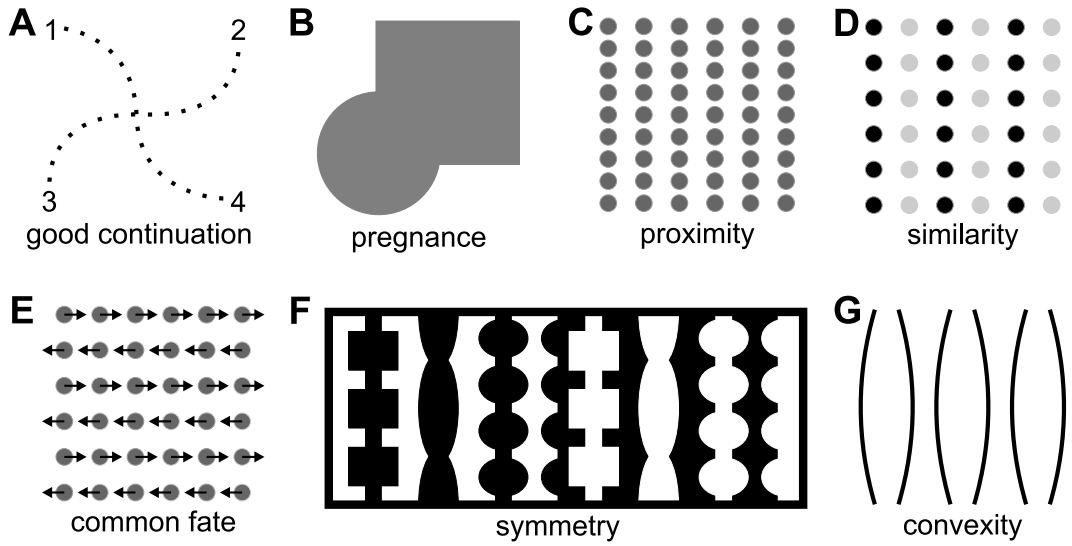

Figure 1.1: *Gestalt laws define basic rules for visual object binding.* **A.** Good continuation expresses the viewer's innate tendency to perceive a line as continuing its established orientation. Line segment 1 is continued to line segment 4; the same holds for line segments 2 and 3. **B.** This law implies that visual input is organized in a predictable way. The unknown form is perceived as a combination of a square and a circle, because we are used to see circles and squares. Perception is influenced by knowledge and expectation. **C-F.** If other cues are missing, objects are perceptually grouped due to their proximity (C), similarity (D), common motion (E) and symmetries (F). **G.** Although all neighboring arcs are separated by equal distances, they are most likely grouped to convex objects. This rule accounts for the fact, that most natural objects have a closed form.

our visual system is confronted with the task to bind local features into a coherent percept. For the example at hand, a neurophysiological counterpart for the Gestalt law of good continuation (Fig. 1.1A) is required. In the following sections, I will present two concepts how distributed features can be bound into a visual object. They should be seen as complementing rather than contradicting each other.

1.2 Convergent feedforward projections and "cardinal cells"

One possible mechanism for feature binding is based on the idea, that the concept of a neuron's cRF can be generalized to more complex representations (Barlow, 1972). Using a layered feedforward scheme, the immense amount of local information is thought to be consecutively compressed and coded by a smaller number of active neurons with

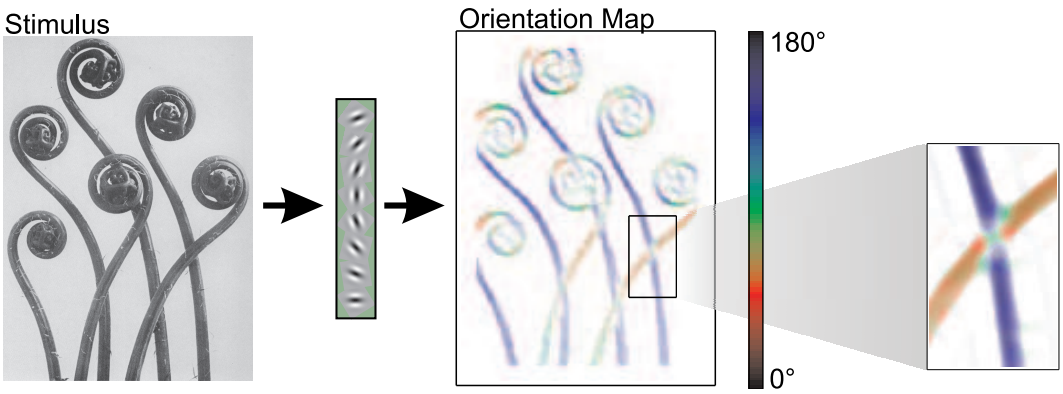

Figure 1.2: *Local orientation properties of a visual stimulus.* A black and white photography of hair ferns (Blossfeldt, 1994) is analyzed by a set of 8 orientation selective filters. The averaged response for each input pixel is shown in the orientation map. The edges of the map are clipped due to boundary effects of the filter functions. Color indicates the dominant orientation and saturation represents its strength. The intersection of two ferns is magnified and indicates the ambiguity of orientation at this point.

increasingly complex features (Fig. 1.3A). At the topmost level, the activity of one or a group of so-called *cardinal cells* (Barlow, 1972) is directly related to the occurrence of specific, complex objects in the visual scene. Since any visual scene would only activate a limited number of cardinal cells, these cells form a sparse representation. Indeed, the cortex heavily uses the principle of convergent connections at various levels of processing, e.g., for the transformation of concentric cRFs in the LGN (lateral geniculate nucleus) to elongated cRFs in the primary visual cortex of cats (e.g., Hubel and Wiesel, 1962; Reid and Alonso, 1995; Ferster et al., 1996).

The concept of cardinal cells also encounters several serious problems. Hard-wired coding of complex objects requires an enormous amount of neurons and connections, because every object has to be coded for every position and various feature combinations to compensate varying stimulus conditions, like view, illumination, size, colors or occlusions. The costs of hard-wired coding can be diminished by using partly invariant representations. The most prominent example is probably the *complex cell* (Hubel and Wiesel, 1962). The cRF of a *simple cell* (Hubel and Wiesel, 1959, 1962) consists of subregions that exert an excitatory or inhibitory influence on the cell's response. A stimulus that drives the cell optimally, must have the right position, the right orientation and the right size. Like simple cells, complex cells respond only to correspondingly

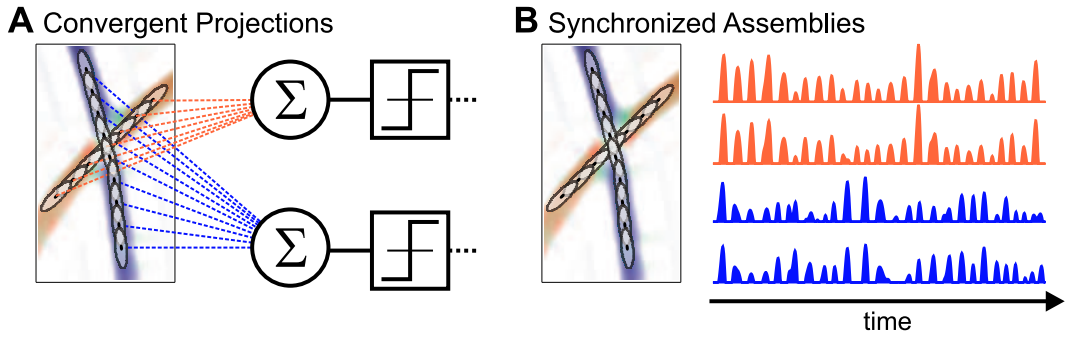

Figure 1.3: *Illustration of two complementary mechanisms for perceptual feature binding.* **A.** Responses of local feature detectors (ellipses in left box) are convergently connected to higher level neurons, illustrated by a summation and a following threshold operation. Higher level neurons will only be activated, if a sufficient number of active feature detectors matches their connection scheme. The upper (lower) neuron binds all red (blue) detectors into the common percept of a long, continuous line. Using only these two neurons, the binding into two vertices consisting of detectors below and above the intersection would not be possible. **B.** Time course of averaged neural activity for the four segments of the X-shaped activation is shown at the right side. Synchronization hypothesis states that neural populations showing synchronized activity belong to the same assembly or object representation. Here, the two red (blue) segments would be bound into the common percept of a long, continuous line. Red and blue time traces are not correlated. The underlying neural distributions therefore belong to different assemblies according to the synchronization hypothesis.

oriented stimuli, but unlike simple cells, the exact position of the stimulus does not matter, as long as it falls inside the receptive field (Hubel and Wiesel, 1962). The cell's response is therefore partly invariant of the stimulus position. Another example are object and face selective cells in the inferotemporal cortex. Their responses are often relatively invariant to the position in the visual field, size and even view of the object (Booth and Rolls, 1998; Tovee et al., 1994).

While invariant representations mitigate the costs for hard-wired object properties, they introduce a binding problem on their own. High-level cells do not account for the information that was disregarded during invariance processing. However, this information can still be important and is typically not lost in perception. To acquire full unambiguous information about an object, it is necessary to combine one or several invariant high-level cells with a fair number of lower-level cells. Mechanisms to bind these cells remain unsettled.

1.3 Synchronized neural assemblies

The large number of neurons representing a single object is the starting point for a competing view on feature binding. In the *assembly* concept (Hebb, 1949), the representation of a visual object is formed by the activation of the same distributed neurons, that represent the object's local features. Since a single neuron can participate in the representation of numerous objects, this coding strategy uses available neurons very efficiently.

However, the flexible binding of neurons to assemblies has a drawback: a visual scene usually contains several objects at once, each represented by an assembly of neurons. The assignment of individual neurons to a specific assembly is ambiguous. This equivocality may be solved by structuring neural activity in the temporal domain (Milner, 1974; Reitboeck, 1983; von der Malsburg and Schneider, 1986). Synchronized neural activity in this view indicates that the participating neurons contribute to the same assembly, while neurons from different assemblies are not synchronized (Fig. 1.3B). Thereby, *temporal binding* can maintain the average response of a neuron, that will still be determined by its receptive field properties, and so still can represent local stimulus features.

Synchronized signal components have been found in the γ-frequency range (30–90 Hz) of microelectrode recordings in cats and monkeys (Eckhorn et al., 1988; Gray et al., 1989; Engel et al., 1991a,b; Kreiter and Singer, 1996; Frien and Eckhorn, 2000b). Their occurrence is stimulus specific and depends on global stimulus properties, in accordance with simple Gestalt laws. The interdependence of γ-oscillations and their synchronization is not clear: on the one hand, synchronized oscillations are also found in other frequency bands (e.g. von Stein and Sarnthein, 2000; Bruns and Eckhorn, 2004), and on the other hand, synchronization is also found in non-oscillatory signal components (Eckhorn, 1994; König et al., 1995). The relevance of synchronized oscillations for perceptual grouping is hotly debated. The state of the discussion can be obtained from several recent reviews: Gray (1999); von der Malsburg (1999); Shadlen and Movshon (1999); Singer (1999); Eckhorn et al. (2001a, 2004a,b).

Closely related to synchrony is the phenomenon of *traveling waves*, which are observed in many cortical areas in several species (review: Ermentrout and Kleinfeld, 2001). Although theoretical studies predict that traveling waves are an emergent property of cortical networks with spatially restricted connectivity (Kuramato, 1984),

they were surprisingly not reported in studies investigating synchrony in the visual cortex of cats and monkeys. By re-evaluating part of these data, Gabriel and Eckhorn (2003) recently demonstrated not only the existence of traveling γ-waves in monkey, but also their dependence on the rules of figure-ground segregation (Eckhorn et al., 2001a, 2004a).

1.4 Plasticity induced by synchronous activity

In his famous work, Donald Hebb did not only develop a simple concept of cell assemblies, but also proposed a mechanism how they might be established (Hebb, 1949):

> When an axon of cell A is near enough to excite cell B or repeatedly or consistently takes part in firing it, some growth or metabolic change takes place in one or both cells such that A's efficiency, as one of the cells firing B, is increased.

The central feature of this postulate is, that neural activity, especially its temporal structure, is decisive for changes in cortical wiring. In the past decades, this postulate has been verified down to the cellular level and provides the basis for all biologically plausible learning mechanisms.

1.4.1 Role of activity for cortical development

The early formation of cortical circuitry involves a phase of initial axon path finding, which can occur over substantial distances and is largely directed by molecular cues. A second developmental phase includes the selection of targets and the formation of appropriate synaptic connections. Today it is generally accepted that neuronal activity is essential for this refinement of developing cortical circuits (reviews: Katz and Shatz, 1996; Zhang and Poo, 2001).

Early experiments on monocular deprivation (Wiesel and Hubel, 1963) and artificial strabism (Hubel and Wiesel, 1965) show that missing or conflicting visual information can substantially disturb the refinement process of ocular dominance. Similarly, the development of orientation selectivity can be deteriorated by artificial, synchronous stimulation of optic nerves (Weliky and Katz, 1997). In another series of experiments, projections from the retina were directed to the immature auditory pathway. After some

weeks, the auditory cortex exhibited orientation maps and characteristic horizontal connectivity. This shows that prominent properties of the primary visual cortex can be transferred to other modalities by activity-dependent mechanisms alone (review: Sur and Leamey, 2001).

The experiments above show that neural activity, induced by the visual input can be very important for the refinement of developing circuits. However, visual input cannot account for the initial development, because several neural properties and cortical maps are already present before eye opening (Wiesel and Hubel, 1974; Godeke and Bonhoeffer, 1996; Horton and Hocking, 1996; Crair et al., 1998). These findings suggest that endogenous neural activity, generated by the nervous system without sensory stimulation, is responsible for development before sensory input is available. One source of this activity are spontaneously generated waves of action potentials, which are present in the retina before photoreceptors are developed (Meister et al., 1991; Wong et al., 1995; Weliky and Katz, 1999). Another source for endogenous activity may be giant depolarizing potentials that are found in the immature hippocampus (review: Spitzner, 2004). Blocking this endogenous activity results in a severe disruption of the developmental process (review: Penn and Shatz, 1999).

In conclusion, the initial development of cortical circuits seems to be driven by endogenous, correlated activity before eye opening, while these circuits are refined by visually driven correlated activity after eye opening. The cellular mechanisms underlying this development will be described in the following section.

1.4.2 Temporal Hebbian learning

The information transfer between two neurons occurs most frequently at one or several chemical synapses. Presynaptic action potentials evoke synaptic potentials at the dendrite of the postsynaptic cell (postsynaptic potential, PSP). The form and amplitude of these PSPs are determined by the properties of the synapse. Under certain conditions, these properties can be due to changes. The amplitude of the postsynaptic potential (PSP) can be potentiated by a brief but intense activation of the presynaptic axon (Bliss and Lømo, 1973). This synaptic change lasts for hours, days or weeks and is therefore called long-term potentiation (LTP). In the past 30 years, the occurrence of LTP was demonstrated in many areas and species (review: Bi and Poo, 2001), using a stimulation protocol with low-frequency presynaptic spikes and a simultaneous depolarization of the

postsynaptic neuron. The exact temporal specificity of LTP effects was not addressed, since pre- and postsynaptic stimulations were applied for several seconds or minutes.

The finding, that action potentials do not only propagate along the axon, but also back-propagate into the neuron's dendrite (Stuart and Sakmann, 1994), was a first sign for the importance of action potentials in synaptic plasticity. Final evidence came from experiments, where a back-propagating action potential, that was triggered 10 ms after onset of the postsynaptic potential, induced LTP (Markram et al., 1997; Magee and Johnston, 1997). Reversing the order of PSP and action potential weakened the synapse, called long-term depression (LTD). The action potential or the PSP in isolation were not sufficient to evoke any synaptic changes. The critical time window for LTP and LTD is about 40 ms in width (Bi and Poo, 1998; Zhang et al., 1998).

In conclusion, synaptic changes rely critically on the temporal order of pre- and postsynaptic action potentials at a millisecond scale.

1.5 Transmission delays

Synchronization, γ-oscillations and plasticity are phenomena that depend critically on the precise timing of neural activity. The interactions between neurons are mediated by action potentials that travel along axons with finite velocity. The resulting transmission delays critically affect the dynamics that can emerge in neural networks. Model investigations (Mirollo and Strogatz, 1990; Kuramato, 1991; Ernst et al., 1995; Nischwitz and Glünder, 1995) have shown, that two mutually connected neurons synchronize with zero-phase difference, if the action potentials are transmitted instantaneously and evoke excitatory postsynaptic potentials. For inhibitory interactions, the synchronous solution is unstable and both neurons show a counterphasic activation. Delayed interactions completely change these dynamics: neurons with mutually inhibitory connections can now synchronize with zero phase difference, while excitatory connections act desynchronizing (Mirollo and Strogatz, 1990; Kuramato, 1991; Ernst et al., 1995; Nischwitz and Glünder, 1995). For an understanding of cortical dynamics, it is therefore important to quantify cortical conduction delays.

Cortico-cortical axons make up 99% of the white matter underlying the cortex (Abeles, 1991). In order to limit the brain volume, it is therefore reasonable to conserve the axonal volume. This is possibly the reason why most cortico-cortical axons have diameters smaller than 1 μm (review: Nowak and Bullier, 1997). The axonal diameter

has important consequences for the conduction velocity of action potentials: There is a linear relationship between conduction velocity and fiber diameter for myelinated axons (Waxman and Bennett, 1972), while conduction velocity varies as a square root of fiber diameter for nonmyelinated axons (Rushton, 1951). The axonal diameter can vary largely between the main axon trunk and its cortical ramifications, which are often nonmyelinated (Houzel et al., 1994). This implies that even myelinated (fast) axonal connections exhibit non-vanishing delays.

While there are numerous velocity measurements between cortical areas, little is known about conduction velocities within a cortical area (Nowak and Bullier, 1997). The typical speed of action potential propagation along horizontal excitatory connections is in the order of a few tenth of m/s (Komatsu et al., 1988: 0.3 m/s; Murakoshi et al., 1993: 0.15–0.55 m/s; Hirsch and Gilbert, 1991: 0.3–0.6 m/s; Nowak and Bullier, 1998: 0.4 m/s). Inhibitory connections seem to be slightly slower (Salin and Prince, 1996: 0.06–0.2 m/s, mean: 0.1 m/s).

Axonal delay is not the only factor that limits the speed of information transfer. The second parameter is the *neural integration time*, that is the duration it takes a depolarizing event to drive the membrane potential of the target neuron to the firing threshold. It strongly depends on the state of the target neuron. For a neuron at rest it is at least 5 ms and can range up to several tens of milliseconds. If the neuron is already near the firing threshold, the neural integration time can be shorter than one millisecond and is mainly determined by the rise time of the PSP (review: Nowak and Bullier, 1997).

The measured velocities of intra-area information processing are consistent with the slow spread of synaptic activity in monkey revealed by optical imaging (Grinvald et al., 1994: 0.1–0.25 m/s). Slow conducting axons may also be the source of slow activity waves in cat, triggered by visual stimulation in peripheral parts of the receptive field (Bringuier et al., 1999, mean: 0.1 m/s).

In conclusion, there are significant transmission delays between cortical neurons that may support or perturb the emergence and stability of synchronized γ-oscillations.

1.6 Aim of the study

In the preceding part of this introduction, several aspects of temporal information processing in the visual cortex and the emergence of related neural circuitry have been

addressed. First, the development of the immature visual system depends crucially on correlated activity, that is either evoked by visual experience or generated by the cortical periphery. On the cellular level, synaptic changes depend on the relative timing of pre- and postsynaptic action potentials in a critical time window of 40 ms. Second, synchronous γ-oscillations (oscillation period $\approx$10–30 ms) as well as stochastic synchrony are found in the mature visual cortex. They extend several millimeters across the cortical surface and show properties that are consistent with perceptual feature binding and segregation. Third, the vast majority of axons remaining in V1 show transmission velocities in the order of 0.1–0.6 m/s. When taking into account that intra-area axonal ramifications in V1 can reach several millimeters (e.g., cat: Gilbert and Wiesel, 1979; Martin and Whitteridge, 1984; Gilbert and Wiesel, 1989; tree shrew: Rockland and Lund, 1982, Bosking et al., 1997, 2002; monkey: Sincich and Blasdel, 2001; Stettler et al., 2002), transmission delays are in the order of at least 5–30 ms.

The synchronization hypothesis states that local features belonging to the same object are synchronized. Delays are likely to have a substantial influence on γ-synchronization and the underlying γ-oscillations, since their time scales are comparable. This work tries to uncover, if groups of neurons can synchronize despite the constraint of slow interactions. Are there critical velocities or distances that limit the emergence of γ-oscillations or γ-synchronization? Do delayed interactions act differently on inhibitory and excitatory, short- and long-range connections?

Synchronization hypothesis additionally demands that features belonging to different objects are not synchronized. Several models (Dicke, 1992; Stoecker et al., 1996; Ursino et al., 2003) realize this by separating objects in phase, i.e. the oscillation period is subdivided and all feature detectors of one object are exclusively active within one time slice. While this mechanism is stable for instantaneous interactions, it is unclear if this is also valid using delayed connections.

In addition to γ-synchronization, the primary visual cortex also exhibits traveling γ-waves (Gabriel and Eckhorn, 2003). What network properties are responsible for this property? Is the spatially restricted connectivity sufficient or are axonal delays required? What is the necessary network design to produce traveling waves, that are consistent with findings from the visual cortex? How is learning influenced by delayed interactions? Can delays assist the development of structures in the cortex?

To investigate the effects of finite axonal velocities, I have performed simplified, numerical simulations of a small area of the primary visual cortex. The basic processing

unit is a spiking neuron, in order to account for the importance of action potentials and their exact timing. Several mesoscopic measures are derived from the network's activity and analyzed with identical methods used for experimental data. This allows easy quantitative comparisons of modeling and experimental results. I will focus on two recent studies from our group dealing with the decoupling of γ-signals across the contour representation of an object in V1 (Gail et al., 2000), and with the emergence of traveling γ-waves within the surface representation of an object (Gabriel et al., 2004).

1.7 Thesis outline

The thesis consists of 3 chapters, each containing a separate introduction and discussion. Chapter 2 deals with the refinement of delayed connections in a simple model of the immature cortex using spiking neurons. Since most of the generic connectivity evolves before eye opening, globally correlated spontaneous activity will be used as input. I will show, that structured intra- and inter-area connections evolve under the influence of temporal Hebbian learning. Chapter 3 presents a simplified model of the mature primary visual cortex. The effects of distance-dependent delays on γ-oscillations and synchronization are investigated in numerical simulations of spiking neurons. The network properties will be discussed using elementary visual configurations for object binding and separation. In Chapter 4, the same network will be used to demonstrate the emergence of traveling γ-waves and their interdependence to γ-synchronization.

2 Plasticity

Lateral spike conduction velocity in the visual cortex affects spatial range of synchronization and receptive field size without visual experience: a learning model with spiking neurons

Classical receptive fields (cRF) increase in size from the retina to higher visual centers. The present work shows how temporal properties, in particular lateral spike velocity and spike input correlation, can affect cRF size and position without visual experience. We demonstrate how these properties are related to the spatial range of cortical synchronization if Hebbian learning dominates early development. For this, a largely reduced model of two successive levels of the visual cortex is developed (e.g., areas V1 and V2). It consists of retinotopic networks of spiking neurons with constant spike velocity in lateral connections. Feedforward connections between level 1 and 2 are additive and determine cRF size and shape, while lateral connections within level 1 are modulatory and affect the cortical range of synchronization. Input during development is mimicked by spike trains with spatially homogeneous properties and a confined temporal correlation width. During learning, the homogeneous lateral coupling shrinks to limited coupling structures defining synchronization and related association fields (AF). The size of level-1 synchronization fields determines the lateral coupling range of developing level-1-to-2 connections and, thus, the size of level-2 cRFs, even if the feedforward connections have distance-independent delays. AFs and cRFs increase with spike velocity in the lateral network and temporal correlation width of the input. Our results suggest that AF size of V1 and cRF size of V2 neurons are confined during learning by the temporal width of input correlations and the spike velocity in lateral connections without the need of visual experience. During learning from visual expe-

rience, a similar influence of AF size on the cRF size may be operative at successive levels of processing, including other parts of the visual system.

The content of this chapter has been published in Saam and Eckhorn (2000). The results are also summarized in Eckhorn et al. (2001a, 2004a,b). Preliminary versions had been published as conference proceedings (Saam and Eckhorn, 1998a,b, 1999; Saam et al., 1999).

2.1 Introduction

2.1.1 Receptive and association fields

The best explored and most accepted concept of visual processing is that of the classical receptive field (cRF; Hubel and Wiesel, 1962) which characterizes the spatiotemporal coupling between small visual stimuli and the spike response of single visual neurons. Less intensely investigated is the influence of visual context outside the cRF. Context can modulate the cRF properties strongly over a broad range in visual space (Allman et al., 1985). In recent years synchronization fields were found in the lower areas of the visual cortex. Their size has been defined by the cortical extent of coherence among fast cortical oscillations (35–90 Hz; Frien et al., 1994; Frien and Eckhorn, 2000b). According to the cRFs of single neurons, the projections of synchronization fields to visual space have been termed the association fields (AF; Eckhorn et al., 1990) or context fields (Phillips and Singer, 1997) of local groups of neurons. One intensely discussed hypothesis for the AFs' function is that feature grouping is supported in their field by synchronizing those neurons currently representing the same visual object (reviews in Eckhorn, 1999; Gray, 1999).

Grouping of features into whole objects may also be coded by the convergence of their relevant feature detectors (Barlow, 1972; Riesenhuber and Poggio, 1999). If convergence is present over all levels of visual processing, it would produce a systematic increase in cRF size from retina to higher centers. This principle may become operative during early visual experience if objects to be learned appear transiently and alone in a scene. The component feature detectors of an object would be coactivated, and Hebbian learning could establish stable convergent connections. However, real visual objects are parts of complex scenes and their segregation from other objects is a formidable

problem. One potential solution for scene segmentation is provided by the concept of transient synchronization within the representational range of an object. In such a scheme, Hebbian learning would only stabilize feedforward connections of synchronized inputs. In this way, the synchronization and related association field at a lower level would determine the cRF type and size at the next level of processing and hence, cRFs would increase within the hierarchy of visual cortical areas.

2.1.2 Input to visual cortex during development

Evidence of cortical plasticity by visual experience is rarely disputed (e.g., Hubel and Wiesel, 1970; Crair et al., 1998). However, many functional units of the visual cortex emerge before eye opening, demonstrating that visual experience is not required for initial development (Crair et al., 1998; Chapman et al., 1999). Spike activities, already present in the retina before eye opening, probably provide instructive cues for guiding the development within the striate cortex (Weliky and Katz, 1999). This activity consists of stochastic spike trains, simultaneously modulated in their rates over large retinal regions (Meister et al., 1991; Wong and Oakley, 1996). For the present model we assume (as a working hypothesis) precise correlations (2–10 ms) among inputs to the V1 level over ranges of several hypercolumns. This seems reasonable because activities in the developing retina are dominated by tight junctions among neighboring neurons (Penn et al., 1994), which are known to mediate fast electrical coupling in the millisecond scale. Precise temporal structuring of cortical input may also be introduced by rhythmic cortico-thalamic feedback (5–10 Hz) and via fast intracortical inhibition (20–30 Hz). Thus, precise correlations in maintained activities at thalamic and primary cortical levels are probably present before visual experience and may guide the early development of connectivity patterns.

2.1.3 Hebbian learning supports the emergence of functional cortical units during development

Several correlational properties of afferent spike trains to the striate cortex are consistent with predictions of activity-dependent models of cortical map and cRF development in V1 before eye opening. One model proposes that the observed differences in correlated firing between ON- and OFF-thalamic afferents can drive the segregation of a simple cell's cRF subregions (Miller, 1994). Other models show that the competing requirements

of joint ocular dominance and orientation map development in V1 can be resolved if within-eye activity is more strongly correlated than between-eye activity (Miyashita et al., 1997; Stetter et al., 1997), a fact that has recently been confirmed experimentally (Weliky and Katz, 1999).

Most models of striate cortical development based on Hebbian learning use partially synchronized input activities, while few assume differences in delays. For instance, Gerstner et al. (1996a) explain the temporal precision in auditory direction discrimination by sorting out axons of differing delays by correlation learning, resulting in coincident spikes. Other recent work assumes correlation-dependent learning of synaptic delays by a rule decreasing the correlation delays in synaptic signals and generating coincident inputs (Hüning et al., 1998; Eurich et al., 1999). Finally, Ritz et al. (1994) demonstrate that the average activation delay among reciprocally connected excitatory neurons restricts the size of cortical synchronization fields in which zero-delay phase-locking is possible for a given oscillation frequency.

In our present model of visual areas V1 and V2, the main properties are lateral spike conduction delays increasing systematically with distance, in addition to partial correlations of the external signals. Their relevance is tested for the emergence of functional cortical units without visual experience (an abstract was published in Saam et al., 1999).

2.2 Methods

2.2.1 Model neuron

We use pulse coding model neurons with spike inputs, realistic post synaptic potentials, and an adaptive spike encoder with dynamic threshold (Eckhorn et al., 1990). The input part of a neuron n_i consists of synapses S_{ij}, which have an impulse response $h(t)$ and a synaptic efficacy w_{ij}.

$$S_{ij}(t) = w_{ij}^S \, I_j(t - \Delta_{ij}) * h(t, \tau_{S1}, \tau_{S2}), \tag{2.1}$$

where $*$ denotes the convolution operator, i is the index of the postsynaptic neuron n_i, I_j the spike output of a presynaptic neuron n_j and Δ_{ij} the conduction delay for

spikes between n_i and n_j. The synaptic response $h(t)$ is modeled by a second-order leaky integrator:

$$h(t, \tau_1, \tau_2) = \mathrm{H}(t)(\exp(-t/\tau_2) - \exp(-t/\tau_1)). \tag{2.2}$$

$\mathrm{H}(\,\cdot\,)$ denotes the Heaviside function. Time constants are chosen such that the excitatory postsynaptic potential (EPSP) reaches its maximum value at t=1. Two types of inputs are processed separately: external feeding input F_{ij} and lateral linking input L_{ij} (Eckhorn et al., 1990).

$$S_i(t) = \sum_j S_{ij}(t), \tag{2.3}$$

where S may be F or L. While the feeding inputs F_i have conventional synapses (non-NMDA), the linking inputs L_i exert multiplicative influence on the feeding inputs. The resulting membrane potential, driving the spike encoder, is therefore calculated as:

$$U_i(t) = F_i(t) \cdot (1 + L_i(t)), \tag{2.4}$$

which enables the feeding input to drive the spike encoder even with zero linking input, while the reverse is not possible. Multiplicative interactions have been chosen for the following reasons: Lateral interactions in developing visual cortex area V1 are mainly located in the upper layers where synapses are dominated by NMDA channels (Fox et al., 1989). In V1, NMDA channels have been reported to mediate gain control, due to their voltage dependences and the differences in the Hill coefficients for binding glutamate at the NMDA receptors. Both properties affect the response to afferent visual input in a graded multiplicative fashion (Fox and Daw, 1992). Thus, a multiplicative interaction among forward and lateral connections seems biologically plausible. In our model, this modulatory action of the linking on the feeding inputs ensures that the local coding of single neurons (here the cRF) is not deteriorated by lateral connections (Eckhorn et al., 1990).

In the spike encoder, the membrane potential $U_i(t)$ is compared to a threshold $\theta_i(t)$. If $U_i(t)$ exceeds $\theta_i(t)$, a spike is generated:

$$O_i(t) = \mathrm{H}(U_i(t) - \theta_i(t)). \tag{2.5}$$

The threshold $\theta_i(t)$ has a static offset value θ_0 and a dynamic part, which is an impulse response of two leaky integrators to the spike output $O_i(t)$:

$$\theta_i(t) = \theta_0 + O_i(t) * [(V_{\theta\mathrm{r}} \exp(-t/\tau_{\theta\mathrm{r}}) + V_{\theta\mathrm{s}} \exp(-t/\tau_{\theta\mathrm{s}}))\mathrm{H}(t)]. \tag{2.6}$$

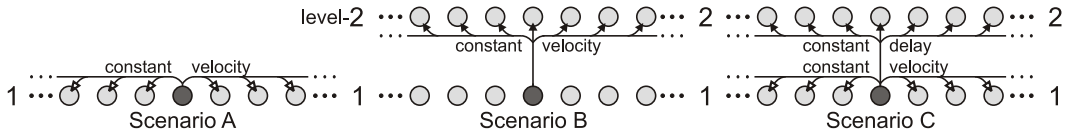

Figure 2.1: *One-dimensional sketch of the connectivity scheme for a single level-1 neuron in the three different scenarios A, B, and C. Open arrow heads:* linking synapses; *filled:* feeding synapses

One leaky integrator has an amplitude $V_{\theta \mathrm{r}}$ and a short time constant $\tau_{\theta \mathrm{r}}$ modeling fast refractory components, while the other ($V_{\theta \mathrm{s}}$, $\tau_{\theta \mathrm{s}}$) is slower, mimicking spike rate adaptation. Additionally, an absolute refractory period of 1 ms is introduced. The above equations are solved for different temporal resolutions ($\Delta t = 0.2, 0.5, 1.0$). The higher resolutions are important for realizing precise distance-dependent delays in the network. A physiologically realistic time scale is 1 ms for $\Delta t = 1$.

2.2.2 Network topology and signal properties

Level 1 and 2 each consist of 441 neurons arranged on a two-dimensional Cartesian grid. To avoid artifacts from boundaries, toroidal boundary conditions are used. All neurons have the same time constants and threshold properties (Table 2.1). We expected complex intermingled effects on the learning process in lateral and feedforward synapses by the different types of temporal spike dispersion, including the partial correlation of the stochastic external inputs and the systematic delay dispersion in lateral and feedforward axons. In order to keep these effects separate we built and analyzed the model in three consecutive steps (Fig. 2.1: scenario A, B and C).

Scenario A: Learning the level-1 linking synapses of lateral connections with distance-dependent delays

Lateral axons project to neighbors up to a distance of 10 neurons. The initial strengths w_c of these linking synapses are low and chosen randomly. The axons transmit spikes at constant velocity v_{ax} (Table 2.1) so that delays increase proportional to lateral distance (for the choice of realistic velocities see the Discussion). Other delays, including synaptic and dendritic ones, are assumed to be constant in their average values so that their sum Δ_0 is also constant and can be compensated in the present simulations by a temporal

offset Δ_0 in the learning function (arguments for these simplifications are given in Discussion).

The external input to level-1 neurons has no spatial structure in its correlation properties because here we are interested in the effects of lateral transmission delays on the formation of spatially confined coupling structures during learning. Therefore, we composed the input of the following components: (1) Independent Gaussian white noise (GWN) is directly superimposed on the feeding potential with the same mean m_{GWN} and standard deviation σ_{GWN} for all neurons. These continuous signals resemble the postsynaptic potentials evoked by a large number of statistically independent spike trains (Fig. 2.2a). (2) Correlated spike trains with a Poissonian interval distribution (mean rate f_p) are applied to a fraction (p_p) of all neurons (randomly selected for each correlated burst of activation). These spike trains are temporally correlated (Fig. 2.2b) according to a common modulation by a Gaussian impulse probability (SD: σ_p). Thus, the input has weak paired spike correlations with a peak at zero time shift and a correlation width of $2\,\sigma_p$. Despite the presence of the independent GWN, the input spike trains reproduce their mutual correlations approximately among the neurons' outputs (Fig. 2.2c,d). These are the spike trains that affect learning in the linking synapses after being delayed in the lateral axons.

Scenario B: Learning of level-1-to-2 feeding projections with distance-dependent delays while lateral connections at level 1 are absent

Here, the effect of delays in feedforward connections is studied in isolation (without the influence of level-1 delays). Level-1 neurons project completely onto level-2 neurons. The initial strengths of the feeding synapses are randomly distributed around a common mean (Fig. 2.7a) sufficient for initiating spikes in level-2 neurons. Level-1-to-2 axons have the same increase in delays with lateral distance as in scenario A (i.e., constant axonal velocity). The interareal delay between all retinotopically corresponding positions is assumed to be equal. A constant delay does not change the relative timing of incoming spikes at level-2 neurons, and since there is no feedback in our simplified model, this additional delay will have no influence on the learning results. Hence, the effective input spike trains for learning the level-2 synapses have the same statistical properties as those for learning the lateral linking connections at level 1 in scenario A (because they are collaterals of the same layer-1 neurons). This means, that their correlations (Fig. 2.2d) are spatially homogeneous.

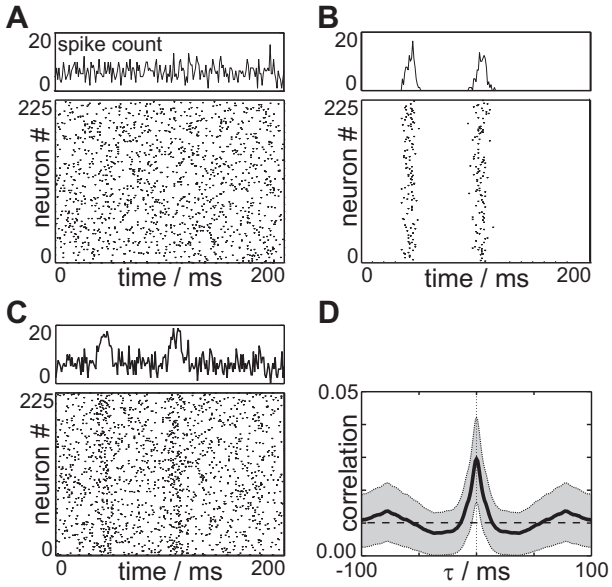

Figure 2.2: *Scenario A, B: Statistical properties of the spike trains at the output of level 1 that are effective during learning.* **A.** *Lower panel*: spike patterns of level-1 neurons (each *dot* denotes the occurrence of a spike) and temporal spike count of all neurons (*upper panel*), driven exclusively by the independent Gaussian white noise (GWN) at the inputs. **B.** Correlated spike patterns and temporal spike count at the output of level-1 neurons; two events of modulation in spike rate are shown. **C.** Spike patterns and temporal spike count at the output of level-1 neurons if GWN (A) and the spike patterns (B) drive their inputs. Such spike patterns are effective during learning of the lateral linking connections at level 1 and the level-1-to-2 feeding connections. Note that the statistical properties of these signals are spatially homogeneous. **D.** Cross-coincidence histogram among pairs of output spike trains, averaged over all combinations of level-1 neurons

Scenario C: Learning level-1-to-2 feeding connections with constant axonal delay and input from the learned version of level 1

Here we test the temporal effects emerging in a learned version of level 1 (scenario A) on feedforward convergent projections to the next level. To obtain separable effects, we kept all delays from level 1 to 2 identical. Level-1 neurons project retinotopically to level-2 neurons, initially with a broad Gaussian weight function (A_{12}, SD: σ_{12}), modeling the large diverging axonal trees present during development. To exclude the possibility that learning results arise from initialization, we trained the network with independent noise inputs as a control. In these simulations all weights decreased below 10^{-5}, which is three decades below the effects obtained with temporally correlated input.

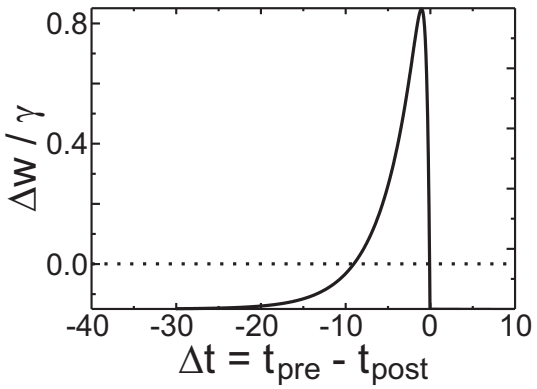

Figure 2.3: *Synaptic weight change $\Delta w/\gamma$ as a function of the relative timing Δt (in milliseconds) between presynaptic t_{pre} and postsynaptic firing t_{post}.*

If the learned version of level 1 (scenario A) is excited by a localized activity blob at random positions, damped traveling waves of laterally propagated activity are evoked, conducted by the constant velocity connections. To obtain a more precise control over this wave-like input to level 2 we replaced the lateral level-1 connectivity and its input spike trains by a simulated version of the level-1 outputs with a well defined firing probability:

$$p(r,t) = \exp(-r^2/(2\sigma_b^2))\,\delta(v_b t - r). \tag{2.7}$$

Here, r denotes the distance of the neuron from the center of the input blob, v_b is the velocity of a wave front and t the time relative to the occurrence of the blob. During learning, the centers of these wave-like activations are uniformly distributed over the neural grid, chosen in a random sequence with Poissonian interval distribution at a rate f_b.

2.2.3 Learning

We use a temporal Hebbian learning rule similar to that of a recent work (Gerstner et al., 1996a). The weight changes exclusively depend on the relative timing of pre- and postsynaptic spikes in the following way. Each presynaptic spike initiates a synaptic learning potential

$$L_{ij}(t) \;=\; O_j(t-\Delta_{ij}) * h(-t,\tau_{p1},\tau_{p2}) - \alpha. \tag{2.8}$$

The time course of L_{ij} in response to a single presynaptic spike is shown in Fig. 2.3. If the postsynaptic neuron generates a spike, the synaptic efficacies are changed according to the present values of the learning potentials:

$$\Delta w_{ij}(t) = \max\{\gamma\, L_{ij}(t) O_i(t), -w_{ij}(t)\}, \tag{2.9}$$

$$w_{ij}(t + \Delta t) = w_{ij}(t) + \Delta w_{ij}(t), \tag{2.10}$$

where γ denotes the learning rate. With this rule, weights cannot change their sign and it ensures that causality plays a prominent role. With the parameters given in Table 2.1 the effective duration of the facilitatory (positive) part of the learning window is about 10 ms. The overall learning process lasted 100 000 ms.

To measure the signal correlations introduced by the learned lateral connections of level-1, their neurons are activated by the same input as during learning. Cycling artifacts are avoided by open boundary conditions and the restriction in calculating the cross-coincidence histograms (CCH) to the spike trains of the central neurons. The spatial strength profile of signal coupling is quantified by a single correlation index from CCHs among neurons of different distances (Juergens and Eckhorn, 1997). This index measures the coupling-related area of the central peak and yields values from 0 (uncorrelated) to 1 (completely correlated).

2.3 Results

2.3.1 Learning of lateral linking connections (scenario A)

Emergence of lateral coupling kernels

Learning of the lateral linking connections is achieved with temporally correlated input, lacking any spatial structure (Fig. 2.2c, and see Sect. 2.2.2). The cross-coincidence histogram among outputs of level-1 neurons (Fig. 2.2d) shows an average coupling width similar to that of the inputs (not shown). With these outputs affecting learning of the lateral connections, several new spatial network properties emerge. Most important is the laterally restricted coupling kernel with strong weights to direct neighbors and a monotonous decline with increasing distance (Fig. 2.4a). The confined coupling structures cause a related spatial restriction in the correlations of the spike trains (Fig. 2.4b). More precisely, the half height width of the spatial distribution of the correlation index varies proportionally with the width D of the lateral coupling kernel.

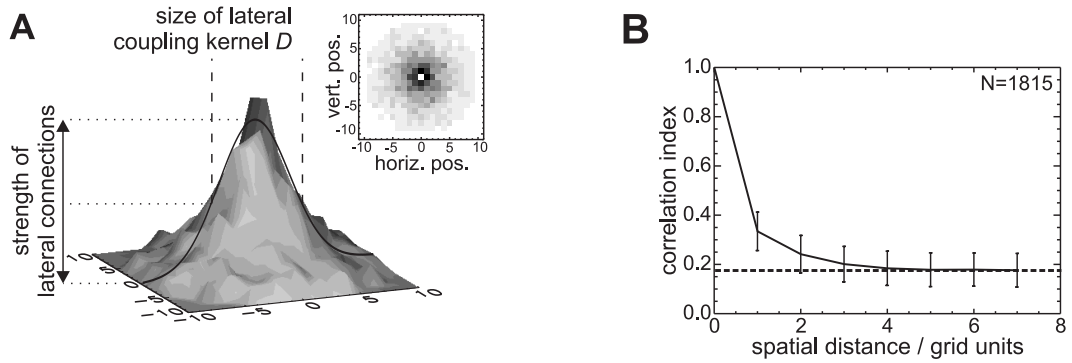

Figure 2.4: *Scenario A: Average spatial coupling profile between level-1 neurons after learning.* **A.** Synaptic strength to neighboring neurons is maximal and decays with increasing distance. The inset shows an intensity plot of the same data (grey scale coding; *black*: highest coupling strength). **B.** Correlation index of spike output depends on spatial distance. The average correlation strength introduced by the input is indicated by the *dashed line*.

This confined coupling emerges due to combined interactions of the distance-dependent spike delays and the temporal jitter of the input correlations in conjunction with the learning window. To understand this, consider the probabilities of relative spike timings at the learned synapses. Assume for the noiseless case that each neuron has a temporal Gaussian probability distribution $u(\Delta t)$ to fire with other neurons during the events of simultaneous input modulations according to Fig. 2.2b:

$$u(\Delta t) = 1/(\sqrt{2\pi}\sigma_p)\exp[-\Delta t^2/(2\sigma_p^2)]. \tag{2.11}$$

In addition, let us consider the projection from a presynaptic neuron n_j to a postsynaptic one n_i. The spikes of n_j need a time interval Δ_{ij} to reach the synapse; therefore, n_i receives a temporally shifted distribution of spikes $u(\Delta t - \Delta_{ij})$ from n_j. Hence, their relative spike timings (pre- and postsynaptic) are a convolution of the distributions:

$$\begin{aligned} \tilde{p}_{ij}(\Delta t) &= u(\Delta t) * u(\Delta t - \Delta_{ij}) && (2.12)\\ &= 1/(2\sqrt{\pi}\sigma_p)\exp[-(\Delta t - \Delta_{ij})^2/(4\sigma_p^2)], && (2.13) \end{aligned}$$

which is also a Gaussian with shifted mean and increased standard deviation. This holds only approximately here because it requires statistical independence, whereas in our model pre- and postsynaptic activities are weakly correlated. However, (2.13) is

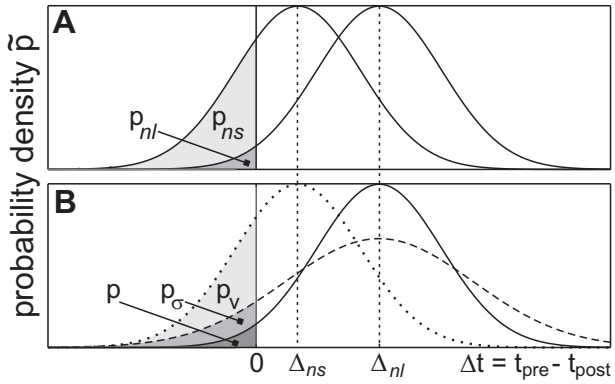

Figure 2.5: *Probability density functions $\tilde{p}$ of the relative spike timings Δt in the idealized, noiseless case.* **A.** Connections with a short delay Δ_{ns} have a high probability p_{ns} to be strengthened, while long delay connections have a low probability p_{nl}. **B.** p is increased by a broader temporal input jitter (p_σ) or a faster axonal velocity (p_v)

not used for simulations, but is introduced for a better understanding of the simulation results. Weight increase only occurs for negative Δt (Fig. 2.3). Thus, the integral

$$p_{ij} = \int_{-\infty}^{0} \tilde{p}_{ij}(\Delta t)\,\mathrm{d}\Delta t \tag{2.14}$$

gives the probability for increasing the synaptic strength between n_j and n_i. The emergence of the lateral coupling kernel can now be understood if we look at two neurons n_n and n_s with a short axonal delay Δ_{ns} in their connection (Fig. 2.5a). In this case, p_{ns} is large so that the synapse is strengthened quite often. In contrast, a distant neuron n_l has a long delay, so that p_{nl} is low (Fig. 2.5a). Since weight increasing events are seldom, the resulting strength will be small after learning has converged. Hence, the spatial coupling kernel depends both on the temporal correlation width among spikes at the (inputs and thus at the) outputs of level-1 neurons and the temporal dispersion introduced along the lateral connections.

Variation in the temporal correlation width of the external input σ_p

This variation results in a proportional change of the spatial width D of the lateral coupling profile. Broader input correlations cause broader coupling profiles (Fig. 2.6a). If we look at a broadened distribution of relative spike timings (Fig. 2.5b, dashed curve), more events comply with the timing condition set by the learning rule. Even for distant

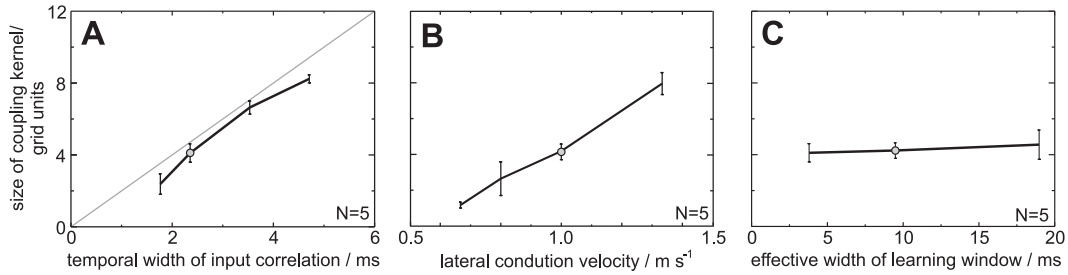

Figure 2.6: *Scenario A: The width of the synaptic weight profile of the lateral linking connections depends on the temporal width of the input correlations.* (**A**) and the lateral conduction velocity (**B**), while the decay of the learning window plays only a minor role (**C**). *Grey dots* indicate simulations with identical parameters

neurons the synaptic weights grow and therefore the spatial weight distribution becomes broader.

Variation of lateral conduction velocity

A narrow coupling width D emerges with a low lateral conduction velocity, and D increases with velocity (Fig. 2.6b). To explain this effect, let the distance between two neurons n_n and n_l be l_{nl}. As axonal transmission velocity is v_{ax}, the delay between them is $\Delta_{nl} = l_{nl}/v_{\mathrm{ax}}$. Increasing the velocity v_{ax} shifts the distribution of relative spike timings p_{nl} in (2.13) nonlinearly towards zero (Fig. 2.5b, dotted curve). Thus, the probability of negative time differences, and therefore the number of positive learning events, increases. In the idealized case of infinite conduction velocity, the resulting coupling structure would exhibit no decay at all.

To summarize, the action of increasing lateral propagation velocity and increasing temporal correlation width at the inputs both enlarge the spatial size of the coupling kernel in the lateral network.

Influence of the learning function

The convergence speed of the learning process and the maximal weights depend on the effective duration of the learning window's strengthening epoch (positive part, Fig. 2.3). If this epoch is elongated beyond the width of the relative spike timings (2.13), the contribution of random spike correlations to the synaptic weight change increases and, therefore, specific learning is slowed down. If the epoch is shortened, the number of

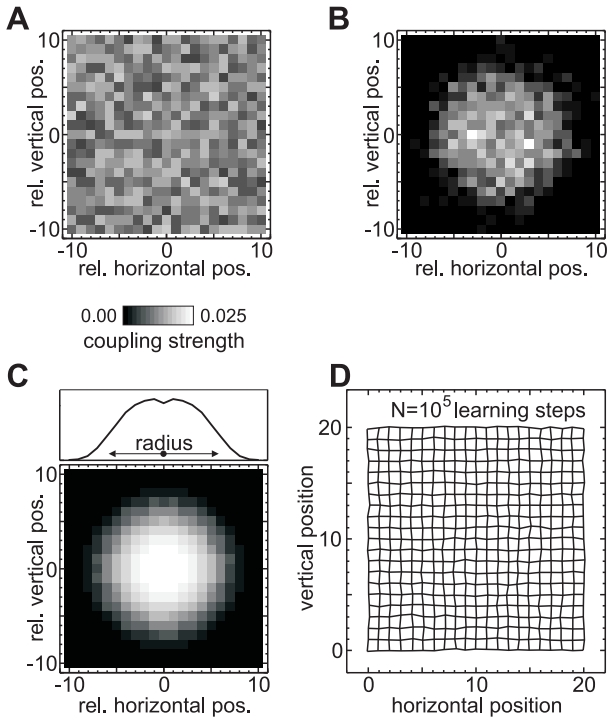

Figure 2.7: *Scenario B: Synaptic weight distribution at level-2 synapses of feedforward projections from a single level-1 neuron.* **A.** Example of randomly initialized weights before learning. **B.** Example of weight distribution after 10^5 learning steps. **C.** Average weight distribution of all level-2 neurons. The dip in the center is due to the decay of the learning window. **D.** Spatial distribution of the centers of synaptic weight profiles of level-1-to-2 connections, characterized by the line crossings. In real visual representations these positions would define the centers of cRFs. Note that the retinotopic organization evolves from complete randomness without spatially structured visual input. Only temporal structure was introduced by distance-dependent spike delays

positive learning events decreases (the signal-to-noise ratio for learning effects), so that stable and fast convergence is difficult to obtain. However, in a broad range the duration of the strengthening epoch has no effect on the size of the spatial coupling kernel (Fig. 2.6c).

2.3.2 Learning of level-1-to-2 feeding connections (scenarios B, C)

In scenario B (Fig. 2.1) the distance-dependent connections between level 1 and 2 are learned with the same input as in scenario A, while lateral connectivity among level-1 neurons is absent. After learning, the following structures emerge from the

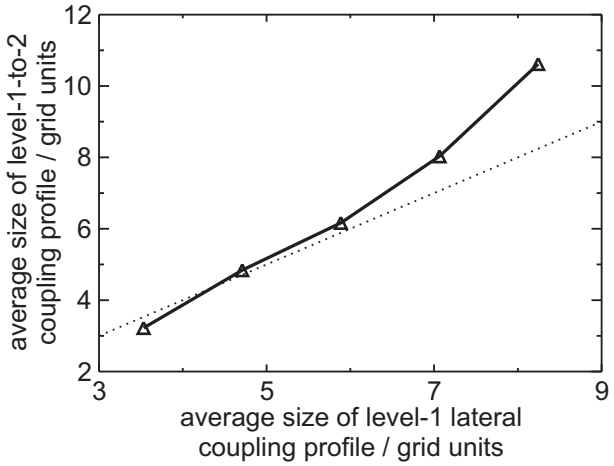

Figure 2.8: *Scenario C: Size of level-1-to-2 connection profile is correlated with lateral synaptic weight profile of level-1 neurons.* (simulations with constant level-1-to-2 delays and damped spreading wave activation at level 1, mimicking a learned version of scenario A). Similar relations are obtained with distance-dependent delays between level 1 and 2 in scenario B (not shown).

randomly chosen weights (Fig. 2.7a). The coupling strength of collaterals from the same level-1 neuron decays with distance (Fig. 2.7b,c). This effect is comparable to the development of the lateral weights at level 1 in scenario A. If neurons at level 1 generate a correlated spike packet, action potentials, transmitted with short delays, arrive first at retinotopically corresponding level-2 neurons. The evoked EPSPs lead to an increase in the membrane potential and finally, the neuron fires. Since delays are distance-dependent on an evenly spaced grid, few connections with short delays exist. The first EPSPs at a given target neuron are only small in number and are generally not sufficient to evoke a postsynaptic spike. However, additional spikes arriving from more distant neurons eventually cause the neuron to fire. The connections leading to threshold transition are strengthened most, while connections with shorter delays have already fired and therefore have a negative Δt (Fig. 2.3). Thus, the weights of proximal connections are less strengthened compared to distal ones, which is reflected in the central dip of the weight distribution (Fig. 2.7c). This dip resembles the decay in the learning function (Fig. 2.3).

After learning, the centers of the coupling kernels in the neural lattice (corresponding to cRF centers in real systems) are retinotopically well organized (Fig. 2.7d). This retinotopic sorting is due to the systematic distance-dependent delays in level-1-to-2

connections which define a temporal neighborhood detected by the Hebbian learning function. We would like to note that this retinotopic sorting does not require spatially structured input signals at level 1.

In scenario C (Fig. 2.1) identical delays in all level-1-to-2 connections are used, and learning started with a broad coupling distribution in the feedforward connections. External inputs are spatially localized blobs of spreading (wave-like) spike activity presented sequentially at random positions (2.7). After learning, the centers of the feedforward coupling kernels have maintained their initialized topography and have increased their spatial resolution by reducing their size and, thus, reducing the size of level-2 cRFs. The cRF size is monotonically related to the size of the synchronization field and the corresponding AF size at level 1 (Fig. 2.8).

2.4 Discussion

We demonstrate how lateral spike propagation velocity can influence the emergence of spatially confined synaptic weight distributions during Hebbian learning without visual experience. Essential for mimicking the developmental phase in visual cortex are also short (< 20 ms) common spike rate fluctuations at its external inputs from the thalamus. As these inputs have no spatially structured correlations in our model, the emerging weight distributions are exclusively due to the temporal dispersion of network spike delays and the temporal width of input correlations. If we relate our model structures to visual cortical areas V1 and V2, the weight distributions of the level-1-to-2 feeding connections determine the cRF size in V2, while the weight distributions of level-1 linking connections (V1) define the potential cortical range of synchronization (its projection to visual space is called the association field or AF).

Our learning function is particularly sensitive to precise spike correlations according to the steep gradient between the negative (unlearning) and the positive (learning) epoch and its asymmetric shape (Fig. 2.3). Recent experimental results support its biological plausibility (Markram et al., 1997). Fast and stable convergence is obtained when the random temporal dispersion of the external input correlations and the systematic dispersion introduced by lateral spike conduction are matched to the positive epoch of the learning function.

Other models applied learning to continuous mean firing rates (e.g., Kohonen, 1984; Phillips and Singer, 1997; Stetter et al., 1997; Wiemer et al., 2000) instead of using

discrete spike patterns. The former is appropriate if the correlated signals vary slowly. This assumption does not hold for the temporally precise input correlation in our model, which hardly influences the mean firing rate of single neurons (Kempter et al., 1999). However, models based on mean firing rates can, in principle, also transform temporal dispersion into spatially confined coupling structures by learning. Yet, this is restricted to the slow time scale of rate modulations (Wiemer et al., 2000) and does not work on a millisecond time scale as in our model.

Temporal dispersion and variability due to synaptic and dendritic delays are neglected in our model. Introducing biologically plausible values for them will broaden the size of the coupling kernels at level 1 in scenario A (Fig. 2.4) and level 2 in Scenario B (Fig. 2.7), accordingly. However, such a broadening effect is already present in our model and is reflected in its results: maintained stochastic input (GWN) to level-1 neurons introduces large variability in activation delays because the membrane potential fluctuates and the threshold can be in any state at any moment. This activation variability is large (> 10 ms, Fig. 2.2) compared to what is expected in cortical neurons from synaptic and dendritic delays (< 5 ms) under the conditions of rather constant spike rates as in our simulations (Agmon-Snir and Segev, 1993).

Lateral conduction delays in the visual cortex (related to scenarios A and B) have been measured only indirectly. If we fit the lateral profile of signal correlations (Fig. 2.4) to the cortically measured coupling profiles in V1 and V2 (Eckhorn, 1994; Frien and Eckhorn, 2000b) by changing the lateral conduction velocity and keeping the temporal jitter of correlated input spikes small ($\sigma_{in} = 2.5$ ms), the model proposes a velocity of about 0.7 m/s. This value is difficult to compare with real velocities, e.g., in the monkey visual cortex, for several reasons. First, there is a broad distribution of velocities, according to the different fiber diameters of lateral connections. Second, no direct measurements of intra- and interareal conduction delays are available from monkeys. Third, the fitted velocity from the model depends on the temporal correlation width of its input spikes.

As no direct measurements of lateral intraareal conduction velocities (scenario A) have been made in the monkey striate cortex, they have to be estimated by indirect methods, yielding 0.1 to 0.5 m/s for the dominating velocity in V1 in different preparations (review in Nowak and Bullier, 1997).

Interareal delays (scenario B) are also relevant for our present work. We concentrate here on V1-V2 delays. They have been measured in monkey revealing delays of a few

milliseconds, mostly due to synaptic delay and integration times (Nowak and Bullier, 1997). Their shortness is probably related to the myelination between retinotopically corresponding positions of V1 and V2. However, each V1-V2 axon sends collaterals to V2 targets that are generally not myelinated, so that they conduct as slowly as other lateral intraareal connections (on average at 0.3 m/s).

Summarizing, we have to realize that the measured average velocities are too slow by a factor of about two for directly explaining the above mentioned fit to the lateral coupling kernels in V1 and V2. We have to note, however, that the experimental data were collected from visually experienced animals. Therefore, a variety of arguments can explain the differences. (1) The effective fibers determining AF and cRF sizes are indeed as slow as 0.3 m/s. Then we have to assume that the correlation width (jitter) of the input spike trains is broader by a factor of about two, because larger temporal jitter also causes wider coupling profiles (Fig. 2.6a). (2) There are few fast conducting fibers determining AF and cRF size while the slower conducting axons play no role in determining size. (3) Visual experience, in particular the spatial correlation of visual object features, reshapes the widths of AFs and cRFs on the basis of stimulus-locked synchronization of the input over the range of average object sizes. (4) Other static and dynamic network properties dominate the emergence of spatial structures of visual function, including dynamics at synapses and dendrites and their potential adaptability (e.g., Markram and Tsodyks, 1996). These possibilities are not mutually exclusive and the presently available data are not sufficient for giving realistic weights to any of them.

Neuron parameters			
τ_{f1}	0.2789 ms	τ_{f2}	9.0 ms
τ_{l1}	0.3866 ms	τ_{l2}	4.0 ms
θ_0	0.3	v_{ax}	1.0 grid/ms
$V_{\theta r}$	5.0	$\tau_{\theta r}$	5.0 ms
$V_{\theta s}$	1.0	$\tau_{\theta s}$	80.0 ms
m_{GWN}	1.0	σ_{GWN}	0.3
Learning level-1 connections (Scenario A)			
p_p	0.25	f_p	10.0 Hz
σ_p	2.5 ms	w_c	0.005
τ_{p1}	0.3866 ms	τ_{p2}	4.0 ms
α	0.15	γ	0.005
Learning level-1 to level-2 connections (Scenarios B, C)			
A_{12}	0.03	σ_{12}	6.0 grid units
f_b	10.0 Hz	v_b	1.0 grid/ms
τ_{p1}	0.2789 ms	τ_{p2}	9.0 ms
α	0.25	γ	0.005

Table 2.1: Network parameters

3 Finite Transmission Delays

Finite Transmission Delays Affect Emergence and Spatial Range of γ-Coherence in a Model of the Primary Visual Cortex

The emergence of coherent γ-oscillations (30–90 Hz) has been investigated in numerous neural network models. Most models do not incorporate realistic neural transmission delays, although physiological studies confirmed that the majority of axonal conduction in the cortex is slow and should have a significant impact on the synchronization of neural populations. We investigated the influence of distance-dependent delays on γ-synchronization, using a strongly reduced model of a visual area with spiking excitatory and inhibitory neurons that are topographically organized. Delays in the local inhibitory feedback loop have a direct impact on the frequency of γ-oscillations, but do not affect the spatial extent of γ-coherence. On the other hand, fast long-range horizontal connections can enhance γ-coherence even between distant sites. γ-coherence is maximal for zero transmission delays and attenuates with decreasing lateral conduction velocities. Below a velocity of 0.5 m/s, γ-power and γ-coherence were even smaller than without these connections at all, i.e., slow horizontal connections actively desynchronized neural populations. In conclusion, the enhancement of γ-coherence by horizontal excitatory connections critically depends on fast conduction velocities.

3.1 Introduction

3.1.1 Coherent γ-activity in the visual cortex

Local populations of neurons in visual cortical areas often show increased power in the γ-range (30–90 Hz) when they are visually activated with a static optimally oriented grating or a slowly moving bar (Eckhorn et al., 1988; Gray et al., 1989; Engel et al., 1991a; Kreiter and Singer, 1996; Frien and Eckhorn, 2000a; reviews: Singer, 1999; Eckhorn et al., 2004a). γ-activities that are simultaneously recorded from two different cortical populations reveal a considerable amount of coherence, if the contributing neurons are involved in co-processing of the same object (Gail et al., 2000; reviews: Eckhorn, 1999; Gray, 1999). In a common experimental paradigm the responses of two groups of neurons are measured while using either a pair of spatially separate optimally oriented stimuli or a single stimulus with an orientation intermediate between the preferred orientations of both groups. Several studies found that the cross-correlations between both groups are stronger for the single stimulus condition than for the pair of stimuli, e.g., in cat (A17: Gray et al., 1989; Engel et al., 1991a; Engel et al., 1991b; Brosch et al., 1997; A18: Brosch et al., 1997, Castelo-Branco et al., 2000) and alert monkey (V1: Livingstone, 1996; MT: Kreiter and Singer, 1996; Palanca and DeAngelis, 2005). Although increased γ-correlations have been found between areas and even between hemispheres (Eckhorn et al., 1988; Engel et al., 1991a; König et al., 1995), the recorded neurons seem to require either overlapping receptive fields (Engel et al., 1991a,b; Kreiter and Singer, 1996; Castelo-Branco et al., 2000) or non-overlapping receptive fields with similar preferred orientations (cat: Gray et al., 1989; Brosch et al., 1997). Comparable studies using both, non-overlapping and non-iso-oriented classical receptive field (cRF) arrangements, did not find significant differences in γ-correlation for the two stimulation paradigms (cat: Golledge et al., 2003; monkey, V1: Roelfsema et al., 2004; monkey, MT: Palanca and DeAngelis, 2005).

3.1.2 Neural basis for mediating long-range γ-correlations

There are probably three potential sources for correlated γ-activity in the primary visual cortex (V1): common input from the lateral geniculate nucleus (LGN), common input

via feedback connections from higher cortical areas and active synchronization mediated by the intra-areal 'lateral' connectivity.

Neurons that are separated by more than 2 mm have non-overlapping cRFs (cat: Reid and Alonso, 1995; Ferster et al., 1996; monkey: Hubel and Wiesel, 1974), implicating that they share no *common input* from the same thalamic circuits. Since γ-correlations in the primary visual cortex are found between groups of neurons separated by a cortical distance of more than 3 mm (e.g., Eckhorn et al., 1988; Gray et al., 1989; Engel et al., 1991a; Kreiter and Singer, 1996; Frien and Eckhorn, 2000b), they can not entirely be due to common input originating from visual thalamic input.

Feedback connections from V2 or MT have large projection areas (Angelucci et al., 2002) and can considerably modulate the responses of V1 neurons as shown by inactivation of higher areas (cat: Mignard and Malpeli, 1991; monkey: Hupé et al., 1998; Hupé et al., 2001b). While the contribution of feedback connections to response properties in V1 is unquestionable, it is a matter of dispute, if they preferably connect to neurons with similar orientation preferences (orientation specific feedback: Angelucci et al., 2002; Angelucci and Bullier, 2003; orientation unspecific feedback: Stettler et al., 2002; all data from monkey but different labeling techniques). It is therefore unclear, if feedback connections can mediate orientation specific correlations between neurons in V1.

The third potential source for γ-correlations are intra-areal *horizontal connections* that primarily emanate from pyramidal cells, extend up to a few millimeters (e.g., 3.5 mm in Stettler et al., 2002) parallel to the cortical surface (Rockland and Lund, 1982; Gilbert and Wiesel, 1983; Martin and Whitteridge, 1984) and terminate in two distinct areas with probably distinct functions: for distances below approx. 0.5 mm, connections are diffuse and unspecific, wiring neurons with a wide range of orientation preferences (Malach et al., 1993; Roerig and Chen, 2002) and axial alignments of their cRFs (Bosking et al., 1997). Outside a radius of approx. 0.5 mm, the projection topography is patchy, preferably connecting distinct cell clusters that share similar orientation preferences (cat, monkey: Gilbert and Wiesel, 1989; Ts'o et al., 1986; Kisvàrday et al., 1997; Schmidt et al., 1997; Stettler et al., 2002) and are placed along an axis in visual space (cat, tree shrew: Nelson and Frost, 1985; Bosking et al., 1997; Chisum et al., 2003). These long-range connections make 80% of their synapses onto excitatory neurons (Kisvàrday et al., 1986; McGuire et al., 1991). Activating the horizontal network at a distant patch results in monosynaptic and polysynaptic excitatory postsynaptic potentials followed by disynaptic inhibitory postsynaptic potentials (Hirsch and Gilbert, 1991; Weliky et al.,

1995; Tucker and Katz, 2003). The summation of postsynaptic potentials (PSP) on the basal dendrites is non-linear under certain conditions: PSPs arriving simultaneously from the apical dendrite and the horizontal circuitry are summed supralinearly when the postsynaptic membrane was depolarized to a certain level (Yoshimura et al., 2000). The summation of nearby input on the same dendritic branch is supralinear when PSPs arrive within an interval of 40 ms (Margulis and Tang, 1998; Polsky et al., 2004).

The different anatomical connections are likely to account for coherence on different spatial scales. First, correlated γ-activity of neurons with overlapping cRFs would originate from LGN common input in combination with dense direct connections that have been found between neurons with overlapping cRFs (Gilbert and Wiesel, 1979; Rockland and Lund, 1982; Gilbert and Wiesel, 1983; Kisvàrday et al., 1993, 1997). Second, the properties of horizontal connections are compatible with γ-correlations found in the primary visual cortex when assuming that correlations require monosynaptic connections between cells of both populations. γ-correlations between neurons with iso-oriented cRFs may be mediated by the widespread network of long-range horizontal connections in layer 2/3 (Gilbert and Wiesel, 1983, 1989), which preferentially connect neurons with similar orientation preference (tree shrew: Bosking et al., 1997; Chisum et al., 2003; cat: Ts'o et al., 1986; monkey: Angelucci et al., 2002). In the tree shrew, correlations and anatomic connections are strongest for iso-oriented neurons with collinearly aligned cRFs (Bosking et al., 1997; Chisum et al., 2003).

In conclusion, the spatial range, the specific wiring scheme and the facilitatory action of horizontal connections strongly suggests, that they play an important role in mediating correlations between neurons with non-overlapping cRFs.

3.1.3 Transmission delays of horizontal connections within area V1

Temporal properties of neural responses including the emergence of γ-correlations are crucially affected by delayed transmission of action potentials from one neuron to another. While there are numerous velocity measurements between cortical areas, little is known about conduction velocities within a cortical area (review: Nowak and Bullier, 1997). Indirect measurements from cat and rat primary visual cortex reveal a broad distribution of conduction velocities. The speed of action potential propagation along horizontal excitatory connections is in the order of a few tenth of m/s (Komatsu et al., 1988: 0.3 m/s; Murakoshi et al., 1993: 0.15–0.55 m/s; Hirsch and Gilbert, 1991:

0.3–0.6 m/s; Nowak and Bullier, 1998: 0.4 m/s). Inhibitory connections seem to be slightly slower (Salin and Prince, 1996: 0.06–0.2 m/s, mean: 0.1 m/s). These measured velocities of intra-areal signal transmission are consistent with the spread of synaptic activity in the primary visual cortex revealed by optical imaging (Grinvald et al., 1994: 0.1–0.25 m/s, monkey; Tucker and Katz, 2003: 0.25 ± 0.2 m/s, ferret). Slow conducting axons may also be the source of slow activity waves in cat V1, triggered by visual stimulation in peripheral parts of the receptive field (Bringuier et al., 1999, mean: 0.1 m/s).

3.1.4 Correlated γ-activities and transmission delays

The slow transmission of action potentials within area V1 raises several questions concerning the temporal aspects of intra-areal information processing. Correlated γ-activity has been found between groups of neurons that are separated by a cortical distance of 3–6 mm (e.g., Eckhorn et al., 1988; Gray et al., 1989; Engel et al., 1991a; Kreiter and Singer, 1996; Frien and Eckhorn, 2000b). These γ-correlations occur at zero time-lag in the majority of cases; the same holds for non-oscillatory signals (cat: Michalski et al., 1983; monkey: Krüger and Aiple, 1988). Monosynaptic interactions spanning these distances therefore take 5–30 ms, when assuming an axonal velocity of 0.1–0.6 m/s. This is long compared to the cycle length (11–33 ms) of γ-range oscillations (30–90 Hz). Delays in signal transmission are therefore likely to have a substantial influence on γ-correlations and the underlying γ-activities.

3.1.5 Goal of the model

In this paper, we show how delays influence the emergence of correlated γ-activity in a structured network of spiking neurons. Each synaptic connection exhibits a delay that is proportional to the distance of the respective neurons, i.e., constant axonal velocity. Velocities were independently varied for two subcircuits: the local inhibitory feedback loop and the long-range excitatory horizontal connections. We derived realistic signals and used a signal analysis that alleviates a direct comparison with experimental data. We asked if the slow transmission velocities are compatible with the spatial and temporal aspects of observed γ-correlations and if other interactions like fast feedback from higher areas have to be taken into account (Hupé et al., 2001a; Angelucci et al., 2002).

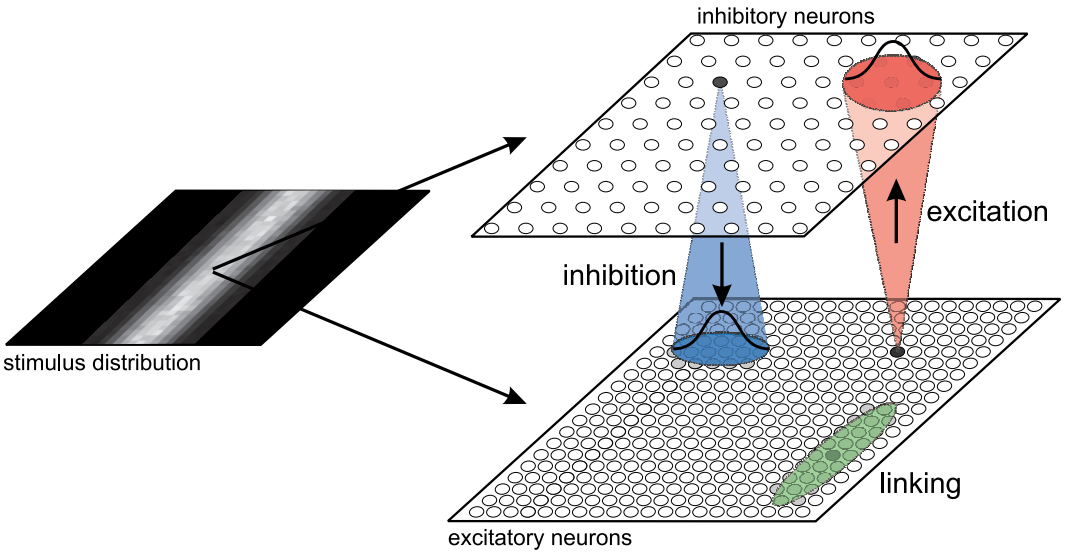

Figure 3.1: *Sketch of the network connectivity.* The network consists of two topographically organized subpopulations. Locally corresponding excitatory and inhibitory neurons are reciprocally connected, forming local feedback loops. Adjacent excitatory neurons were additionally connected via mutual linking synapses in the vertical neighborhood. The connection schemes are exemplary shown for one neuron per connection type. All synaptic efficacies decay like a Gaussian with increasing distance. The spatial separation of both populations is for visualization purposes only. They are supposed to be in the same functional layer. The stimulus amplitudes are directly applied to excitatory and inhibitory neurons at the corresponding positions.

3.2 Methods

3.2.1 Network

The network (Fig. 3.1) contained 961 excitatory and 225 inhibitory model neurons (Section 2.2.1). Both cell types were regularly placed on a two-dimensional Cartesian grid that was supposed to span $4 \cdot 15\,\mathrm{mm}^2$ in the primary visual cortex (V1). The minimal distance between two adjacent excitatory (inhibitory) neurons was accordingly set to 0.25 mm (0.5 mm). Each excitatory neuron projected topologically to a group of inhibitory neurons (E→I), and each inhibitory neuron projected back to a group of excitatory neurons (I→E). Therefore both cell types form local recurrent inhibitory loops (E↔I). The axonal field of laterally projecting large basket (inhibitory) cells in cat covers a maximal diameter from 1.6 mm (Martin et al., 1983) up to 3 mm (Kisvarday

and Eysel, 1993). The synaptic connection strengths (I→E) of a single inhibitory cell were set to decay Gaussian with increasing distance $\hat{\sigma}$=1.0 mm, where $\hat{\sigma}$ denotes the full-width at half-height (FWHH). Using these settings, the maximal projection diameter of approx. 2 mm is in accordance with the previously cited experimental data. The same connection profile was used for the excitatory (E→I) neurons, because connections between neurons are often reciprocal (Braitenberg and Schüz, 1991). In some simulations, excitatory neurons were mutually connected (E↔E) via modulatory linking synapses using a vertically elongated Gaussian coupling kernel ($\hat{\sigma}_x = 0.5$ mm, $\hat{\sigma}_y = 3.0$ mm). They are supposed to imitate long-range horizontal connections that were found between pyramidal cells with similar orientation preference in the superficial layers of the primary visual cortex (Gilbert and Wiesel, 1979). Initial synaptic strengths were jittered by ±0.05 of their assigned value (temporally constant). Open boundary conditions were

A. Neuron parameters				**C.** Input parameters	
τ_{f1}	0.2789 ms	τ_{f2}	9.0 ms	$w_{S\to E}$	0.2
τ_{l1}	0.2789 ms	τ_{l2}	5.0 ms	$w_{S\to I}$	0.075
τ_{i1}	0.45 ms	τ_{i2}	3.0 ms	σ_{U_E}	0.4
θ_0	1.0			σ_{U_I}	0.1
$V_{\theta r}$	1.0	$\tau_{\theta r}$	5.0 ms	σ_I	0.5
$V_{\theta s}$	0.5 (0.2)	$\tau_{\theta s}$	80.0 ms		
B. Connections					
$w_{E\to I}$	0.15	$\hat{\sigma}_{EI}$	1.0 mm		
$w_{I\to E}$	0.35	$\hat{\sigma}_{IE}$	1.0 mm		
$w_{E\to E}$	0.02	$\hat{\sigma}_{EE}$	3.0, 0.5 mm		
$v_{E\to I}$	0.25 m/s	$v_{I\to E}$	0.125 m/s		
$v_{E\to E}$	1.0 m/s				

Table 3.1: *Network parameters.* **A.** Parameters for excitatory and inhibitory neurons are identical except for the lower spike rate adaptation $V_{\theta s}$ of inhibitory neurons. **B.** w denotes the connection strength for neurons at corresponding positions, $\hat{\sigma}$ the full-width at half-height (FWHH) of the Gaussian weight distribution. **C.** Parameters denote input strength and noise. See text for details.

used, to prevent artifacts due to cycling activity. By restricting all quantitative analyses to the central area of the network, we found that boundary effects can be ignored.

All connections exhibited a constant signal transmission velocity. This simplifying assumption is motivated by the observation that the latency of a depolarization is linearly related to the eccentricity of the receptive field center relative to the position of the stimulation (cat, V1, intracellular recordings: Bringuier et al., 1999). The axonal velocity was set to 0.25 m/s for E→I, 0.125 m/s for I→E and 1 m/s for E→E connections, increased by a uniformly distributed random delay of up to 2 ms. Parameters are summarized in Tab. 3.1.

3.2.2 External stimulation

For simplicity, the visual periphery such as the retina and the LGN were excluded from the model. We applied amplitude-continuous input directly to each of the modeled neurons, disregarding all cRF properties (e.g. orientation, color, motion) except cRF position.

During the entire simulation period, independent Gaussian white noise (GWN) $\xi(t)$ was directly added to the membrane potential $U(t)$ of all excitatory (amplitude: σ_{U_E}) and inhibitory neurons (σ_{U_I}). This approach neglects input correlations that are due to overlapping receptive fields (Reid and Alonso, 1995; Ferster et al., 1996) or feedback from higher visual cortical areas (review: Salin and Bullier, 1995). Although these processes are likely to be of importance for processing in V1, their exclusion was necessary to separate internal correlations generated by the modeled network from external correlations. Since external correlations always enlarge the coupling profiles, uncorrelated input gives a lower bound for strength and extent of coupling profiles.

A simulation run started with a pre-stimulus period lasting 512 ms, during which only the noise input was present. After that, the stimulus was linearly faded in, taking 20 ms to reach its maximum amplitude. The stimulus S used here was either a continuous or a disrupted bar (Fig. 3.2A), which should mimic the single- and the two-stimulus condition of the experiments described in the introduction:

$$S_X(x,y) = w_{S\to X} \cdot \cos((x-\bar{x})/\sigma_x) \cdot (1 - D \cdot \exp(-(y-\bar{y})^2/(2\sigma_y^2))) \quad , \tag{3.1}$$

where X may be E for the excitatory and I for the inhibitory sublayer, $\bar{x} = 7$, $\sigma_x = 14/\pi$, $\bar{y} = 30$, $\sigma_y = 1/\sqrt{2\ln 2}$, $D = 0$ for continuous and $D = 0.75$ for a disrupted bar. All

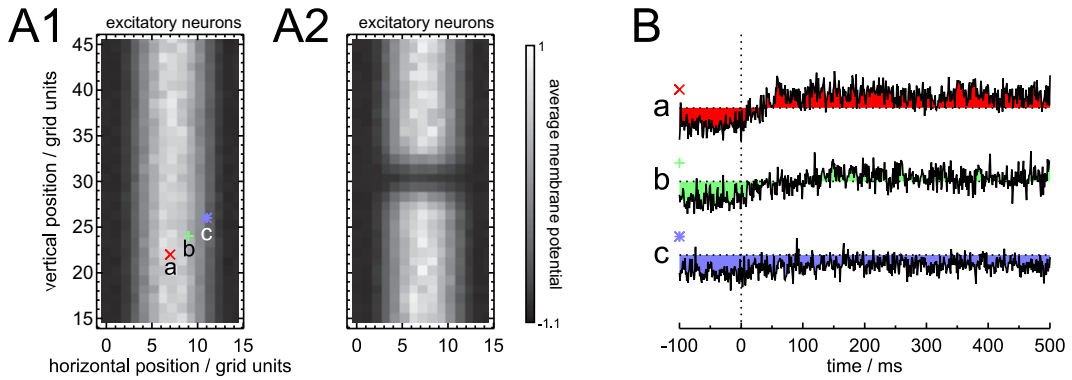

Figure 3.2: *Network input.* **A1.** Spatial distribution of temporally averaged membrane potentials for a stimulation period of 1024 ms (vertically cropped). **A2.** Averaged membrane potentials for an alternative stimulus used for investigating decoupling effects. **B.** Single membrane potentials for a maximally (a), a medium (b) and a weakly (c) activated neuron. Stimulus is switched on at $t = 0$. The neurons' resting thresholds θ_0 are denoted by dotted horizontal lines.

neurons received independent GWN input with each mean and standard deviation modulated according to the spatial structure of a stimulus S.

$$I(x, y, t) = S_X(x, y)(1 + 0.05\,\zeta(x, y, t)) \quad , \tag{3.2}$$

where ζ is a normally distributed random variable with zero mean and a standard deviation of 1. The strength of the input noise therefore increased with the mean input to the neuron. $I(x, y, t)$ was applied to the feeding inputs of the model neurons and therefore low pass filtered. The spatial distribution of the mean membrane potentials and a sample of time-resolved membrane potentials are shown in Fig. 3.2. For a convenient comparison with electro-physiological results, the stimulus may be interpreted as a vertical bar composed of a vertically oriented sinusoidal grating (Fig. 4.1B1).

3.2.3 Signals

The stationary phase used for all spectral and coherence analyses started 200 ms after the stimulus onset. Despite directly available membrane potentials $U_i(t)$ and single unit activity $O_i(t)$, we extracted two mesoscopic measures from these data: multiple unit activity (MUA) is a measure for the collective spiking activity of a small local neural group in real experiments ($\approx$0.05 mm half-height decline; tetrodes, cat: Gray et al., 1995; theoretical: Rall, 1962). The local field potential (LFP) in real recordings is a local

superposition of somato-dendritic potentials, so it gives some indication of average local activity (≈ 0.5 mm half-height decline; Mitzdorf, 1985). Both measures are generated from the model by weighting raw signals with a spatial exponential distribution. For LFP, the full-width at half-height was set to 0.5 mm in accordance with experimental data. The low spatial density of neurons in the model enforces a diameter of 0.12 mm for MUA (compared to the proposed value of 0.05 mm), to ensure that the signal captures a local population of neurons. The result of the spatial convolution for LFP was band-pass filtered (5–140 Hz) similar to experiments (Gail et al., 2000: 1–120 Hz). Power spectra were obtained using a sliding Hamming window (duration: 256 ms, shift: 64 ms, sampling interval: 1 ms). We used coherence to quantify coupling strengths between pairs of signals. It was calculated across the number of trials with identical stimulation (Bartlett-smoothing, N=50 for all results) and corrected after Benignus for small N (Glaser and Ruchkin, 1976). Coherence, as used here, is sensitive to phase and amplitude covariations. All normalized values were averaged using the Fisher Z-transformation. Normalized coherence as used in Section 3.3.5 is defined as:

$$C_N = \frac{C_{\text{dis}} - C_{\text{pre}}}{C_{\text{cont}} - C_{\text{pre}}} \quad , \tag{3.3}$$

where C_{pre} is the γ-coherence without, C_{cont} with a continuous and C_{dis} with a discontinuous stimulus.

3.3 Results

3.3.1 Stimulus-induced γ-activity

To get an impression of the network dynamics, we first looked at the single unit activity of the excitatory cells (Fig. 3.3) in response to a vertical bar stimulus (Fig. 3.2A1). Without stimulation all neurons were spontaneously active with an average rate of 3.4 impulses/s. Shortly after stimulus onset, the stimulated neurons fired with an increased rate, which can be seen by an increased dot density in the spike raster (Fig. 3.3A) and, more clearly, in the temporally averaged individual firing rates (Fig. 3.3B). The summed activity across all neurons (Fig. 3.3C) showed damped oscillations for 128 ms that were phase-locked to the stimulus onset.

Similar temporal properties can be found in the time-courses of MUA and LFP at strongly activated network positions (Fig. 3.4). Both show γ-oscillations in single trials.

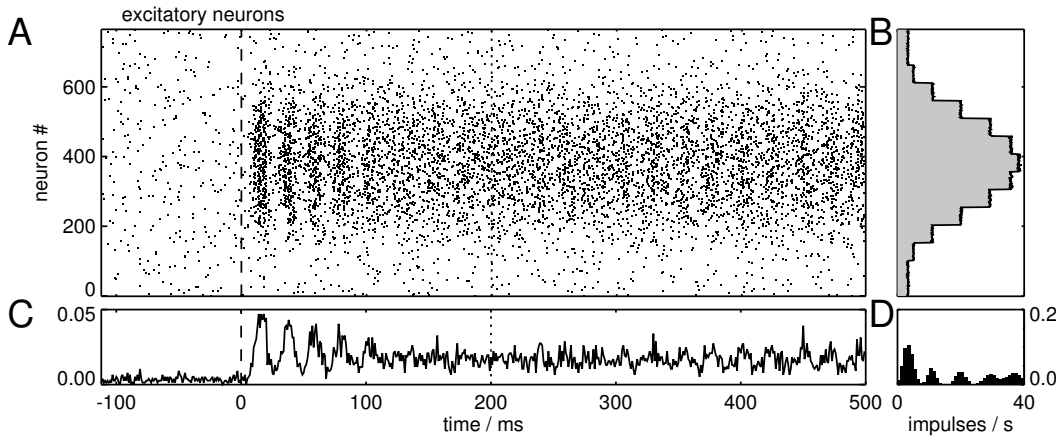

Figure 3.3: *Single unit spike activity of excitatory neurons.* **A.** Single trial spike activity of excitatory neurons for a bar-like stimulus. All neurons of the two-dimensional excitatory sub-population are displayed on the vertical axis. Each dot denotes the occurrence of an action potential. **B.** Distribution of temporally averaged single neuron firing rates for the tonic phase ($t > 200$ ms). The step-like structure of the graph reflects the input with 15 columns, each containing neurons with a similar average firing rate (Fig. 3.2). **C.** Spike density across all neurons shown in A, divided by the total number of neurons. **D.** Histogram of mean firing rates shown in B (N=50).

These are locked to the stimulus-onset for 150 ms and occur randomly at later times: phase-locked components can be seen in the peri-stimulus time histogram (PSTH), while events occurring at arbitrary times cancel out (Fig. 3.4). The fine-structure of the phase-locked component looks different in monkey MUA and LFP but the duration is comparable (Frien and Eckhorn, 2000a, their Fig. 2).

During stimulus presentation, membrane potentials in strongly activated regions of the network exhibited oscillations in the γ-range (here: 40 Hz). The time-resolved power-spectrum for a single membrane potential exhibits a large temporal variability for a single trial (Fig. 3.5A). Averaging across trials (N=50) discloses a prominent γ-peak (Fig. 3.5B), that is absent without stimulation (Fig. 3.5C).

3.3.2 Dependency of peak γ-frequency on the feedback loop

The following section will clarify, how the observed γ-activity depends on the E↔I connection parameters. The synaptic strengths of the E→I and the I→E connections are simultaneously scaled by adjusting $w_{E\to I}$ and $w_{I\to E}$ accordingly. Changing each parameter in isolation does not qualitatively change the following results.

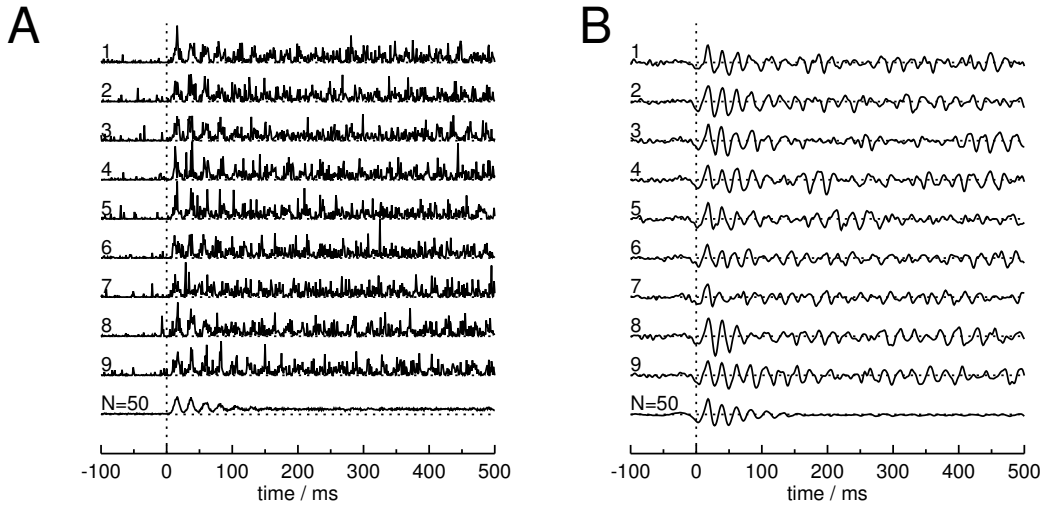

Figure 3.4: *Multi unit (A) and local field potential (B) traces.* The upper traces show 9 single responses to identical stimulus repetitions recorded at the same position. Lower most traces show the peri-stimulus time histogram (PSTH) of 50 traces as shown above at the same amplitude scale. The dotted vertical line indicates stimulus onset. Note the occurrence of fast oscillations during stimulation in the single traces. Only the first oscillations are locked to the stimulus onset and survive averaging in the PSTH. The valleys in B shortly before stimulus onset and after the stimulus transient are due to the filtering kernel (5–140 Hz).

Increasing connection strengths reduce the spike rates for excitatory neurons (Fig. 3.6A). This is due to the following mechanism: strengthened E→I connections increase the excitatory input to inhibitory neurons, resulting in increased spike rates of these inhibitory neurons. This increases the inhibitory input to excitatory neurons, which is in addition amplified by stronger I→E connections. The increased inhibition results in reduced firing rates of the excitatory neurons. These changes in the network dynamics do not have an impact on the peak γ-frequency in LFP signals (Fig. 3.6B), which remains constant in the investigated parameter range. The power of this frequency, however, is not constant, but increases drastically with increasing E↔I connection strengths (Fig. 3.6C). This is due to the increasing inhibition that acts synchronizing on membrane potentials (models: Mirollo and Strogatz, 1990; Ernst et al., 1995; Nischwitz and Glünder, 1995).

The oscillation frequency of LFPs is independent of the E↔I connection strength, but it depends on the transmission velocities of these connections. Fig. 3.6D shows,

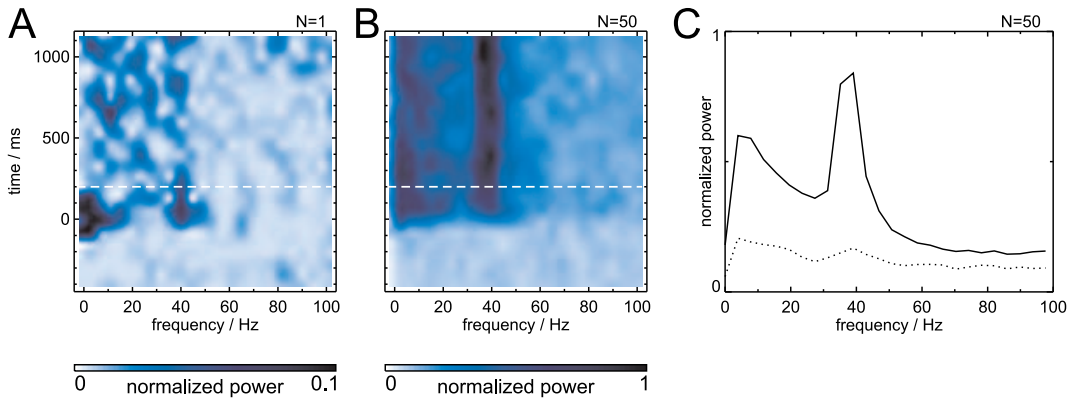

Figure 3.5: *Gamma-activity in membrane potential.* **A.** Time-resolved power spectrum of a single membrane potential in the center of the layer for a single trial (window length: 256 ms). The stimulus onset ($t = 0$) induced large contributions in the low-frequency as well as in the γ-range (here: 30–50 Hz). For $t > 200$ ms, the power is mainly present below 50 Hz without temporally stable peaks. **B.** Time-resolved power spectrum (N=50) for a single membrane potential shows a strong γ-peak (38 Hz) beginning with the stimulation. The stimulus-locked contributions have been removed by subtracting the power-spectrum of the PSTH. **C.** Time-averaged power-spectrum (N=50) for the pre-stimulus period ($t < 0$, *dotted line*) and the stimulus period ($t > 200$ ms, *solid line*). Despite the prominent γ-peak, the power in all frequencies bands is enhanced, dropping with increasing frequency.

that the oscillation frequency with instantaneous E↔I connections is about 60 Hz. This is faster than the highest average firing rate of a neuron in the whole network (all cells on average below 50 impulses/s) and illustrates that the observed γ-oscillations are a population phenomenon. With decreasing velocity of all E↔I connections, the oscillation frequency gets smaller (Fig. 3.6D), while the firing rates of the contributing neurons remained about the same (not shown). The shift in the oscillation frequency can be fully explained by the increasing mean delay of the feedback loop.

3.3.3 Dependency of γ-activity on horizontal connections

The previous results are obtained with mutual connections between excitatory and inhibitory neurons alone. Here, we introduce additional linking connections with a velocity of 1 m/s between vertically aligned excitatory neurons as shown in Fig. 3.1 (look for linking). Increasing the coupling strength of these modulatory E↔E connections among excitatory neurons generally increases the mean firing rates (Fig. 3.7A), while the peak frequency of corresponding LFPs decreases (Fig. 3.7B). A similar relationship

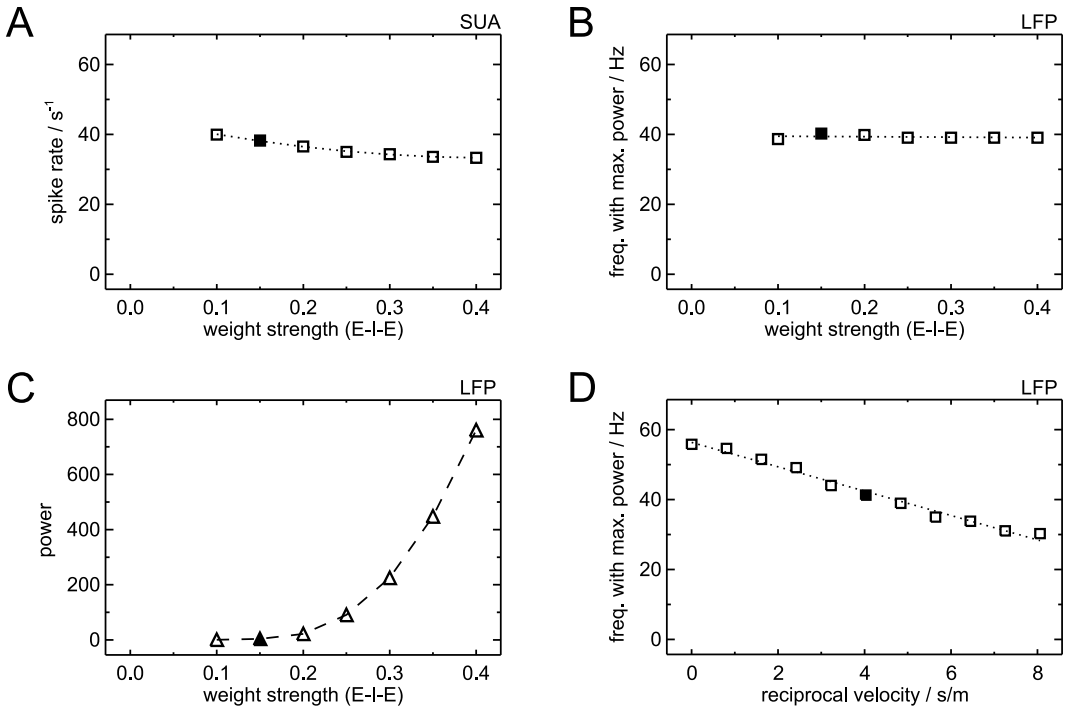

Figure 3.6: *Simulations using different E→I and I→E connection properties.* **A.** Abscissa denotes the connection strength for the E→I connections at corresponding network positions. All other E→I as well as all I→E connections are scaled proportionally. Spike rate of an excitatory neuron placed at the network center decreases with increasing E↔I connection strengths. **B.** The frequency of the maximal spectral LFP power remains constant, while the power at this frequency (**C**) increases drastically with E↔I connection strengths. **D.** In this series of simulations, the connection strengths remained constant, while the transmission delays of the E↔I connections are scaled proportionally. Oscillation frequency scales linearly with the reciprocal velocities of the E→I and the I→E connections. Filled symbols indicate the standard value for this parameter.

has been found by Juergens and Eckhorn (1997) in a homogeneous model with purely excitatory neurons. Engaged linking synapses provide an additional excitatory drive to stimulated excitatory neurons. The firing times of neighboring neurons are already correlated due to their common inhibition. Hence, linking input from spiking neurons reaches their neighbors shortly after or before they have or would have fired themselves, due to external input and their internal dynamics. Activated excitatory neurons in the network therefore tend to burst. For strong E↔E connections, the burst frequency is mainly determined by the time constant of the slow threshold component (τ_{θ_s} =

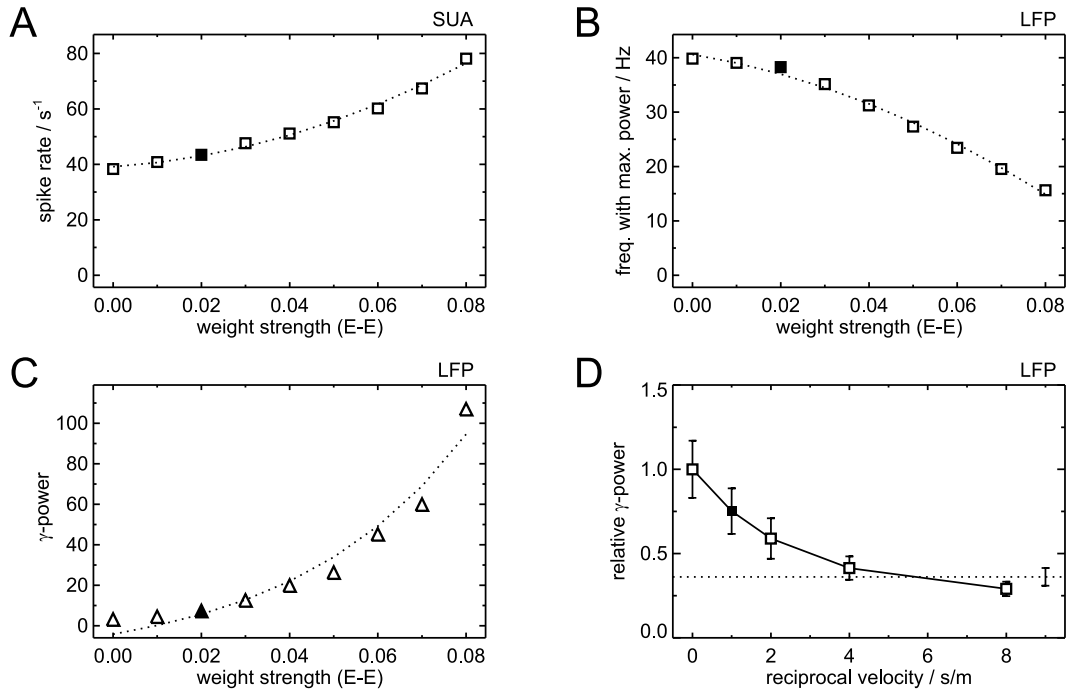

Figure 3.7: *Simulations using differently scaled E↔E connections.* **A.** Spike rate of an excitatory neuron placed at the network center increases with increasing E↔E connection strengths. **B.** The dominating frequency in the LFP at the same position as in A is reduced by the increasing recurrent excitation, due to the occurrence of bursts. **C.** The power of the dominating frequency increases drastically with the E↔E weights. **D.** Relative γ-power decreases with decreasing transmission velocity of the E↔E connections. Dotted line indicates γ-power with disabled E↔E connections. Filled symbols indicate the standard values for the parameters.

80 ms). The power of the peak frequency increases strongly due to the facilitating and synchronizing effect of the mutual E↔E connections (Fig. 3.7C).

The transmission velocity of the E↔E connections has a strong impact on the γ-power of LFP signals (Fig. 3.7D). For instantaneous interactions (i.e., infinite velocity), the relative γ-power is set to 1. Power decreases considerably with decreasing velocity of E↔E connections. For E↔E with a velocity of 0.25 m/s, the power is slightly above 0.36, which is the value obtained with completely disabled E↔E connections. For a velocity of 0.125 m/s, γ-power is even below this value.

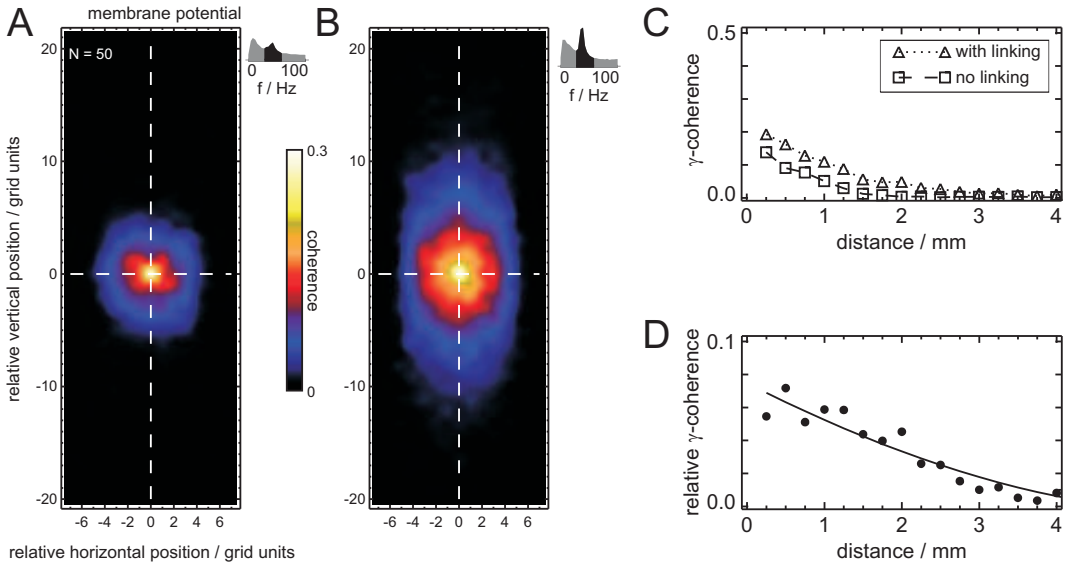

Figure 3.8: *Spatial distribution of γ-coherence of membrane potentials.* Color palette indicates temporally averaged γ-coherence (N=50, 25–60 Hz) with the reference neuron. The *white dashed crosses* mark the position of the reference neuron. *Right insets* show the power spectrum of the reference neuron and are equally scaled. **A.** With disabled E↔E linking connections, γ-coherence monotonically decays with distance. The shape of the profile is approximately circular. **B.** With engaged linking connections, the γ-coherence profile extends elliptically in the direction of the E↔E connections. **C, D.** γ-coherence of neurons placed along the vertical dashed line is compared for A and B. Engaged E↔E connections enhance γ-coherence preferably for short distances.

3.3.4 Horizontal linking connections enhance γ-coherence

In this section we investigate, how recurrent E↔E connections can change γ-coherence of different signal types in the network.

Input signals fed to neurons in the network are completely uncorrelated (not shown). Recurrent inhibition provided by E↔I connections, induces linear correlations between neighboring neurons. These can be seen, e.g., in the γ-coherence of membrane potentials (Fig. 3.8A). The stimulus evokes a radial symmetric coupling profile that decays with the distance of the observed neuron pair. Membrane potentials separated by 0.25 mm show an average γ-coherence of 0.14; for 0.75 mm, the value is only 0.07 (Fig. 3.8C). The strength and spatial extent of γ-coherence does not depend on the peak frequency. Adding E↔E connections (Fig. 3.8B), clearly enhanced the coherence for all distances in the direction of the asymmetric coupling kernel. This can be seen in Fig. 3.8D, where

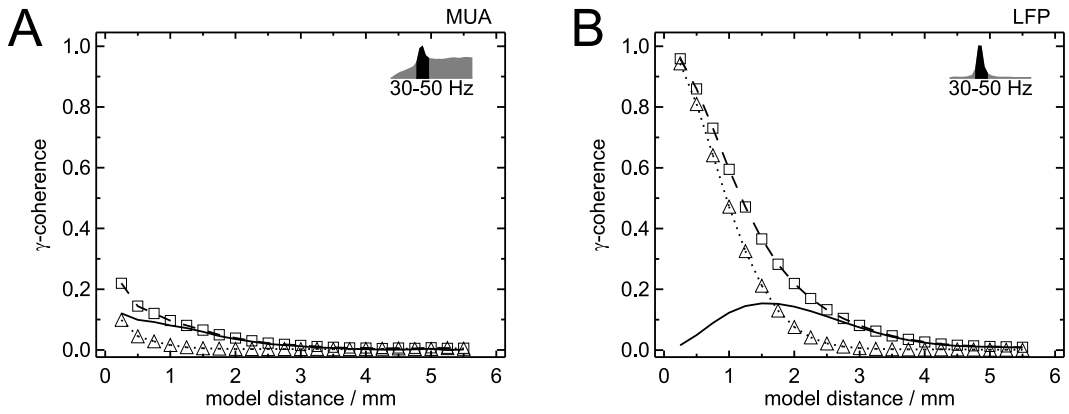

Figure 3.9: *Spatial coherence of MUA and LFP (30-50 Hz).* **A.** Gamma-coherence of MUA monotonically decays with distance. Engaged E↔E linking connections induce generally higher coherence values (*squares*) than E↔I connections in isolation (*triangle*). Differences between both conditions are visible even for lowest distances (*solid line*). **B.** The spatial extent and the absolute γ-coherence values are much larger for LFP than for MUA. Differences between engaged and disabled E↔E connections are most prominent for a distance of 1.75 mm, and differ significantly up to 3.75 mm for LFP and 3.5 mm for MUA (Mann-Whitney-U-Test, $p < 0.001$).

γ-coherences with enabled and disabled E↔E connectivity are compared. The linking connections enhance γ-coherence of membrane potentials preferably for short distances (up to 50%); slight increases can be seen up to distances of 3.5 mm.

Using local field (LFP) instead of membrane potentials (Fig. 3.9B) revealed generally higher coherence values. Differences in γ-coherence between engaged and disabled E↔E connections are small for low distances, increase to a maximum for a distance of 1.75 mm and decrease again for larger distances. This is in contrast to the findings for the membrane potential, where differences in γ-coherence decay monotonously with distance (Fig. 3.8C,D). γ-coherences for MUA signals were generally much lower than for LFP signals (Fig. 3.9A). γ-coherence enhancements by engaged E↔E connections are therefore less pronounced. However, differences were visible even for lowest distances, in contrast to LFP.

The width of the γ-coherence profile does not only depend on the E↔E connection strengths as shown before, but also on the transmission velocity of these connections. Using instantaneous E↔E interactions, the spatial width and strength of the γ-coherence profile is enhanced compared to disabled E↔E connections (Fig. 3.10). With decreasing conduction velocities the width and strength of this coupling is gradually reduced. For

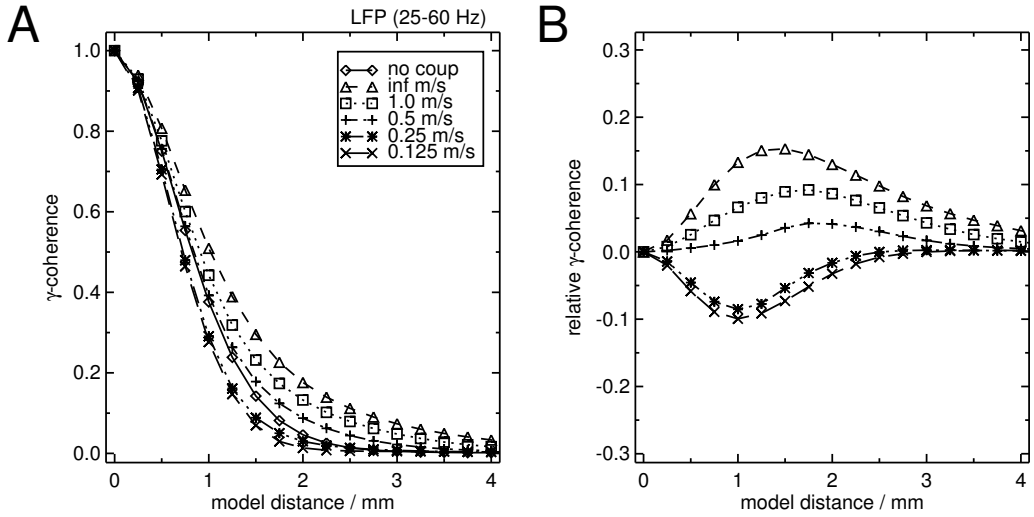

Figure 3.10: *Spatial γ-coherence profiles depend on E↔E velocities.* **A.** The *solid line* indicates the coupling profile that is induced in the presence of recurrent inhibition (E↔I) and in the absence of the linking connections (E↔E). Instantaneous lateral transmissions (*dashed*) revealed the broadest coupling profile, while transmission velocities up to 0.5 m/s exhibited intermediate coupling ranges (*dotted, dash dotted*). Velocities below 0.5 m/s reduced the width of the γ-coherence profile coupling even below the values obtained without any E↔E connections. **B.** Differences between γ-coherence profiles for different E↔E connections and disabled E↔E connections (solid line in A) are shown.

lateral velocities below 0.5 m/s, γ-coherence for all distances is smaller than without any E↔E connections at all. The decrease in coupling strength and range is accompanied by a reduction of the γ-power (Fig. 3.7D).

3.3.5 Decoupling of γ-coherence across stimulus gaps

In the previous sections, we analyzed γ-coherence in a network region that was homogeneously stimulated. Here, the properties of γ-coherence will be investigated near a spatial disruption in input stimulation (Fig. 3.2A2). The attenuation of input stimulation is accompanied by a reduction of γ-power at the positions of the gap (Fig. 3.11), because the reduced spike rates of excitatory neurons are not sufficient to drive the inhibitory feedback loop.

For a reference membrane potential located 2.5 mm away from the stimulation gap (Fig. 3.11B), the γ-coherence profile is not visibly disturbed compared to a homogeneous stimulation (Fig. 3.8B). With decreasing distance to the gap, membrane potentials

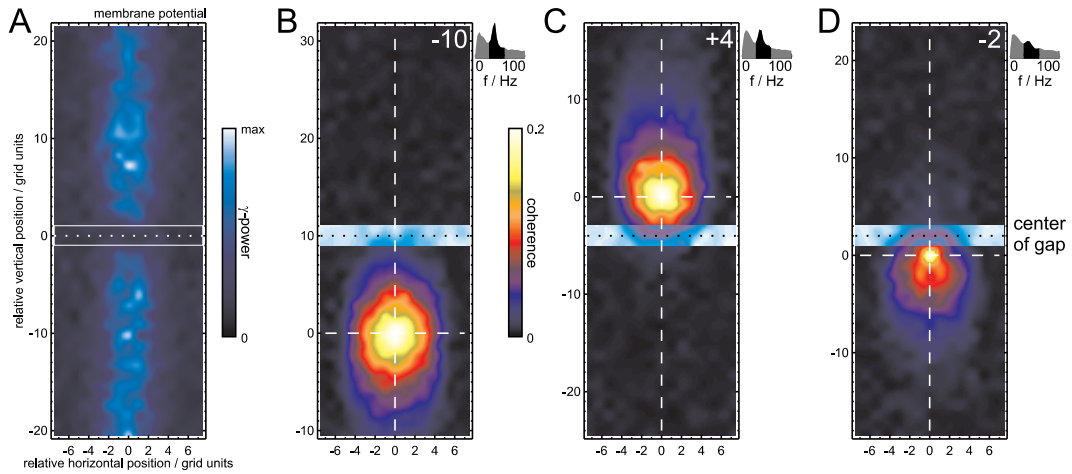

Figure 3.11: *Coherence is reduced in the vicinity of an activity gap. White dashed crosses* mark the positions of the reference neurons. *Horizontal dotted line* indicates the center of the gap. *Right insets* show the power spectrum of the reference neuron (same scaling). **A.** Reduced stimulation in the center of the array (Fig. 3.2A2) results in reduced γ-activity at these positions. **B.** Reference neuron is located 10 grid units (2.5 mm) below the gap center. The elongated γ-coherence profile is not affected by the presence of the gap. **C.** The γ-coherence profile with the reference neuron placed 1 mm above the gap center is deformed in the direction of the gap. Neurons on opposite sides of the gap are not coupled. **D.** γ-coherence profile (distance: 0.5 mm from gap center) is generally reduced in strength compared to B and C.

show a generally reduced γ-coherence with their neighbors (Fig. 3.8). Additionally the coupling profile is deformed in the direction of the gap. The membrane potential of neurons near the gap is neither coupled with neurons on the other side of the gap, nor with neurons at the position of the gap (Fig. 3.11).

This qualitative description is confirmed, by comparing the γ-coherence for pairs of LFP signals on the same side and on either side of the gap, using both, continuous bar and two-bar stimulation. Fig. 3.12A shows that γ-coherence of signal pairs on the same side of the stimulus discontinuity is not affected by the presence of the gap (144 combinations, paired t-test, $p > 0.5$). In contrast, γ-coherence is significantly reduced across the gap (144 combinations, paired t-test, $p < 0.0001$). The dependence of γ-coherence reduction on the distance of the recorded signals can be seen in Fig. 3.12C. Averaging across all signal pairs reveals, that gap stimulation reduces γ-coherence on average to 0.37 of the value obtained with continuous stimulation (Fig. 3.12B).

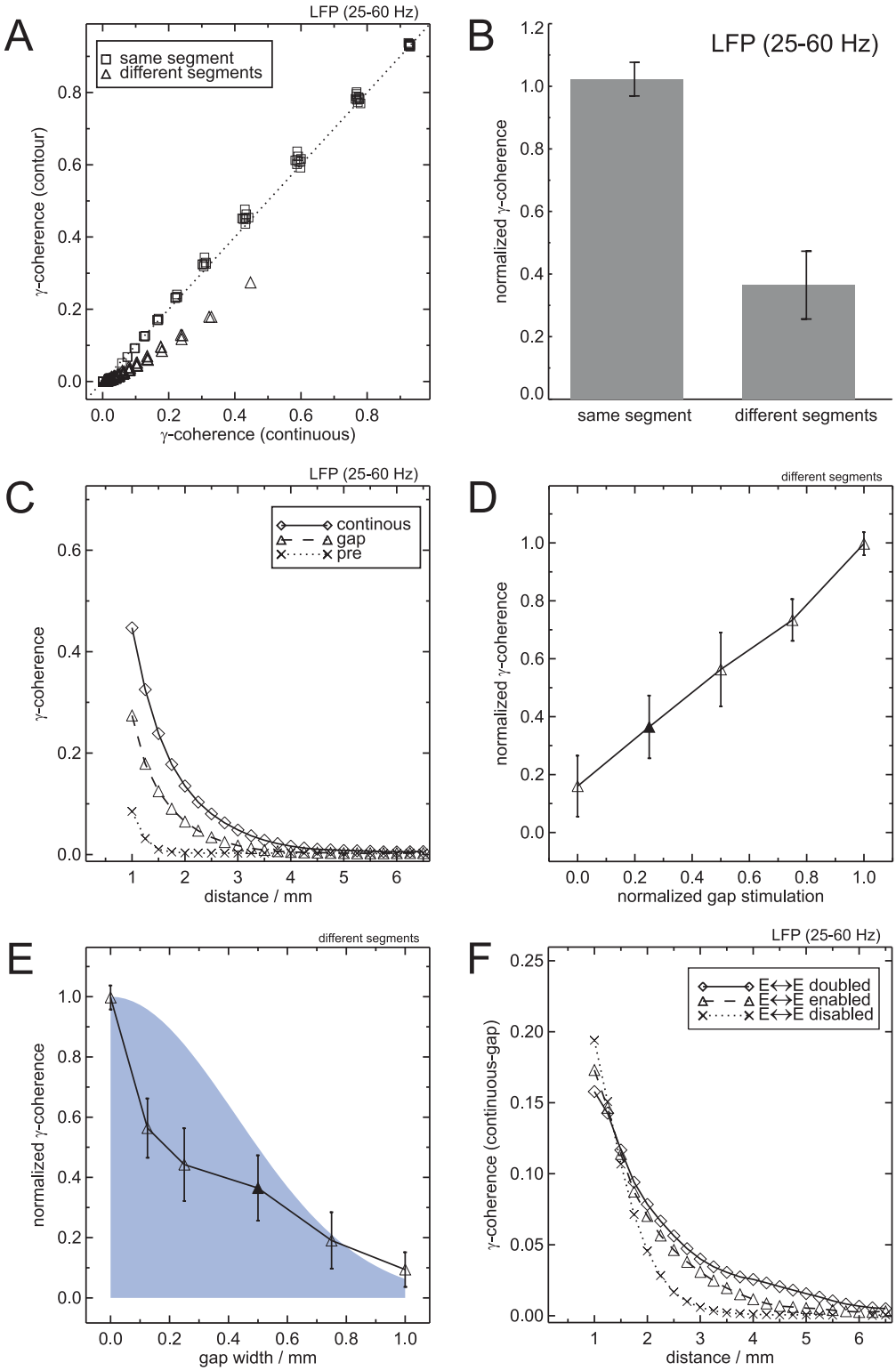
A
LFP (25-60 Hz)
same segment
different segments
γ-coherence (contour)
γ-coherence (continuous)
B
LFP (25-60 Hz)
normalized γ-coherence
same segment
different segments
C
LFP (25-60 Hz)
continous
gap
pre
γ-coherence
distance / mm
D
different segments
normalized γ-coherence
normalized gap stimulation
E
different segments
normalized γ-coherence
gap width / mm
F
LFP (25-60 Hz)
E↔E doubled
E↔E enabled
E↔E disabled
γ-coherence (continuous-gap)
distance / mm

Figure 3.12: *Reduction of LFP γ-coherence across stimulus discontinuity.* **A.** Comparison of γ-coherence for continuous and discontinuous stimulation. γ-coherence for signal pairs derived on the same side of the gap is unaffected by the gap (same segment, *squares*, paired t-test, $p > 0.5$), while γ-coherence is reduced for pairs on either side of the gap (different segments, *triangles*, $p < 0.0001$). **B.** Averaged reduction of γ-coherence by discontinuous stimulation. Modulation of γ-coherence within the same segment (squares in A) is minimal, while a strong reduction can be observed for different segments (*triangles* in A). **C.** Distance-dependence of γ-coherence for continuous (*solid*), discontinuous (*dashed*) and without stimulation (*dotted*). γ-coherence for continuous and discontinuous stimulation is significantly larger than without stimulation (paired t-test, $p < 0.001$ for all distances). Reduction of γ-coherence is maximal for short distances, and decreases slowly with increasing distance (paired t-test, $p < 0.001$ for all distances $<= 5$ mm). **D.** γ-coherence for LFP signals on either side of the gap increases linearly with the stimulation amplitude at the position of the gap. Filled symbol indicates the standard value for the gap amplitude. **E.** Decoupling of γ-LFP signals on either side of the stimulus gap increases with gap width. A prominent γ-coherence reduction is already present for small gap widths of 0.1 mm. The spatial decay of γ-coherence is comparable to the spatial decline of the E↔I connection profile (*shaded area*). **F.** γ-coherence reduction by the presence of the stimulus gap for different E↔E strengths.

γ-coherence across the stimulus gap is linearly reduced with the stimulus amplitude used for neurons at the position of the gap (Fig. 3.12D). The magnitude of γ-coherence reduction also depends strongly on the width of the stimulus gap (Fig. 3.12E). If the gap width matches the projection area of the I→E (or E→I) connections, there is virtually no coupling for LFP signals on either side of the gap.

Note however, that a prominent γ-coherence reduction is already present for small gap widths. E↔E connections enlarge the spatial range of γ-coherence for a continuous stimulation (Fig. 3.9). For distances below 1.5 mm, a stimulus gap reduces γ-coherence most effectively for disabled E↔E connections (Fig. 3.12F). For larger distances, the effect is reversed: the reduction in γ-coherence increases with the strength of the E↔E connections.

The temporal properties of the γ-coherence reduction can be seen in Fig. 3.13. First differences in γ-coherence for gap and continuous stimulation can be seen after 100 ms. The reduction is maximal for $t = 200$ ms and remains constant on average for larger times.

3.4 Discussion

3.4.1 Main results

We addressed the basic question of whether and how finite velocities in the transmission of action potentials affect the emergence of γ-activity, its temporal frequency and γ-correlations in a model of spiking neurons. We found that transmission delays act differently on signal properties in the γ-range depending on the sub-circuit they are part of. First, delays in the inhibitory feedback loop, i.e., axonal projections from and to inhibitory neurons, directly influence the peak γ-frequency, but affect neither the emergence and power of γ-activity nor the spatial extent of γ-coherence. Second, transmission delays between excitatory neurons have a critical impact on both, the power and the coherence of γ-activity. Horizontal connections having infinite transmission velocities between excitatory neurons enhance γ-coherence for all distances ≤ 4 mm. This enhancement is gradually diminished for decreasing velocities. Below 0.5 m/s, γ-power and γ-coherence for all distances are even smaller than without these connections at all, i.e., slow horizontal connections actively desynchronize neural populations. We conclude, that cortical horizontal connections between excitatory neurons have to be fast ($v \geq 0.5$ m/s, maximal delay ≤ 5 ms), to play a role for γ-synchronization.

3.4.2 Spatial decay of γ-coherence

γ-coherence of model MUA and LFP signals gradually decays with increasing distance of the two recording positions (Fig. 3.9; LFP full-width at half-height: 2–2.4 mm). The decay essentially matches the monosynaptic connection scheme of recurrent inhibition in our model (E→I, I→E: 1.0 mm each), which is based on the finding that most connections in the primary visual cortex terminate within a diameter of 1.0 mm, connecting neurons unspecifically with arbitrary orientation preferences (cat: Kisvarday and Eysel, 1993; ferret: Roerig and Chen, 2002; monkey: Malach et al., 1993; Stettler et al., 2002; tree shrew: Bosking et al., 1997; Chisum et al., 2003). The range of LFP γ-coherence observed in cat and monkey primary visual cortex is somewhat larger than the values we obtain in the model (3–6 mm, cat: Brosch et al., 1995; Steriade et al., 1996; monkey: Frien and Eckhorn; Gabriel and Eckhorn, 2000b; 2003). The model coupling profiles are a result of the model circuitry alone, since input to the network

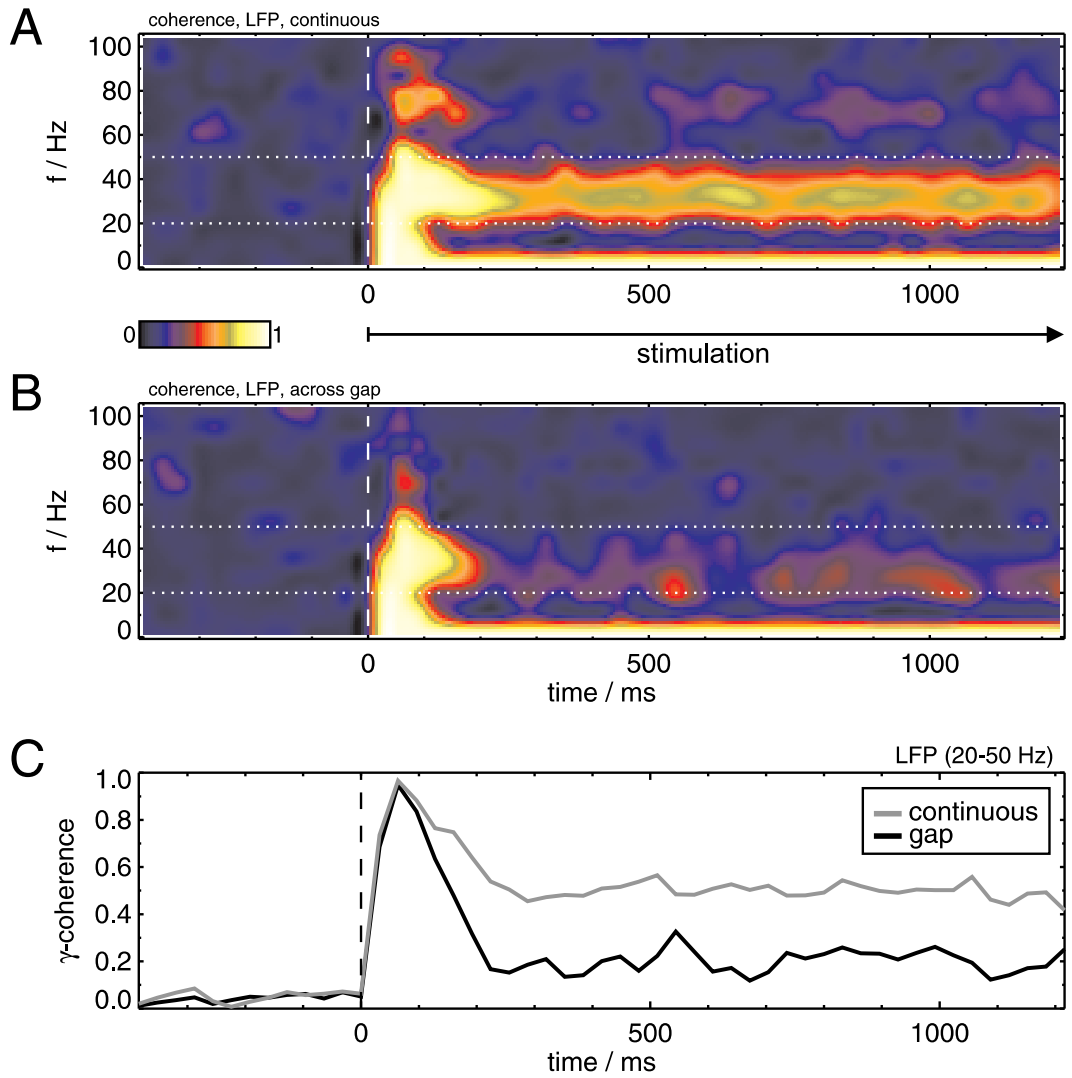

Figure 3.13: *Time-courses of averaged LFP coherence.* Average time- and frequency-resolved LFP coherence is calculated between 2 recording positions (distance: 0.25 mm) on one side and 2 positions on the other side of the gap (gap distance: 1 mm, window size: 128 ms, N=50). **A.** Coherence for continuous stimulation starting at $t = 0$ ms (Fig. 3.2A1). *White dashed lines* mark the lower and upper limit of the investigated frequency range (20–50 Hz) in C. The right edge of the averaging window is aligned with the time scale. **B.** Coherence across the gap (stimulus onset: $t = 0$ ms, input: Fig. 3.2A2) is strongly reduced for $t > 200$ ms in comparison to the continous stimulation in A. **C.** Average coherence (20–50 Hz) for continuous and gap stimulation increases with the onset of the stimulus. First differences in coherence can be observed for $t > 100$ ms.

is uncorrelated and feedback from other cortical areas was not modelled. Intracellular recordings from cat V1 yet revealed, that membrane potentials of neighboring cortical neurons are correlated due to common input from LGN neurons (Llampl et al., 1999, investigated below 0.5 mm). The spatial range of correlated activity due to overlapping receptive fields depends on eccentricity and is at least in the order of 1 mm (cat: Hubel and Wiesel, 1974; Usrey et al., 2000). Incorporating similar input correlations into the model, would allow a better match of experimental with model γ-coherence ranges.

3.4.3 Fast horizontal connections enhance γ-coherence

For all distances, MUA and LFP γ-coherence with engaged fast horizontal connections ($v \geq 0.5$ m/s) is stronger than without these connections (Fig. 3.9). Horizontal connections preferably connect neurons that share similar orientation preferences (cat, monkey: Gilbert and Wiesel, 1989; Ts'o et al., 1986; Kisvàrday et al., 1997; Schmidt et al., 1997; Stettler et al., 2002). We did not explicitly include orientation selective receptive fields in our model. However, we can assume that two neurons with reciprocal long-range horizontal connections have iso-oriented cRFs, while neurons without these connections are cross-oriented. In this sense, the results are in good accordance with data from monkey visual cortex showing that γ-coherence of MUA signals significantly increases with similarity in preferred orientations (Frien and Eckhorn, 2000b, their Fig. 6).

A similar, but weaker dependency of γ-coherence on orientation difference is also visible in their LFP data. However this effect is not significant, which may be due to the large cortical range over which postsynaptic potentials contribute to LFP via extracellular volume conduction (FWHH ≈ 1.0 mm; Mitzdorf, 1985). Our model LFPs are in fact weighted across the same spatial area, but the network topology does not account for ocular dominance, spatial frequency, color, motion and feedback from higher areas and is in that way not comparable to real cortical influences.

3.4.4 Transmission delays vs. synchronized γ-activity

The transmission delays incorporated in our network introduce two opposing effects on synchronized γ-activity. On the one hand, decreasing spike conduction velocities in the E↔I connectivity linearly reduce the peak frequency in LFPs (Fig. 3.6D). Their influence on the power and spatial range of γ-activity is weak, however. Increasing E↔I connection strengths result in increased γ-power, while γ-frequency remains constant.

On the other hand, decreasing velocity in the E↔E connectivity drastically reduces γ-power (Fig. 3.7D) and γ-coherence of LFPs (Fig. 3.10). This reduction is effective for all distances, even where delays are small compared to the oscillation period.

The different action of delays is due to the way, how these connections affect the membrane potentials of excitatory neurons. Let us assume a local group of excitatory neurons that is driven by an external input. If they fire synchronously at a certain time, this activity excites connected inhibitory neurons (E→I), that reach their firing threshold and in turn inhibit the connected excitatory cells via single or bursts of inhibitory postsynaptic potentials (I→E). Synchronized excitatory cells therefore receive a delayed inhibition by the E↔I sub-network.

Analytical (Mirollo and Strogatz, 1990; Kuramato, 1991; van Vreeswijk et al., 1994; Ernst et al., 1995) and simulation studies (Ernst et al., 1995; Nischwitz and Glünder, 1995), using pulse-coupled oscillators, have shown that two mutually connected neurons synchronize stably at zero-phase difference, if the action potentials are transmitted with arbitrary but equal delays and evoke inhibitory postsynaptic potentials. This can be mapped to our network by considering two neighboring excitatory neurons that mutually inhibit each other via common inhibitory neurons. Therefore, finite conduction velocities in the E↔I network delay the inhibitory force of the interneurons, thereby reducing the frequency of the γ-peak, but the power of γ-activity remains unaffected.

The situation is different for the E↔E connections, where mutually connected excitatory cells receive delayed excitation. For this case, van Vreeswijk et al. (1994) could show, that synchronous firing of integrate-and-fire as well as Hodgkin-Huxley neurons is only stable, if the rise time of the synapse is shorter than the duration of an action potential ($\approx$1 ms). For larger delays, the synchronous state is repellent and two neurons show a phase shift in firing time that equals the transmission delay (Mirollo and Strogatz, 1990; Kuramato, 1991; Ernst et al., 1995; Nischwitz and Glünder, 1995). In our model, a single neuron receives excitatory postsynaptic potentials from several proximal and distant neurons with a variety of delays ($\geq$1 ms), which results in a desynchronizing effect, increasing with the variance of delays (i.e. decreasing velocity) in the E↔E connections.

The network's behavior can also be deduced from the "locking theorem" (Gerstner et al., 1996b), that is valid for spatially homogeneous networks with a large number of excitatory or inhibitory interacting neighbors. It states, that coherent oscillations are stable if and only if the postsynaptic potential is increasing in time as the neurons

fire. In our model, coherent γ-oscillations are stable for the E↔I network, because the membrane potentials of the excitatory neurons increase due to the decaying action of the IPSPs, when they touch the slowly decaying firing threshold, resulting in new action potentials. γ-oscillations are also stable for small delays in the additional E↔E network, because linking pulses from neighboring neurons depolarize the membrane potential shortly before it reaches threshold. Linking signals reaching the neuron directly after it has fired have no effect, because the neuron is refractory. The situation is changed for larger delays, where linking signals reach the neuron with high delays compared to the spiking time of the local group. This results in a summed linking signal that shows only weak temporal variations, and reduces the probability that the neuron will fire when the membrane potential is increasing. For decreasing velocities, the synchronizing action of linking signals as seen in γ-power and γ-coherence is therefore successively reduced ($v \approx 0.5$ m/s, Fig. 3.7D, 3.10).

The desynchronizing effect of slow, long-range excitatory connections was also observed in a compartment model with Hodgkin-Huxley dynamics (Wilson and Bower, 1991). They found synchronized γ-oscillations for an average velocity of 0.86 m/s, while synchrony was superseded by traveling waves when the velocity was reduced to 0.43 m/s. Schillen and König (1991) used similar delayed ($\Delta = 4$ ms), next nearest-neighbors excitation to actively desynchronize two separate neuronal populations within a single layer. Their simulation model consisted of nonlinear oscillators (period: $T = 20$ ms) based on the statistical approach of Wilson and Cowan (1972). Ritz et al. (1994) were able to demonstrate that two hemispheres show synchronized γ-oscillation provided that the average delay of interhemispheric all-to-all connections does not exceed 5 ms (oscillation period: T=25 ms). In our model, E↔E connections only act synchronizing if the conduction velocity is 0.5 m/s or larger, corresponding to a maximal (average) delay of 5 ms (2 ms).

Summarizing, γ-synchrony is only stable when maximal delays of E↔E connections are lower than 5 ms (0.2 of the oscillation period). Interestingly, the same value is found, if the connections between two groups of neurons (e.g. cortical columns) are mediated by delayed inhibition (Traub et al., 1996; Bush and Sejnowski, 1996). This finding therefore seems to be independent of the specific mechanism used to establish synchronized γ-oscillations.

3.4.5 Decoupling of γ-activity across stimulus discontinuity

The γ-synchronization hypothesis states, that γ-activities of neural groups, representing the same object are coupled, while γ-activities representing different objects are decoupled. Our model results are compatible with this hypothesis, when interpreting the two stimulated regions (Fig. 3.2A2) as object and background or two different objects, respectively. First, stimulus-specific coupling of γ-activity (measure: γ-coherence) recorded from the same object is significantly stronger than without stimulation. Second, stimulus-specific γ-coherence is strongly reduced across the region separating both objects compared to a homogeneous stimulation, while γ-coherence within the respective object representation is not reduced. The decoupling of γ-activity is not visible in early, stimulus-locked responses, but emerges only for later times (>100–200 ms post stimulus onset).

Discontinuous stimulation caused a decoupling of γ-activity because of two effects: First, neurons representing the stimulus gap are weakly activated and therefore do not participate in the E↔I dynamics on either side of the gap. Second, excitatory neurons in the vicinity of the stimulus gap do not receive modulatory E↔E input from the weakly activated neurons at the position of the gap. The remaining long-distance monosynaptic linking connections between neurons on either side of the gap are too low in number and too weak in action to produce strong γ-coupling. Therefore, the synchronizing effect of lateral linking connections is effectively disabled at the position of the gap. The width of the gap can be much smaller (≤ 0.25) than the width of the E→I, I→E and E→E connections to achieve prominent γ-decoupling. The influence of E↔E connection strength on the magnitude of γ-decoupling depends on the distance. For low distances (≤ 1.5 mm), the stimulus gap reduces γ-coherence by $0.16 - 0.19$. The influence of E↔E connection strengths on this effect is low ($< 20\%$). For larger distances, γ-coherence reduction strongly increases ($> 100\%$) with E↔E connection strength. The influence of the stimulus gap can therefore be detected over much larger distances, when E↔E connections are strong.

The model results are in line with a study investigating γ-decoupling across texture representations in monkey primary visual cortex (Gail et al., 2000). They used a whole field sinusoidal grating (background) as stimulus and defined a square object, by shifting the spatial phase within a square region of the grating. γ-decoupling between positions

of object and background representation solely occurred when the square object was visible.

Two stimulus properties may be responsible for the observed reduction in γ-coherence: on the one hand, object and background are separated by a polarity changing contour, that was introduced by the specific stimulus setup. We have recently shown that the strong activation, that is evoked by such a contour, is capable of disabling the effects of long-range horizontal connections in a model investigation using slow shunting inhibition (Al-Shaikhli, 2001; Eckhorn et al., 2004a,b). On the other hand, the border of object and background is characterized by a discontinuity in the spatial phase of the sinusoidal texture. Neurons that are optimally stimulated by either the object or the background stimulation both exhibit a suboptimal response if their receptive field is at the position of the object's border. In other words, the spatially inhomogeneous visual information at the border of the object results in a reduced activity of neurons representing these positions.

The current model shows, that this reduced activity directly impairs γ-coherence between object and background representations (Fig. 3.12D). In a more elaborate model we could additionally show, that γ-decoupling can be maintained in the presence of a strong contour activation (Saam et al., 2000; Eckhorn et al., 2001a). This mechanism is not restricted to the specific experimental setup, but can be applied generally, since each object border exhibits a discontinuity in at least one visual feature domain (e.g. color, motion, texture).

The available experimental data can not clarify, if decoupling is evoked by either the contour activation or the stimulus discontinuity. We suggest new experiments with modified stimuli to distinguish between both mechanisms: a comparable γ-decoupling using a rectangular frame placed above a continuous grating would support decoupling-by-contour, while γ-decoupling using a phase shifted object where the object borders are smoothed would support decoupling-by-discontinuity. Possibly, both stimulus properties contribute to the observed effects.

4 Traveling γ-waves

Recent studies showed, that coherence in the γ-band (30–90 Hz) is restricted to patches of few millimeters in the primary visual cortex of cats and monkeys. This challenges the role of γ-synchronization to solve the binding problem for larger object representations. To investigate the phenomenon of restricted synchrony, we used a biologically plausible model network with spiking neurons and distance-dependent delays. Local recurrent inhibition generated regions of neurons that were synchronized in the γ-range, when they were driven above threshold by a static input stimulus. These synchronized patches were part of more globally occurring γ-waves, which coupled over much larger distances and extended well beyond the maximal monosynaptic connection distance. Long-range horizontal connections were added to account for the physiology of the primary visual cortex in which contextual modulations outside the classical receptive fields are assumed to be primarily due to these connections. While modulations obtained with conventional linear coupling measures were weak and restricted to low distances (γ-coherence, 1.8 mm half-height decline), modulations of γ-waves were strong and cover larger distances (6.3 mm half-height decline). The model γ-waves observed here are qualitatively similar to those found in the primary visual cortex of awake monkeys (Gabriel and Eckhorn, 2003). The model quantitatively captured experimental properties, e.g., the spatial decay of γ-coherence and γ-waves, except for a fixed scaling factor. In conclusion, we therefore propose that γ-waves may support the coding of object continuity beyond the limits of γ-synchronization.

Some results presented in this chapter have already been published in Eckhorn et al. (2001a, 2004a,b). Preliminary versions had been published as conference proceedings (Saam et al., 2000; Eckhorn et al., 2001b).

4.1 Introduction

4.1.1 Coherent γ-activity is locally restricted

Stimulus-induced oscillations are an emergent phenomenon in many cortical areas and across various species (Freeman, 1978; Eckhorn et al., 1988; Kreiter and Singer, 1992; Traub et al., 1993; Frien et al., 1994; Golomb and Amitai, 1997; Prechtl et al., 1997). Their magnitude and frequency is modulated by the properties of the external stimulus (Eckhorn et al., 1988). In the visual system, oscillations are commonly found in the γ-range (30–90 Hz) of local field potentials (LFPs). Simultaneously recorded LFPs are found to be synchronized, if the contributing neurons are involved in the co-processing of the visual input (reviews: Eckhorn, 1999; Gray, 1999). Synchronization may therefore be one neural mechanism (Reitboeck, 1983; von der Malsburg and Schneider, 1986) to unify locally detected features into perceived objects. While there are many supportive studies for this binding-by-synchronization hypothesis (reviews: Eckhorn, 1999; Gray, 1999), it was also observed, that synchronization of γ-signals is usually limited to a few millimeters in the primary visual cortex (Brosch et al., 1995; Frien and Eckhorn, 2000b). This seems to restrict feature binding-by-synchronization to objects covering only small parts of the visual field.

4.1.2 Coherence fails to detect long-range coupling

In order to understand why γ-synchrony is locally restricted, Gabriel and Eckhorn (2003) analyzed multi-channel LFP recordings obtained from the primary visual cortex of awake monkeys. It turned out, that local γ-synchrony is part of more globally occurring traveling γ-waves. The spatial extent, velocity and direction of these γ-waves changes quickly (within tens of milliseconds) with respect to the time interval used by standard correlation techniques (usually hundreds of milliseconds). For small distances between the electrodes, the variance of phase differences is small, but increases linearly with increasing electrode distance (Eckhorn et al., 2001a). Standard correlation methods, like cross-correlation and coherence, are sensitive to variances in the phase difference and require them to be small across identical stimulus repetitions (trials), to obtain strong coupling values. Hence, pair-wise cross-correlation and coherence are well suited to detect constant phase relations between two recording sites, but they cannot capture

γ-waves over their entire spatial extent, because this phenomenon is concealed by phase averaging across trials. Furthermore these pair-wise methods cannot account for the spatial continuity and extent, which is a key property of γ-waves.

4.1.3 γ-waves cover larger cortical distances than γ-coherence

To overcome these shortcomings, Gabriel and Eckhorn (2003) developed a multi-channel correlation method to detect and quantify the occurrence and velocity of a single wave front in single trial recordings. Applying this method to recordings from awake monkeys revealed, that γ-waves can cover large portions of the primary visual cortex (half-height decline >7.5 mm; Gabriel and Eckhorn, 2003), while coherence as a measure for γ-synchrony decays within 2.5 mm (half-height decline, same data). This indicates, that distant neural populations are coupled for short periods of time by a spatially continuous activation. However, this coupling mode does not rely on stable phase relations between two distant cortical sites and is therefore not captured by coherence.

4.1.4 Existing models do not properly capture properties of γ-waves

Traveling waves are observed in many cortical areas and species (e.g. Freeman, 1978; Traub et al., 1993; Golomb and Amitai, 1997; Prechtl et al., 1997). There has also been much effort in uncovering the underlying neural mechanisms by mathematical investigations using a self-consistency approach (Kuramato, 1984; Crook et al., 1997; Ermentrout, 1998; Bressloff, 1999; Kistler, 2000; Ermentrout and Kleinfeld, 2001). In general, excitable media with spatially restricted connectivity can generate solitary pulses and periodic waves with constant phase relations, that run across the entire one- or two-dimensional network (Kuramato, 1984). The propagation velocity and stability of waves in these models depends on the spike transmission velocities as well as the axonal projection ranges of lateral connections (Crook et al., 1997; Ermentrout, 1998).

Although such investigations can provide valuable insights into traveling wave phenomena, a direct comparison with experimental data is difficult: on the one hand, this is due to necessary simplifications in network architecture, e.g., continuous instead of spiking neurons, one-to-all instead of local connections, absence of inhibitory neurons, no or constant spike transmission delays. Besides, these studies prefer to characterize stable network states, i.e., temporally and spatially periodic, linear waves of constant phase that move over the whole network. For a fixed set of network and input parameters,

there is only one stable solution with one constant propagation velocity (Crook et al., 1997; Bressloff, 1999; Kistler, 2000). γ-waves as described by Gabriel and Eckhorn (2003) differ from these predictions: First, γ-waves with a small spatial extent occur more often than those covering large cortical regions (Eckhorn et al., 2004a). Second, γ-waves are temporally not periodic, but occur at random times. Finally, γ-waves show a wide distribution of velocities and directions even within a single stimulus presentation (Eckhorn et al., 2004a).

4.1.5 Goal of the model

In the previous chapter, we have developed a network that successfully reproduced various experimentally observed coupling phenomena. Here, we want to find out, if the model is additionally capable of producing traveling γ-waves and if the observed effects are similar to the experimental results.

For this, we used a two-dimensional network of topographically ordered integrate-and-fire neurons. Excitatory and inhibitory neurons were reciprocally connected, and modulatory connections between excitatory neurons should account for long-range interactions (e.g., Gilbert, 1983; Allman et al., 1985; Eckhorn et al., 1988).

We found that the model is able to produce traveling γ-waves that extend well beyond the monosynaptic connection range. Their occurrence was sensitive to both, stimulus as well as network properties, and surpassed standard coupling measurements, like the coherence. Results were in accordance with experimental data, specific differences are discussed.

4.2 Methods

4.2.1 Network and input

The model neuron, the network, and the network input are based on previous simulations (for details see Chapter 3). In short, the topographically arranged network consists of excitatory and inhibitory spiking neurons (Eckhorn et al., 1990), reciprocally connected to a distance of up to 1 mm in model space. To network consists of $15 \cdot 61$ excitatory and $7 \cdot 31$ inhibitory neurons, corresponding to 3.5 mm $\cdot$ 15 mm in model space.

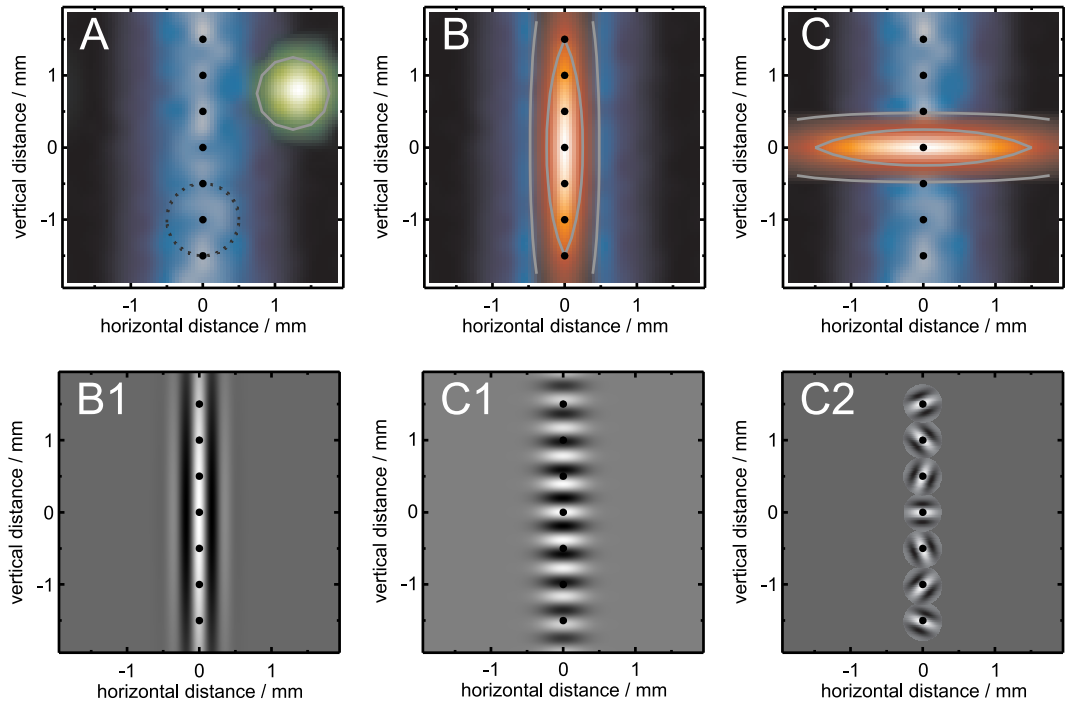

Figure 4.1: *Network and stimulus configurations.* Each figure shows a vertically cropped arrangement of a different stimulus-network configuration. The vertical bar stimulus evokes membrane potential depolarisations in neurons (blue color scheme). Signal sampling positions ('virtual electrodes', black dots) are always aligned with the vertical stimulus. **A.** A sample projection scheme for excitatory-to-inhibitory as well as inhibitory-to-excitatory connections is shown in green (gray circle: half-height decline). The dotted dark line illustrates a sample LFP catchment area for the second lowest sampling position. There were no direct connections between excitatory cells in this case. This scenario serves as reference condition for the effects of horizontal connections. **B.** Lateral connections between excitatory cells are vertically oriented and match the stimulus configuration. The connectivity pattern for the center neuron is shown in red (gray lines: 50% and 10% of the maximum). **C.** Lateral connections between excitatory cells are horizontally oriented and do not match the stimulus configuration. **B1, C1, C2.** Possible visual stimuli for the combinations of input activation, (hypothetical) receptive field configuration and lateral connectivity in B and C.

All simulations used a vertically elongated stimulus (Eq. 3.1, 3.2), with signal sampling positions placed along the stimulus-activated neurons (Fig. 4.1A). The analog stimulus was strong enough, to evoke moderate firing rates at the stimulated neurons (Fig. 3.3). Receptive fields were not explicitely modelled. The input therefore represents a convolution of the local visual stimulus with the corresponding (hypothetical) receptive field for that neuron. To provide a concrete example, the stimulus can be interpreted

as a vertical bar composed of a vertically oriented sinusoidal grating (Fig. 4.1B1). Hypothetic receptive fields may also be vertically oriented, the corresponding neurons are therefore activated (Fig. 4.1A). Cortical neurons with similar orientation preference and a collinear arrangement in visual space are known to be reciprocally interconnected (tree shrew: Bosking et al., 1997; Chisum et al., 2003). This scenario is simulated in scenario B (Fig. 4.1B). The third scenario (Fig. 4.1C) mimics a visual stimulus configuration, where either the collinear configuration (Fig. 4.1C1) or the iso-orientation arrangement (Fig. 4.1C2) of the visual stimulus is not present. In this case, little or no effects are expected by the long-range lateral connections.

4.2.2 Signal acquisition

We used 21 linearly arranged signal sampling positions ('virtual recording electrodes') unless noted otherwise. The distance between adjacent positions was 0.5 mm, so that the complete arrangement covered 10 mm of the network. For each position, we computed the LFP by averaging membrane potentials with a spatially exponential weight distribution. The half-height decline is termed the *catchment radius* and was set to 0.5 mm. With these settings, the neuron placed directly at the sampling position contributed 5% to the total signal. Every LFP signal was band-pass filtered in the γ-range. The filter characteristics were broadly tuned (25–60 Hz) and enclose the maximal γ-power (here: from 35 up to 45 Hz).

We restricted our model analyses to the stationary part of stimulus response and therefore excluded from quantitative analyses all time windows less than 50 ms before (for the pre-stimulus reference) and 200 ms after the stimulus onset.

4.2.3 Wave detection method

To detect and quantify plane traveling waves in the model LFPs, we used a recently developed spatio-temporal correlation method (Gabriel and Eckhorn, 2003). Recorded potentials are analyzed by a short sliding window of 30 ms duration, consecutively shifted by 15 ms (Fig. 4.2 A,B). For each window, a two-dimensional autocorrelation is calculated (Fig. 4.2 C). One dimension is the sampling position, while the second dimension is the time. The resulting correlations range from -1 to 1. If the input signals are statistically independent, the correlation values for all spatial and temporal shifts will be close to zero. If all input signals represent synchronous activity or traveling

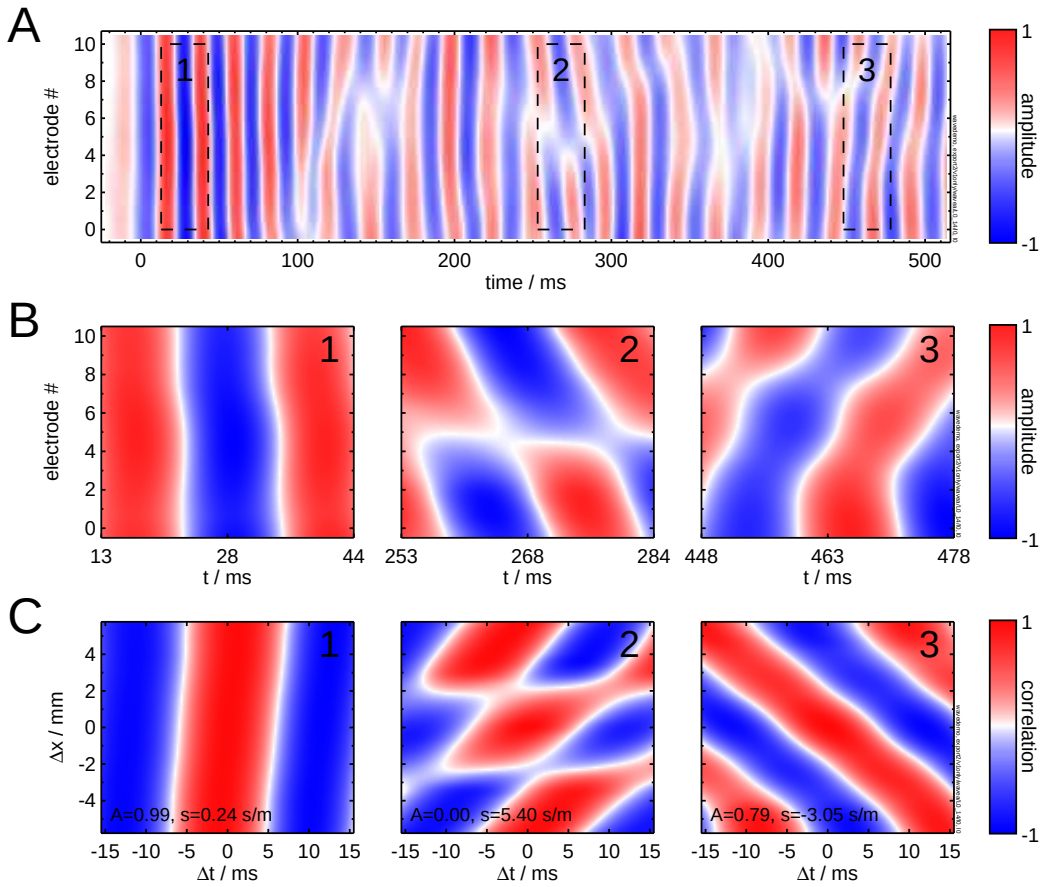

Figure 4.2: Spatio-temporal correlation method. **A.** Single trial time course of 11 simultaneously recorded LFP potentials (25–60 Hz) is analyzed with a sliding window technique (window size: 30 ms). Three sample windows are shown (dashed lines). **B.** Enlarged versions of 3 windows shown in A. A two-dimensional auto-correlation is computed for each window (**C**) and fit to a two-dimensional cos-function. Amplitude (A) and the reciprocal velocity (s) of these fits are shown. For the second window, an amplitude of zero indicates a spatio-temporal independent event, while the other two windows exhibited high amplitudes and therefore show a good spatio-temporal correlation (termed: γ-wave). In the first window, all electrode are stimulated nearly synchronously (v=4.2 m/s), while the propagation velocity of the γ-wave in the third window is quite slow (v=0.3 m/s).

waves, the two-dimensional correlation function will show a linear ridge where the maximal values are close to +1 (Fig. 4.2 C1, C3). To quantify the correlation map with few parameters, the map was fit to the autocorrelation of an ideal planar wave:

$$C_V(\Delta x, \Delta t) = A \cdot \cos\left(2\pi\nu(\Delta t - \Delta x/v)\right) \quad , \tag{4.1}$$

where A, v and ν were free parameters. The fitted amplitude factor A is termed the *γ-wave strength* ($0 \leq A \leq 1$), v is the velocity of the fitted planar wave. The details and the application to artificial as well as monkey data can be found in Gabriel and Eckhorn (2003).

Fig. 4.2 demonstrates 3 typical patterns. The second time window (B2) shows a Y-like activation of the 11 sampling positions. The spatio-temporal correlation (C2) has a blob-like structure. The fitting algorithm therefore failed to fit Eq. 4.1 (γ-wave strength $A = 0$). The time window did therefore neither exhibit a traveling wave nor synchronous activity. The third window (B3) shows an LFP negativity that begins with the first sampling position and spreads slowly to sampling position 10. The fit of the correlation pattern reveals a prominent traveling γ-wave ($A = 0.79$) with a slow propagation velocity ($v = 0.3$ m/s). The propagation velocity of the γ-wave in the first window is high ($v = 4.2$ m/s): for a short period all sampling positions show nearly synchronous activity. Since synchronous activity means an infinite velocity, we used the reciprocal velocity for most plots.

The results of this method were compared with the linear pair-wise coherence method, averaged across the number of trials with identical stimulation (Bartlett-smoothing, $N = 50$ trials) and corrected after Benignus for small N (Glaser and Ruchkin, 1976). To be directly comparable to the wave detection method, the square-root is taken for all coherence values.

4.3 Results

4.3.1 γ-coherence decays with distance

Model γ-coherence is high for distances below 2 mm (Fig. 4.3A). The corresponding phase variances (Fig. 4.3B) are small, showing that local groups of neurons are tightly coupled even across trials. For distances beyond 2 mm, phase variances increase quickly. Although distant neurons may be synchronized for short time intervals, these phase relations are neither stable in time nor across trials.

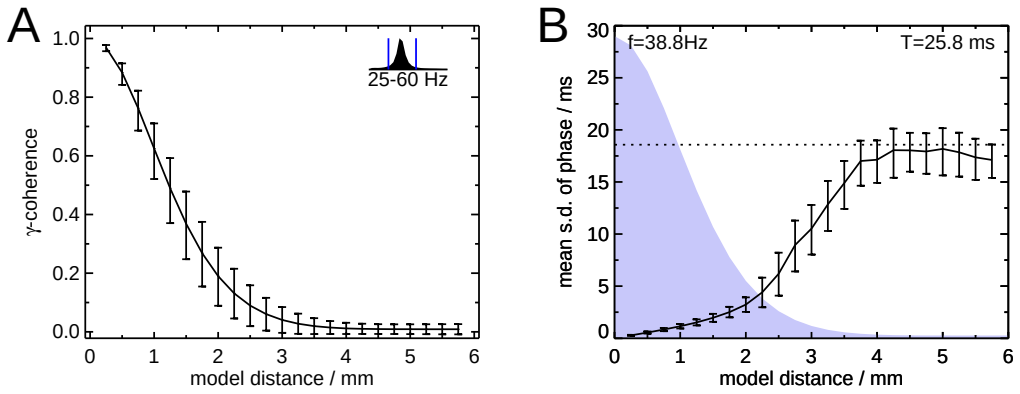

Figure 4.3: *γ-coherence decays with increasing distance due to increasing phase variances.* **A.** Mean γ-coherence drops steeply with increasing distance between pairs of sampling positions (0.5: 1.2 mm, 0.1: 2.3 mm). Local field potentials (25–60 Hz) are derived at 41 linearly arranged sampling positions covering 10 mm in model space. Coherence was calculated for each pair of sampling positions using data from 50 simulation runs with identical stimulus configuration and independent noise. Error bars indicate the mean standard deviation, which is determined, first, by averaging time windows and frequency bins, and second, by averaging electrode combinations showing equal distances. The number of contributing coherence values decreases with increasing distance. **B.** Mean s.d. of phases for pair-wise signals increases with distance up to ≈ 3.5 mm and saturates beyond. Phases are extracted from the spectra and range from $-\pi$ to π. Absolute phase values are transformed to temporal scale using the period of the dominating frequency (here: 38.8 Hz or 25.8 ms for corresponding oscillation period). *Shaded area:* coherence values from the left figure. *Dotted line*: s.d. for uniformly distributed phases (18 ms). Coherence drops down to 0.5 (0.1) for a mean s.d. of 1.6 ms (6.4 ms), corresponding to 6% (36%) of a distribution with uniformly, random phases.

4.3.2 Stimulus-dependent waves

Without stimulation the membrane potentials of all neurons are mostly affected by the dynamic uncorrelated noise fed independently to each neuron. Since this pre-stimulus noise was too weak to evoke high discharge rates, all neurons are near their resting potentials and respond simultaneously to the stimulus (Fig. 4.4). This evokes broad-band activity decaying approximately 200 ms after stimulus onset, introducing a new network state where all membrane potentials exhibit γ-oscillations (Fig. 4.4, top inset). Groups of neighboring neurons form patches of correlated activity with variable spatial extent and duration.

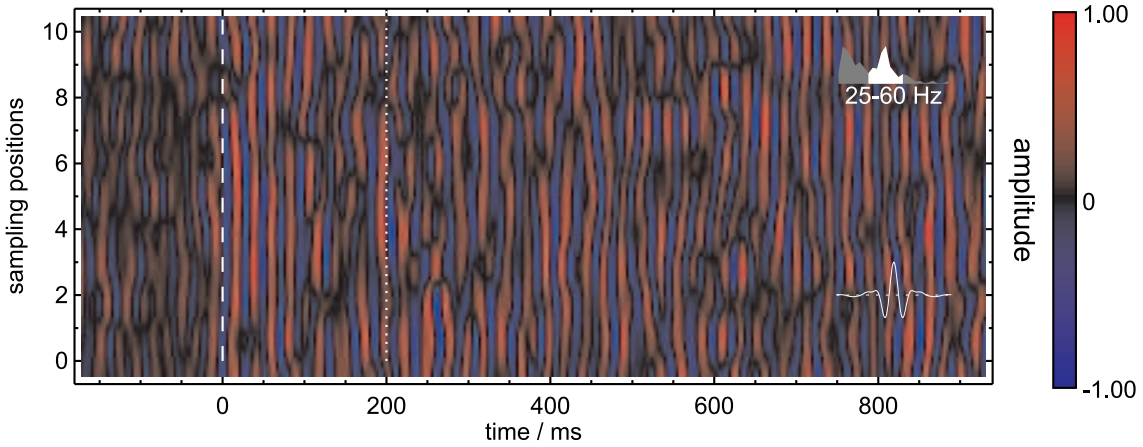

Figure 4.4: *Sample membrane potentials.* Single-trial membrane potentials are obtained from 11 linearly arranged neurons and filtered in the γ-range (25–60 Hz). The stimulus is turned on at $t = 0$ (dashed line). Stimulus locked activity decays approximately after 200 ms (dotted line), followed by spatio-temporal patches of correlated γ-activity. *Top right inset:* average power spectrum of a single unit membrane potential (abscissa: 0–100 Hz). *Bottom right inset:* shape and temporal extent of the filter.

γ-oscillations and their patchy spatio-temporal appearance are much clearer in the corresponding local field potentials (Fig. 4.5A). There are some time intervals, where the maxima of all signals can be aligned to a straight line representing synchrony (e.g., directly after stimulus onset). This event can also be interpreted as a two-dimensional wave of γ-activity traveling perpendicular across the one-dimensional sampling array. It will therefore be termed a γ-*wave*. Velocity and direction of the wave are two-dimensional, but are only measured in direction of the one-dimensional recording array. A sample analysis with the spatio-temporal correlation method (Section 4.2.3) is shown in Fig. 4.5B. We observed extended time intervals, where each time window contained a γ-wave (here: t=450–650 ms). Since the time intervals are much longer than the filter response (t=80 ms covering 0.94 of filter extend) and the duration of the time window (t=30 ms), these periods are no artifact of the evaluation, but a real network effect.

For quantitative analyses, simulations were repeated with identical parameters ($N = 50$) by changing the noise values, but not the underlying noise distribution. It turned out, that γ-waves occur more often with than without stimulation (average γ-wave strength of $\bar{A} = 0.53$ with stimulation compared to $\bar{A} = 0.16$ in the pre-stimulus period, $N = 50$).

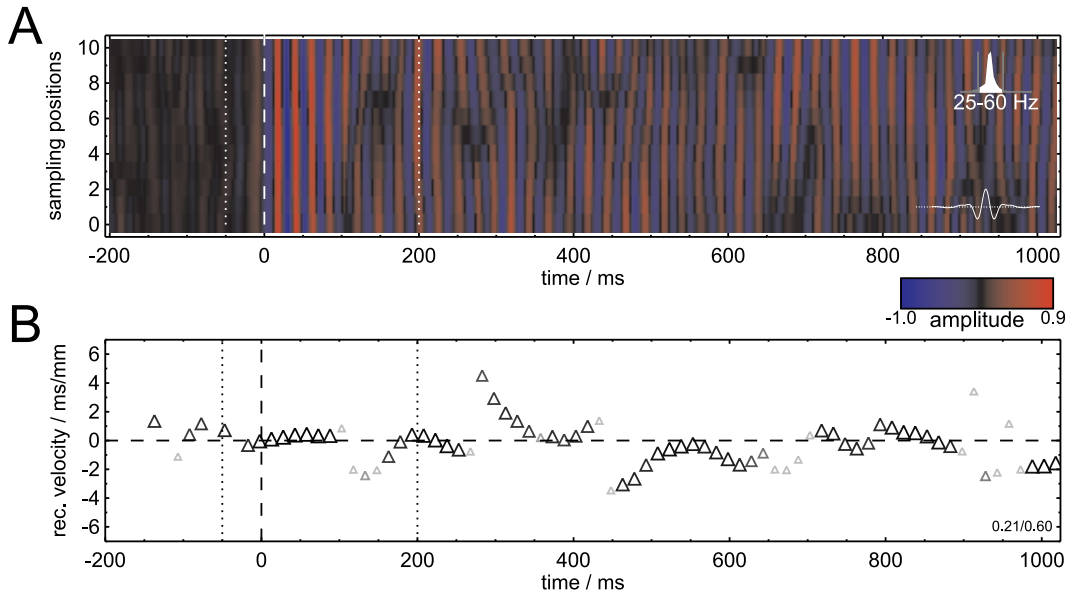

Figure 4.5: *Sample LFPs and γ-wave occurrence in the model.* **A.** Single-trial LFP signals (25–60 Hz) of 11 linearly arranged sampling positions spanning an overall distance of 5 mm in model space. *Top right inset:* average power spectrum of a single local field potential (abscissa: 0–100 Hz). *Bottom right inset:* band-pass filter applied to each LFP. **B.** Occurrence and reciprocal velocity of γ-waves for the signals in *A*. A linear phase relation for all electrodes was required to detect a γ-wave (*triangles*). Symbol size and gray value indicate the correlation strength of the wave detection method. Average γ-wave strength in the pre-stimulus phase was much lower than during stimulation (shown trial: $\bar{A} = 0.21$ compared to $\bar{A} = 0.60$). The γ-wave directly before stimulus onset was due to the band pass filtering of the LFP signal. The dotted region was always excluded from quantitative analyses.

4.3.3 Occurrence and velocity distribution of γ-waves

Before stimulation, model γ-waves occurred rarely ($\bar{A} = 0.16$, Fig. 4.6) and at random times. The wave velocities range from infinity (i.e., synchrony) down to 0.11 m/s (Fig. 4.7). The average reciprocal velocity is approximately zero with a large standard deviation of 1.44 s/m (Fig. 4.7A). When the stimulus was turned on, synchronous (zero phase) γ-waves could be found in nearly every time window ($\bar{A} = 0.81$, $t = -50 \ldots 200$, Fig. 4.6D, 4.7C). This behavior starts even before stimulation (Fig. 4.6), but this is solely due to the temporal extent of the symmetric frequency filter (t=128 ms, Fig. 4.5A, bottom right inset). The variance in the observed velocities (s.d.: 0.80 s/m, Fig. 4.7C) is much lower than in the pre-stimulus phase (s.d.: 1.44 s/m, Fig. 4.7B). After 200 ms, the system's transient response to the stimulus onset has vanished. γ-waves then occurred

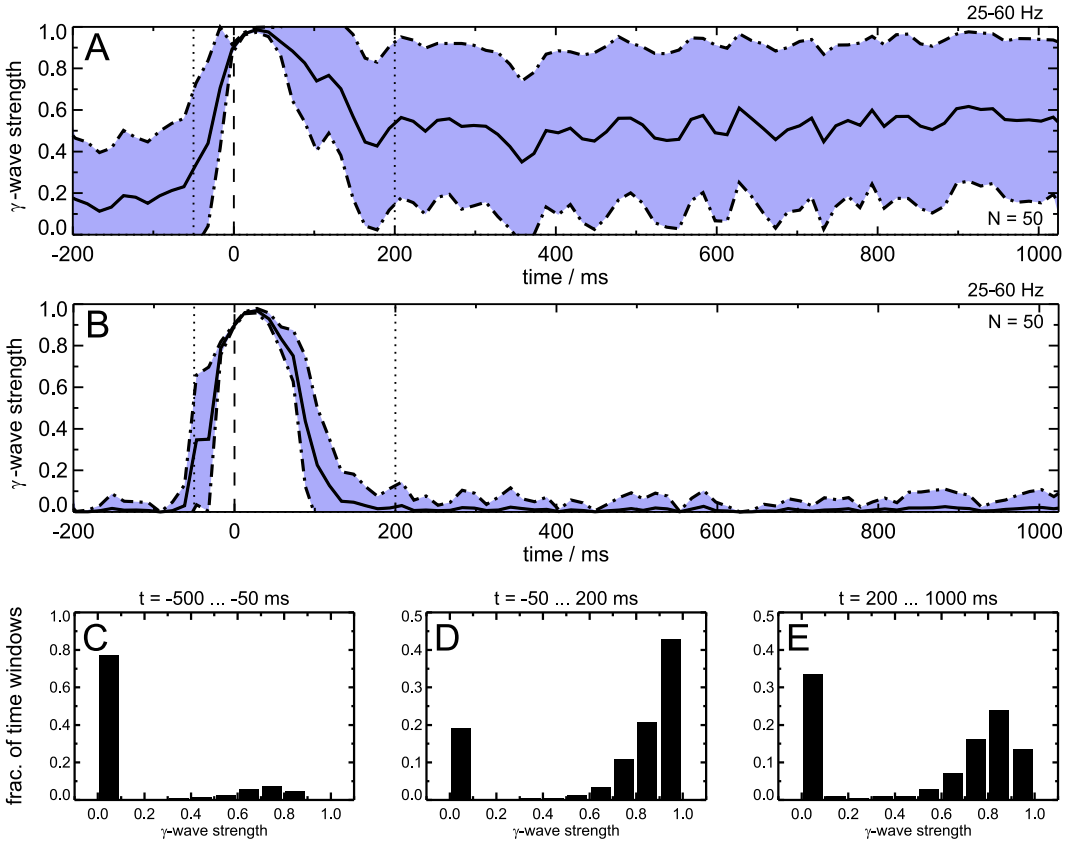

Figure 4.6: *Time-resolved occurrences of γ-waves.* **A.** Average γ-wave occurrence as a function of time (11 electrodes, 5 mm, $N = 50$, s.d.: *dash dotted*). Before stimulation, γ-waves occurred seldom ($\bar{A} = 0.16$) inside the investigated time interval. Beginning with the stimulation at $t = 0$, γ-waves show up in nearly every time window ($\bar{A} = 0.81$), consistently over each trial. Approximately 200 ms after stimulus onset, their occurrence drops down to $\bar{A} = 0.53$ in average, while having a large variance in probability. **B.** Same signals as in A, but mixed between trials (surrogate data), were used to estimate the random occurrence of γ-waves. It shows a strong peak directly after stimulus onset, due to high input correlations. In the tonic phase, random γ-waves are extremely seldom ($\bar{A} < 0.02$). For the three observed time intervals in A, histograms of γ-wave strengths are shown in **C-E**. The left-most bar indicates the relative occurrence for time windows, where no γ-waves were found. Most other events show high correlation values (> 0.5) and are concentrated near the right border of the histogram. This indicates that if a γ-wave was found, it matched an ideal planar wave quite well. The bipartite distributions explain the large s.d. in A.

with an average strength of $\bar{A} = 0.53$ and a constant average reciprocal velocity of zero. In contrast to the stimulus-locked phase, slow traveling waves occur more often (s.d.:

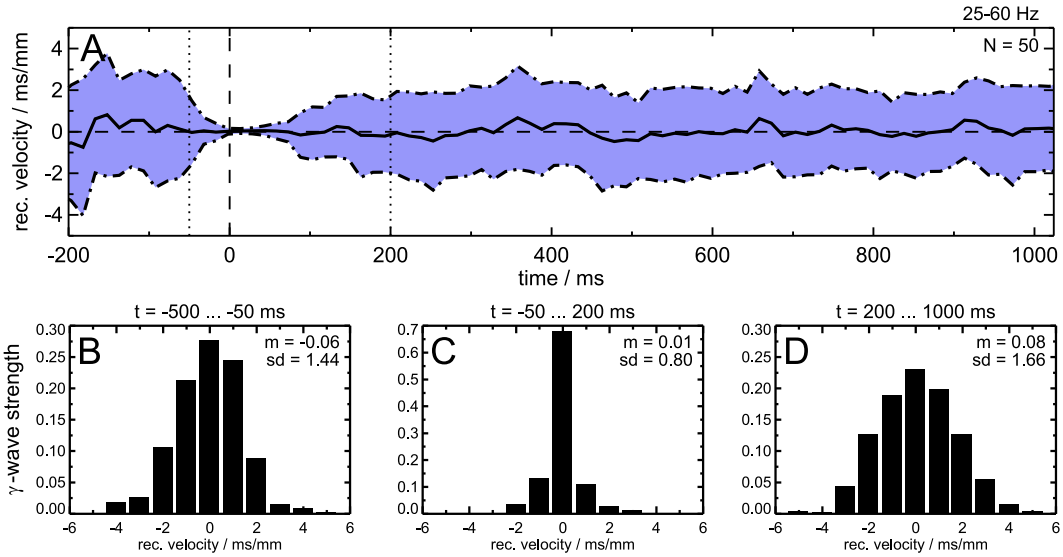

Figure 4.7: *Time-resolved velocities of γ-waves.* **A.** Average γ-wave reciprocal velocities as a function of time (11 electrodes, 5 mm, $N = 50$, s.d.: *dash dotted*). Before stimulation, γ-waves occurred with random velocities. Beginning with the stimulation at $t = 0$, γ-waves showed up nearly synchronously, consistently over each trial. After approximately 200 ms, the variance of the detected reciprocal velocities has nearly reached the pre-stimulus level. The reciprocal velocity distribution is shown for the pre-stimulus (**B**), the stimulus locked (**C**) and the stimulus-induced phase (**D**). Average reciprocal velocity (m) for all three time intervals was nearly zero. Waves with lower velocities occurred with lower probability. The minimal observed velocity was 0.11 m/s. The distributions are nearly symmetric, showing that γ-waves did not prefer any direction.

1.66 s/m, Fig. 4.7D). The lowest observed velocity is 0.11 m/s, which is very similar to the conduction velocity of inhibitory-to-excitatory connections (0.125 m/s).

4.3.4 Spatial properties of γ-waves

All previous analyses were done with a fixed number of LFP sampling positions covering a fixed area of the network. In order to investigate the spatial characteristics of γ-waves, we changed the number of sampling locations, while keeping the distance between adjacent locations constant.

For low distances, the occurrence of γ-waves is maximal (Fig. 4.8A), both for the stimulus and the pre-stimulus period. The γ-wave strength decreases slowly and nearly linear with increasing distance. γ-waves clearly extend as far as 10 mm, the half-height

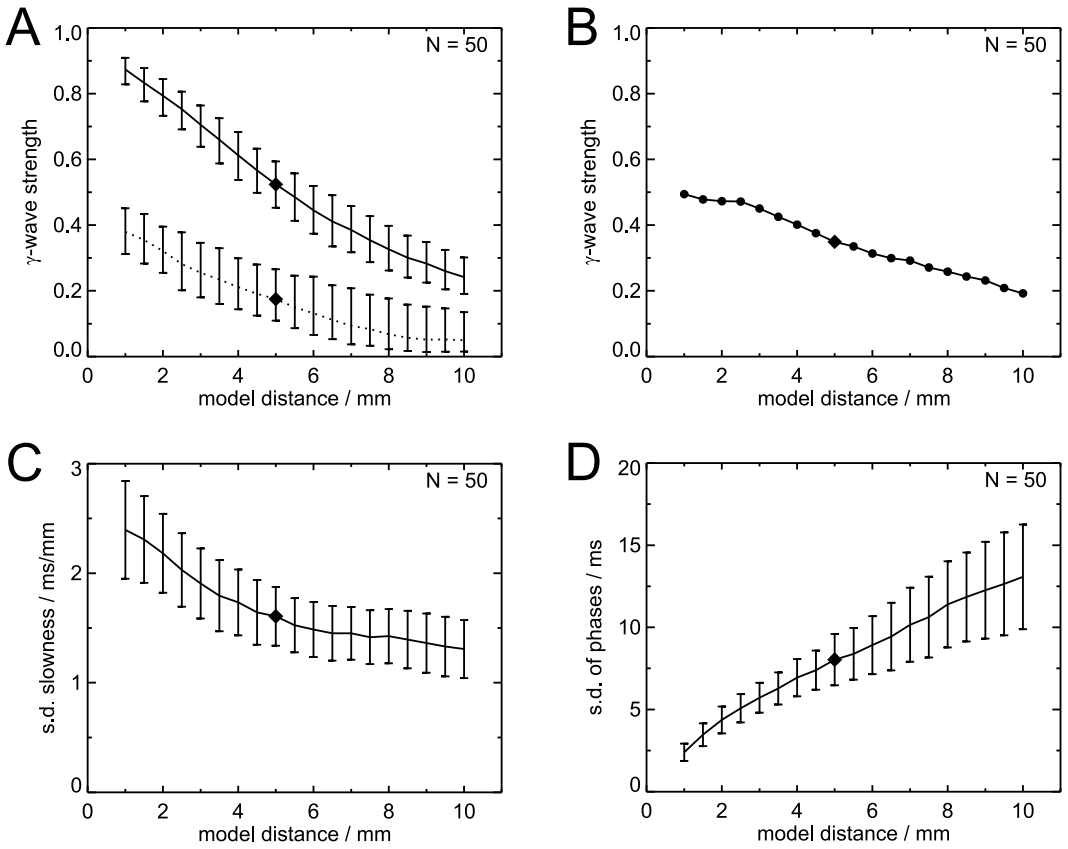

Figure 4.8: *Occurrence of γ-waves dropped slowly with distance.* **A.** γ-waves strength was maximal (≈0.9) for low distances and decayed almost linearly with increasing distance (decay: 0.073/mm). The pre-stimulus γ-wave strength (*dotted line*) for small distances is clearly lower (≈0.4), but decays with a smaller slope (decay: 0.038/mm). **B.** The difference between stimulus and pre-stimulus γ-wave strength decays almost linearly (0.035/mm). **C.** Mean standard deviation of γ-wave reciprocal velocity decreases with distance. **D.** Absolute standard deviation of phase variances increases with distance. *Diamonds* indicate the value that was chosen for all other simulations.

decline with stimulation is 6.3 mm. The spatial decay is 0.073/mm for the stimulus condition and 0.035/mm when subtracting the pre-stimulus occurrence (Fig. 4.8B).

For a fixed distance, the observed reciprocal velocities were distributed around zero with a certain standard deviation (Fig. 4.7). This s.d. decreases with increasing distance (Fig. 4.8C), indicating that more extensive waves showed higher average velocities. The detection of slow waves is limited to velocities that are faster than $v_{\min} = \Delta x/\Delta t$, where Δx indicates the extend of the sampling array, and Δt the duration of the time window. With increasing distance, the minimal detectable velocity also increases. Therefore

slow waves that are well detected using short array lengths, may be missed, when investigating larger distances. However, this does not seem to be relevant here, because the minimal velocity for the largest distance is about 0.33 m/s ($\Delta t = 30$ ms, $\Delta x = 10$ mm), while the respective s.d. of velocities (0.74 m/s, Fig. 4.8C) is clearly above this value.

The average phase differences between both ends of the recording array increases with the size of the array (Fig. 4.8D). They are, however, much smaller than the results obtained for pair-wise signals (Fig. 4.3B).

4.3.5 LFP catchment area

The model LFP is a linear superposition of membrane potentials from neighboring neurons weighted with an exponential spatial decline. The size of this *catchment area* determined the fraction of overlap between adjacent LFP sampling locations.

An increased radius r leads to a higher number of γ-waves, both for the stimulus and the pre-stimulus period (Fig. 4.9). The difference between both conditions increases strongly for small r and saturates for $r > 0.25$ mm. For $r \leq 0.25$ mm, the LFP is mainly determined by few membrane potentials showing a considerable amount of noise that was externally applied to each neuron (Section 3.2.2). Increasing the radius improves the extraction of the local group's common γ-activity in favor of the uncorrelated external noise. LFPs with a very large catchment area integrate membrane potentials all over the network and are therefore less specific to local stimulus properties (not shown). However, they are still selective to global dynamic changes, like the stimulus onset.

4.3.6 Long-range horizontal connections

All previous results were obtained without long-range horizontal modulatory connections. With engaged horizontal connections and using a stimulus that is orthogonal to the preferred orientation of these connections (Fig. 4.1C) reveals nearly the same results as without horizontal connections. This holds for distance and catchment radius dependence for both detection methods, γ-coherence and γ-waves (*diamonds* compared to *triangles* in Fig. 4.10 and 4.11, significance levels: Tab. 4.1B).

The optimal stimulus (Fig. 4.1B) enhanced coherence values slightly (<0.1) showing a weak maximum for a distance of 3.5 mm (Fig. 4.10, left, *squares*). Although barely visible, enhancements are significant for all distances up to 4.5 mm (Tab. 4.1).

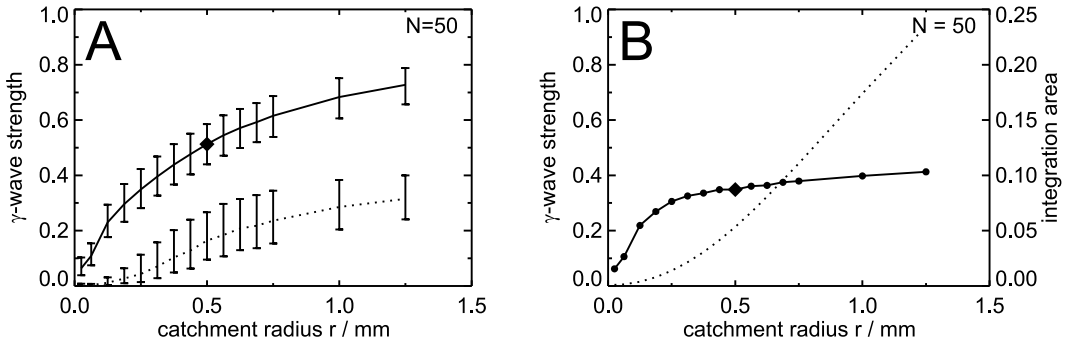

Figure 4.9: *Occurrence of γ-waves depended on LFP catchment radius.* **A.** γ-wave strength increased with increasing catchment radius r for the stimulus and the pre-stimulus condition. Stimulus-related γ-waves increased stronger than the pre-stimulus waves (*dotted*). **B.** Difference of γ-wave strength with and without stimulation increases for larger r. However, the value saturates for $r > 0.25$ mm. The *dotted line* is associated with the right axis and shows the integration area (weighted with the exponential electrode characteristic) of the LFP relative to the area covered by the complete network. *Diamonds* indicate the standard value for this parameter (11 electrodes, 5 mm).

In contrast, γ-waves evoked by the optimal stimulus revealed clearly enhanced occurrences for all distances (Fig. 4.10, right, *squares*). The improvement is most prominent for distances larger than 4 mm, and is significant for all investigated distances (Tab. 4.1B). The half-height decline for the stimulus condition is 15.8 mm compared to 6.3 mm without lateral connections.

The results do not depend on the catchment area of the LFP signals (Fig. 4.11) because the engaged lateral connections improve γ-wave detection equally for all catchment radii $r > 0.1$ mm.

4.4 Discussion

We have presented a neural network model that is capable of producing γ-waves very similar to those found in primary visual cortex of awake monkeys (Gabriel and Eckhorn, 2003; Eckhorn et al., 2004a,b). Their occurrence was sensitive to both, stimulus and network properties as is the case in real recordings. The spatial coupling range indicated by γ-waves surpassed those captured by conventional linear measures (i.e. pairwise coherence, cross-correlation), and extended well beyond the range of horizontal connections.

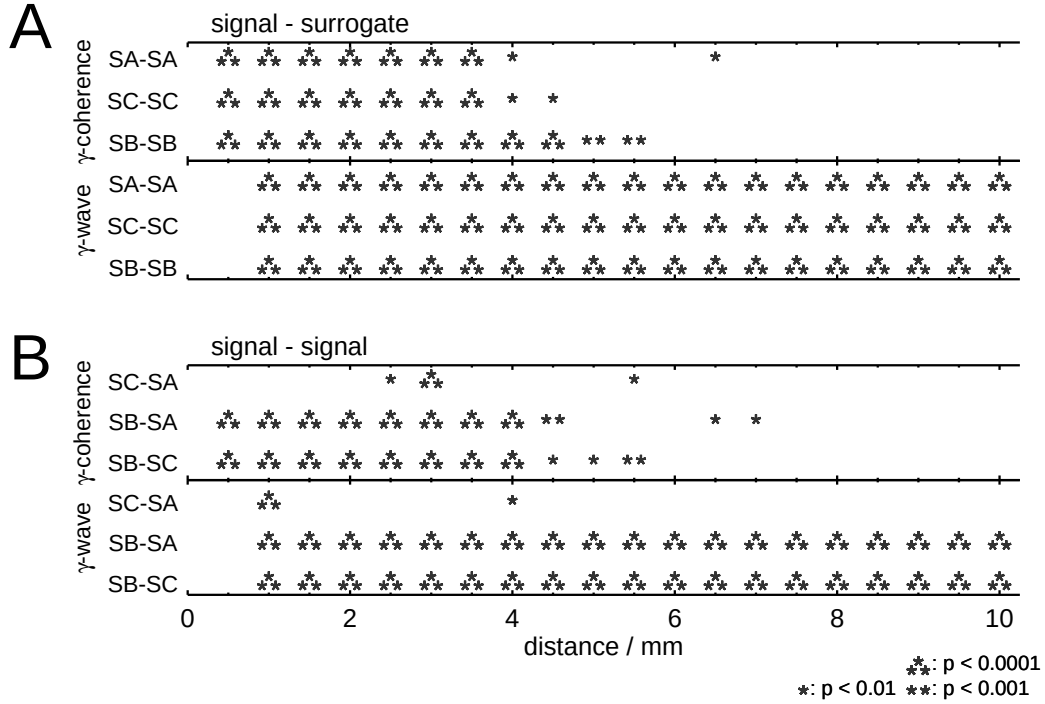

Table 4.1: Mann-Whitney-U-Test on differences between γ-wave strengths. SA,SB,SC: results from scenarios A-C. **A.** The correlation values (γ-coherence, γ-waves) for a specific distance and input-network scenario (SA, SB, SC) are compared to their surrogate counterparts. While coherence breaks down for distances beyond 4 mm, γ-waves occur at higher than chance level up to distances of 10 mm. **B.** Correlation values at a specific distance are compared for different input-network scenarios. For γ-coherence as well as γ-waves, the iso-oriented scenario (SB) reveals higher values than the other two scenarios. There is no clear difference between SA and SC. Similar to *A*, differences in coherence are significant up to 4 mm, while γ-waves in the iso-oriented case (SB) are significantly elevated for all investigated distances. Results were nearly identical when using a T-test with unequal standard deviations (not shown).

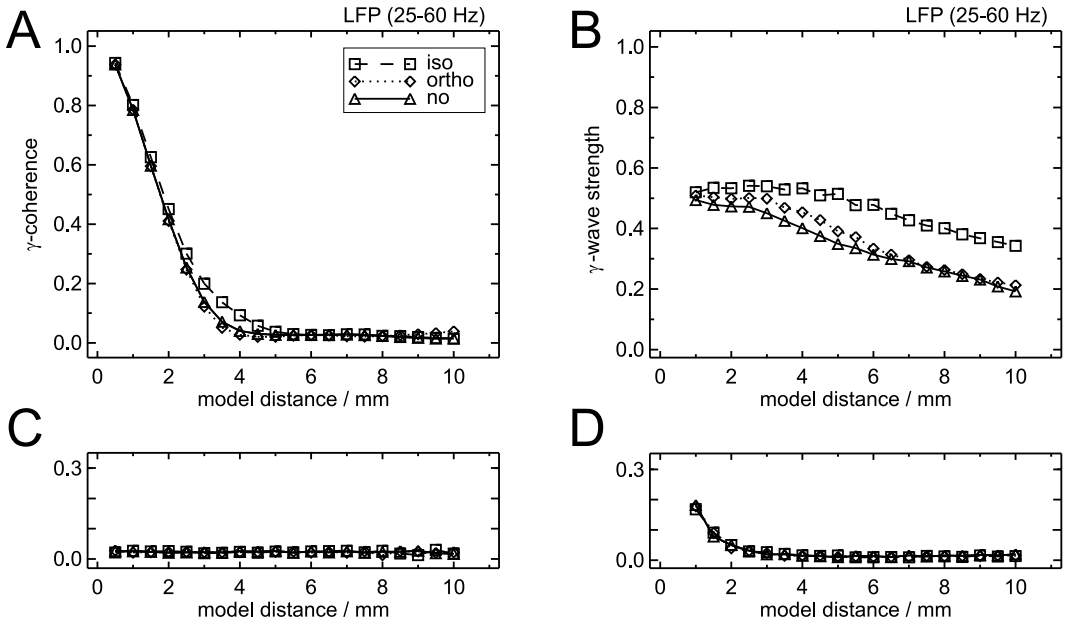

Figure 4.10: *Distance-dependent lateral coupling for γ-coherence and γ-waves.* **A.** γ-coherence quickly decays with increasing distance (half-height decline ≈ 2 mm). Orthogonal lateral connections (*triangles*) did not significantly change the coupling profile, while iso-oriented connections (*squares*) slightly increased coherence up to distances of 4.5 mm. **B.** γ-waves decay slowly with distance (half-height decline > 6 mm). Orthogonal connections enhance occurrences slightly, while iso-oriented connections exhibit most prominent enhancement for each investigated distance ($N = 50$). Surrogate signals, generated by mixing signals of identical recording positions between trials, differed significantly for γ-coherence (**C**, $r \leq 4$ mm) and γ-waves (**D**, see Tab. 4.1 for details).

4.4.1 Binding hypothesis

γ-synchronization was proposed as a possible candidate to solve the binding problem (Reitboeck, 1983; von der Malsburg and Schneider, 1986), i.e., neural groups that represent features of the same object, are supposed to be synchronized, while groups that represent separate objects are desynchronized (Gail et al., 2000). However, recent experiments show that γ-synchronization is restricted to few millimeters in monkey primary visual cortex, even if the representation of the stimulus is much larger (Brosch et al., 1995; Frien and Eckhorn, 2000b). Our previous model investigations revealed that this is due to spatially restricted connectivity and finite conduction velocities (Chapter 3). Accepting the original formulation of the synchronization hypothesis would therefore imply that widely distributed features couldn't be integrated into a single

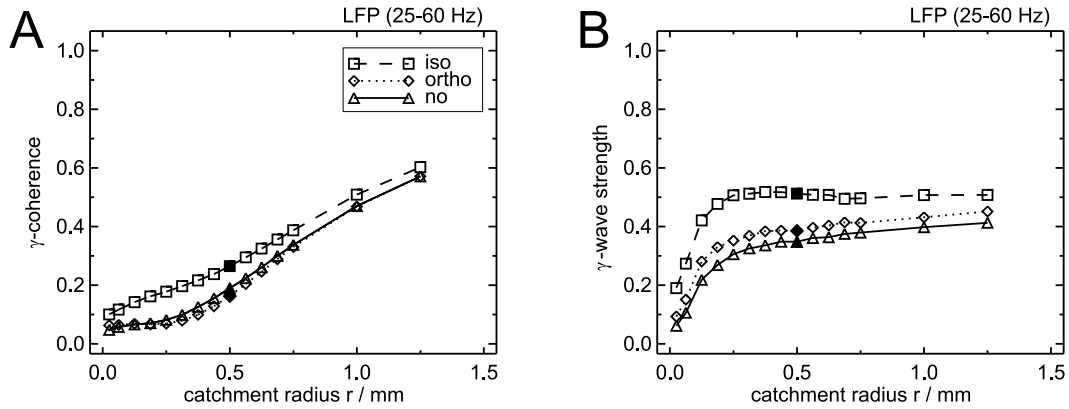

Figure 4.11: *γ-coherence and γ-wave strength depended on LFP catchment radius.* **A.** γ-coherence increases nearly linear with growing catchment radius r. For small r, iso-oriented coupling is larger than orthogonal or no coupling ($N = 50$, 7 electrodes, 3 mm). **B.** γ-wave occurrences quickly increase for low catchment radii and saturate for $r > 0.25$ mm. Filled symbols indicate the standard value for this parameter ($N = 50$, 11 electrodes, 5 mm). Please note, that there is no significant coherence at the standard distance used for γ-wave analyses (5 mm, see Fig. 4.10). The investigated distance for coherence is therefore set smaller, to provide comparable results.

object. This prediction is obviously in conflict with perception. Therefore, we searched for alternative mechanisms and found that γ-waves are well suited to mediate coupling across larger distances.

4.4.2 Stimulus-locked and stimulus-induced γ-waves

Occurrence of γ-waves was markedly increased by the model input and preferentially occurred in the area representing this stimulus. The stimulus transient introduced a correlation between all input signals. This resulted in many, nearly synchronous γ-waves for the restricted time of 100 ms directly after stimulus onset. Before and after this time, input signals were pair-wise uncorrelated. We therefore conclude that γ-waves are emergent properties of the network itself. Most important is the recurrent inhibition, but lateral connections between excitatory neurons also play a role by selectively enlarging the strength of γ-waves.

4.4.3 Spatial properties of γ-waves

In terms of a generalized synchronization hypothesis, the maximal spatial extent of γ-waves limits grouping of features into a unique perception of a visual object. Coherence of LFP signals revealed that coupling dropped quickly with increasing distance (half-height decline: 1.8 mm), comparable to LFP signals from monkey V1 (Gabriel and Eckhorn, 2003: half-height decline 2.5 mm; Frien and Eckhorn, 2000b: decrease to noise level at $\approx$ 6 mm). The extent of model γ-coherence essentially matched the monosynaptic connectivity scheme of the recurrent inhibition in the model (half-height decline: 2 mm[1]). The axonal field of laterally projecting large basket (inhibitory) cells in cat covers a maximal diameter from 1.6 mm (Martin et al., 1983) up to 3 mm (Kisvarday and Eysel, 1993). Assuming reciprocal connectivity between pyramidal and basket cells (Braitenberg and Schüz, 1991) reveals a half-height decline of 1.6 mm up to 3 mm, which is comparable to model assumptions. γ-waves, on the other hand, extend well beyond this limit and cover large distances comparable to the size of the model network (15 mm; Eckhorn et al., 2004a: estimated half-height decline of 9.5 mm in monkey V1).

The differences between the spatial extent of γ-coherence and γ-waves become even larger, when taking into account that low coherence values, as obtained for larger distances, are not reliable because they can easily be obscured by other processes that are not incorporated in our simplified model. On the other hand, the detected model γ-waves are reliable for large distances because the analysis involves signals from multiple channels simultaneously that all have to be linearly correlated. However, the assumption of a linear spatio-temporal correlation is also a strong restriction for the detection of traveling waves. Fig. 4.8C shows, that the propagation velocities of γ-waves increase with their spatial extent. This phenomenon is probably caused by the restrictions of the detection method. It is likely, that the shape of slow large-distance γ-waves is disturbed from the linear structure by noise and therefore not (or seldomly) captured by the γ-wave analysis used here.

Summarizing the observed effects, the spatial extent of γ-coherence is mainly restricted to the area of monosynaptic connections, where phase variances are sufficiently small. It seems to reflect mainly the connection structure of the investigated network.

[1]Both, the excitatory-to-inhibitory and the inhibitory-to-excitatory connections exhibit a half-height decline of 1 mm. The resulting half-height decline is the sum of both, because the distributions are Gaussian.

γ-waves rely on network properties as well, but they are also influenced by the dynamics occurring within the network and can therefore overcome limitations set by restricted network connectivity.

4.4.4 Orientation specificity of lateral coupling

Though our model does not explicitly incorporate orientation selective neurons, we can nevertheless set our results in relation to experimental findings in the primary visual cortex. Long-range horizontal connections link patches of neurons that have similar orientation preferences (Ts'o et al., 1986; Bosking et al., 1997; Angelucci et al., 2002; Chisum et al., 2003). In the model, neural groups with similar orientation preference are simulated in scenario B (Fig. 4.1B1), while dissimilar orientations conform to scenario C (Fig. 4.1C2). In the tree shrew, a collinear arrangement of iso-oriented texture segments (Fig. 4.1B1) evoked higher discharge rates than other stimulus arrangements (Fig. 4.1C1, Chisum et al., 2003). This property is not found in the monkey, where the coupling profiles are nearly symmetric (Angelucci et al., 2002; Stettler et al., 2002) and γ-coupling does not depend on the relative spatial position as long as the distance between recording electrodes and the preferred stimulation at these positions are kept constant (Frien and Eckhorn, 2000b). Hence, stimuli like Fig. 4.1B1 and C1 produce similar coupling profiles in the monkey V1, while they are different in the tree shrew.

Analogous to monkey data, γ-coherence in the model is very similar for scenarios B and C (Fig. 4.10). For short distances, γ-coherence is dominated by the strong inhibitory feedback that acts synchronizing on the excitatory neurons. For intermediate distances (3–5 mm), enabled horizontal connections can enhance γ-coherence slightly. With increasing distance, the enhancement of γ-coherence by horizontal connections is covered by the general decay of coherence that is due to increasing phase variations. Therefore, γ-coherence seems to be an inadequate measure to detect the effects of horizontal connections.

Contrasting this, γ-waves are highly sensitive to horizontal connections for all investigated distances (Fig. 4.11, Tab. 4.1). This is confirmed by Gabriel et al. (2004), showing that LFPs of similar orientation tuning at separate sites are highly correlated by traveling waves.

4.4.5 Model scaling

We have already shown, that the model describes qualitatively several experimental findings. In this section, we will try to map model to cortical dimensions.

The γ-power in the model signals peaks at 39 Hz, while in typical experiments (Frien and Eckhorn, 2000b; Gail et al., 2000) the maxima are usually around 55 Hz, depending on the stimulation. This introduces a temporal scaling factor of 0.71 between both. Comparing the spatial half-height decline of γ-coherence for both introduces a spatial factor of 0.72 (model: 1.8 mm, experiment: 2.5 mm, obtained from Gabriel and Eckhorn, 2003, Fig. 6A), that is very similar to the temporal scaling factor. The decline of γ-wave strength for monkey data (0.05/mm) was obtained from Gabriel and Eckhorn (2003), Fig. 6 and is 0.71 times smaller than in our model data (0.07/mm). Note that the spatial dimension is in the denominator (model decay is larger than experimental decay). The scaling of γ-wave and γ-coherence decline is therefore consistent. As the last quantity, we compare the mean phase variance between model and experiment. From Gabriel and Eckhorn (2003), Fig. 6B, we could determine a value of 0.27 s/m for the mean s.d. of phases (valid between 3 and 7 mm). The model data reveals 0.57 s/m for the adequate spatial scale (valid between 2.2 mm and 5 mm, because of the spatial scaling factor). Both values are related by a factor of 0.69^2. The square respects the different scaling in the temporal and the spatial dimension.

All results are summarized in Tab. 4.2. The model's spatial scale was defined by the range of excitatory and inhibitory connections. Both covered 4 neurons and were set to 1 mm. This mapping could be changed either, by defining, that 4 neurons cover 0.7^{-1}mm or by extending the coupling range to approximately 6 neurons (factor 0.7^{-1}). The model's temporal scale (e.g., oscillation frequency) is mainly determined by the axonal velocity and the inhibitory postsynaptic potential time constant. Adjusting one of theses parameters would allow the model to match experimental data.

In other words, the model quantitatively captures all investigated experimental properties except for a scaling factor. Even this could be reduced to 1, by adjusting some common model parameters within the range of anatomically and physiologically plausible values.

	model	experiment	factor
γ-frequency (main peak)	39 Hz	55 Hz	0.71
γ-coherence (half-height decline)	1.8 mm	2.5 mm	0.72
γ-waves decay	0.07/mm	0.05/mm	$(0.71)^{-1}$
mean s.d. of phase	0.57 s/m	0.27 s/m	$(0.69)^{-2}$

Table 4.2: Comparison of model and experimental properties. The factor indicates the ratio between the respective values. All experimental data are directly taken from Gabriel and Eckhorn (2003) or derived from their Figure 6.

4.4.6 Other models

There are numerous studies dealing with wave-like phenomena in biological models. In one type of investigations (Golomb and Amitai, 1997; Ermentrout, 1998; Bressloff, 1999; Kistler, 2000), the mean membrane potential of contributing neurons is below threshold, i.e. the network is silent if not driven from external sources. Neurons are placed in a one-dimensional chain and are connected by excitatory synapses, exclusively. If a current is applied to neurons at one edge of the network, a slow solitary pulse is traveling across the whole network. The average velocity is in the order of 0.2 m/s (Golomb and Amitai, 1997, Hodgkin-Huxley type models with direct comparisons to data from neocortical slices) and is mainly determined by the synaptic rise time and the number of excitatory postsynaptic potentials required to reach the firing threshold (Ermentrout, 1998; Bressloff, 1999; Kistler, 2000). Adding inhibitory neurons (Kistler, 2000) or extending the network with a second dimension (Bressloff, 1999; Kistler, 2000) does not significantly change the models' properties.

In another type of investigations (e.g., Kistler et al., 1997; Bressloff and Coombes, 1998; Ermentrout and Kleinfeld, 2001), the mean membrane potential of contributing neurons is above threshold, i.e. neurons tend to spike regularly. There are two mechanisms for stable waves. For the first, neurons are weakly coupled and show a slight gradient in their intrinsic oscillation frequencies from one side of the array to the other. Waves are then traveling from the high frequency to the low frequency region. The second mechanism requires neurons to have identical intrinsic oscillation frequencies and an interaction function that is non-zero for neurons that are in phase. The (perfectly) synchronous state is therefore unstable: the slightest noise can push

synchronized neurons out of phase. This last mechanism seems to underly the generation of γ-waves in our model and probably the associated experiments. With finite synaptic rise times as well as axonal and dendritic delays, traveling waves evolve naturally for the underlying architecture.

Although analogies between oscillator and integrate-and-fire neurons are obvious, there are also serious structural differences. Our neurons are no oscillators but fire irregular due to external noise and are therefore more comparable to cortical neurons (Softky and Koch, 1993). Cortical oscillations are a network phenomenon involving many neurons. With the underlying network topology it is not clear, what parts of the network should be defined as oscillators without violating constraints required for the analytical treatments (e.g., weak interaction). A recent study (Cremers and Herz, 2002) shows that, at least for simple networks, both approaches can be mapped by a non-trivial transformation of the synaptic connectivities.

4.4.7 Origin of waves

In contrast to the experiment, the origin of γ-waves is clearer in the model. With disabled lateral connections, neighboring excitatory cells are not directly connected at all. Instead, they share connections from and to a common group of interneurons that indirectly induces coupling between them. This synchronizing effect of inhibition has been described earlier (Ermentrout and Kopell, 1998; Ermentrout et al., 2001; Kopell et al., 2000; Nischwitz and Glünder, 1995; Whittington et al., 1995). However, the range of these inhibitory monosynaptic connections is restricted (model: 1 mm full-width at half-height; maximal diameter 1.6–3 mm, cat, Martin et al., 1983; Kisvarday and Eysel, 1993) and their conduction velocity is slow (model: 0.25 m/s; rat and cat: 0.15–0.6 m/s, Komatsu et al., 1988; Murakoshi et al., 1993; Hirsch and Gilbert, 1991; Nowak and Bullier, 1998). The activation of a single inhibitory neuron seems not sufficient to evoke a wave that propagates widely (>10 mm) and fast (average: 1.25 m/s) across the network. It seems more plausible, that neighboring oscillating local groups, which share a similar driving input are transiently synchronized by their overlap and mutual connectivity. The interaction is locally tight and attenuates with increasing distance, similar to a rubber band. Additional direct connections between the excitatory cells support the coupling due to their larger projection range.

In the current paper, waves of activity were only detected when they showed a linear phase-relation. These are found in several species (review: Ermentrout and Kleinfeld, 2001). Other patterns like rotating waves have also been found in experiments (Prechtl et al., 1997) and models (Kistler et al., 1997). Visual inspection of our two-dimensional model LFP signals does not show other than linear waves. This is most likely due to the bar-like stimulus extending preferentially in one direction. Using two-dimensional stimulation and more complex lateral connections would possibly allow other types of waves. This has to be tested by future investigations.

5 Concluding Remarks

All models presented in the previous chapters deal with the interplay of synchronization and finite spike conduction velocities. In Chapter 2, the refinement of feedforward and lateral connectivity in a model of the developing visual cortex is analyzed. Chapter 3 systematically investigates how delays influence the emergence of γ-oscillations and γ-coherence in a simplified model of a mature visual area. Chapter 4 puts these findings into a broader concept of neural coupling by a quantitative analysis of traveling γ-waves. Detailed discussions can be found in the respective chapters, while this chapter will focus on more comprehensive aspects of this work.

5.1 Development of the visual cortex

Neural activity is essential for the development of synaptic connections in the visual cortex (reviews: Katz and Shatz, 1996; Zhang and Poo, 2001). The change of synaptic strength depends on the relative timing of pre- and postsynaptic potentials in the millisecond range (Markram and Tsodyks, 1996; Bi and Poo, 1998).

In Chapter 2 we could show, that constant axonal conduction velocities can support the development of topographic connections within and between visual processing levels (e.g., V1 and V2). The formation of a single processing stage, i.e. a level of retinotopic representation, occurs in two consecutive steps:

1. Excitatory feedforward connections, that originate from a lower, mature level and terminate in the considered layer, have random efficacies (all-to-all) and one constant axonal velocity. After Hebbian learning using partially synchronized but spatially unstructured input, these connections become topographically organized and spatially restricted.

2. Lateral modulatory connections (all-to-all) within the considered level are modified using the same input and learning rule. The resulting connections have a similar structure as the previously learned feedforward connections. Lateral connections are responsible for increased γ-coherence during normal network operations. Their spatial width determines the width of developing connections that terminate at the next processing level (step 1).

The succession of these two steps is consistent with the experimental finding, that apical (feedforward) dendrites develop before basal (lateral) dendrites (Tyzio et al., 1999; Khazipov et al., 2001). The model additionally proposes a hierarchical development of the visual cortex, since higher processing levels depend on structured input from lower levels. There is experimental evidence for a sequential development of the visual cortex starting in V1, continuing in V2, up to the higher-order regions of the inferior temporal cortex TE (e.g., Condé et al., 1996; review: Guillery, 2005), although there is also evidence for parallel development in other regions of the brain (review: Guillery, 2005).

5.2 Development of inhibitory connections

For the sake of simplicity, inhibitory neurons were completely omitted in the learning model. However, recurrent inhibition as used in Chapters 3 and 4 would not invalidate the results, because its dynamics rarely overlaps with the learning process: inhibitory postsynaptic potentials are solely transmitted by E↔I feedback loops which are slow (E→I: 0.5 m/s, I→E: 0.25 m/s) compared to E↔E (1 m/s) connections. Within an oscillation period, Hebbian learning of E↔E connections would therefore have been completed before inhibition reaches the affected neurons.

A more realistic model would have to incorporate the refinement of connections forming the inhibitory feedback loop (E→I→E). Perez et al. (2001) have shown, that excitatory neurons can induce long-term potentiation (LTP) in mature hippocampal inhibitory interneurons (E→I). In our model, the plasticity of these connection could be implemented with the same learning rule as in Chapter 2, since the underlying neurotransmitters and receptors are identical. The learning process would then be similar to the development of level-1-to-2 connections (Section 2.3.2), resulting in topographically organized receptive fields having a Gaussian weight profile (similar to

Fig. 2.7). Both, long-term depression (LTD) and potentiation of inhibitory transmission in mature pyramidal neurons (I→E) have been reported for several brain regions (Holmgren and Zilberter, 2001, and references therein), including the visual cortex (Komatsu and Iwakiri, 1993). The activation pattern of pre- and postsynaptic neurons seems to be important for these synaptic changes. However, the limited number of reports, different stimulation protocols and the diversity of inhibitory neurons impede the formulation of a general learning rule at present.

The initial development of inhibitory synapses seems to follow a different mechanism: the neurotransmitter GABA that mediates inhibition in mature cortical neurons, is excitatory in the early development as a result of a higher intracellular chloride concentration (review: Ben-Ari, 2002). Furthermore, the release of GABA can induce action potentials and an influx of calcium ions, that is required for long-term learning, i.e., LTP and LTD. The development of these synapses occurs before glutamatergic (excitatory) synapses are functional (e.g., Khazipov et al., 2001; review: Ben-Ari, 2002). Summarizing, the initial development of I→E connections seems to follow common Hebbian laws and takes place before E→I and E↔E connections are functional. A lot of modeling and experimental work remains to be done, before the details of this complex interplay are clarified.

5.3 Delays and γ-coherence

Neural groups that are separated by few millimeters and interact only with excitatory forces, can synchronize in the γ-range with zero delay even in the presence of non-vanishing delays (Ritz et al., 1994; Chapter 3). A closer investigation of cortical (Gabriel and Eckhorn, 2003) and model network dynamics (Chapter 4) shows however, that this finding can be due to temporal averaging. γ-waves are subsequently traveling across the recording positions in random directions, so that phase differences average out. The interplay of γ-coherence and constant transmission velocities influences both, the formation of a topographically organized area and the neural dynamics within it: the size of developing lateral connection profiles (E↔E) increases with the spike transmission velocity. This implicates, that the range of these connections determines the maximal spatial range of γ-coherence in the learned network. To achieve γ-coherence ranges similar to those found in the primary visual cortex, the model predicts that action potentials between excitatory neurons must be conducted with at least 0.5 m/s.

While a fraction of transmission velocities within an area is above this critical value, many connections are slower (Section 1.5). However, studies (review: Nowak and Bullier, 1997) do not reveal the velocity distribution for different types of connections (E→E, E→I, I→E). It is therefore possible that most slow connections are part of the E↔I network, which generates stable γ-oscillations for a wide range of conduction velocities (Chapter 3). The remaining slow connections in the E↔E network would still actively desynchronize the underlying neural populations. This may be a desired property in terms of the binding-by-synchronization hypothesis, e.g., to impede that two conflicting features are bound into the same object representation. Besides, it could be beneficial to impede the early binding of certain neural populations by the use of slow connections, because inadvertently coupled neurons can barely be separated later.

5.4 Interareal connections

While the majority of connections within a visual area is slow (≈ 0.5 m/s, see Section 1.5 for details), feedforward connections between areas have rapid conduction velocities (≈ 3 m/s, review: Nowak and Bullier, 1997). Synchronized γ-activity in lower areas may therefore be transmitted and maintained in higher areas. Several studies are consistent with this view: γ-synchronization between areas was found for neuronal groups in V1 and V2 with overlapping receptive fields (cat: Eckhorn et al., 1988; monkey: Eckhorn, 1994; Frien et al., 1994). In an optical imaging experiment, synchronized γ-activity was observed between three visual areas simultaneously (V1, V2 and V4; Liu et al., 2003).

However, the hierarchical organization of areas (Felleman and van Essen, 1991) does not impose the temporal order in which information is processed (Nowak and Bullier, 1997; Schmolesky et al., 1998). A higher area like MT (V5) can modulate even the earliest responses in lower areas like V1, V2 and V3 (Hupé et al., 2001b). Synchronized γ-activity could therefore as well be transmitted from higher to lower areas.

This idea is supported by the fact that feedback connections share several properties with feedforward connections: first, there is a strong reciprocal connectivity between neural groups of both areas, if their receptive fields are overlapping (review: Salin and Bullier, 1995). Second, transmission velocities of both connection types can have comparable fast transmission velocities (e.g., ≈ 3 m/s between V1 and V2: Nowak and Bullier, 1997; Girard et al., 2001). Correlated activity may therefore not only travel from lower to higher areas but also vice versa. It is therefore likely that synchronized

γ-activity and the more generalized γ-waves do not only occur within one area, but also between several areas. Synchronized γ-activity that occurs with zero phase between V1 and V2 (Frien et al., 1994) may then be due to temporal averaging, similar to the findings within V1 (Gabriel and Eckhorn, 2003).

The significant difference between fast feedforward/feedback connections and slow lateral interactions poses questions on the functional implication. One possible advantage may be to allow neurons in lower areas to integrate information that has already been processed by higher areas. The feedback could be used to modulate the local processing of input signals (models: e.g., Stoecker et al., 1997; Grossberg and Raizada, 2000; Siegel et al., 2000). Since the density of feedforward/feedback connections is at least an order of magnitude smaller than the intraareal connectivity (money, V1 and V2: Stettler et al., 2002), the feedback information cannot be as comprehensive as intraareal information. Yet, the specificity of this feedback is a controversial issue (Angelucci et al., 2002; Stettler et al., 2002; Angelucci and Bullier, 2003) and requires further investigations.

Bibliography

Abeles M (1991) Corticonics: Neural Circuits of the Cerebral Cortex. Cambridge University Press

Agmon-Snir H, Segev I (1993) Signal delay and input synchronization in passive dendritic structures. J Neurophysiol 70:2066–2085

Al-Shaikhli B (2001) Figur/Hintergrund-Trennung durch Signalentkopplung. Diplomarbeit, AG Neurophysik, Marburg

Allman J, Miezin F, McGuinness E (1985) Stimulus specific responses from beyond the classical receptive field: Neurophysiological mechanisms for local-global comparisons in visual neurons. Annu Rev Neurosci 8:407–430

Angelucci A, Bullier J (2003) Reaching beyond the classical receptive field of V1 neurons: horizontal or feedback axons? J Physiol Paris 97:141–154

Angelucci A, Levitt JB, Walton EJS, Hupe JM, Bullier J, Lund JS (2002) Circuits for local and global signal integration in primary visual cortex. J Neurosci 22:8633–8646

Barlow HB (1972) Single units and sensation: A neuron doctrine for perceptual psychology? Perception 1:371–394

Ben-Ari Y (2002) Excitatory actions of GABA during development: The nature of the nurture. Nat Rev Neurosci 3:728–739

Bi Gq, Poo Mm (1998) Synaptic modifications in cultured hippocampal neurons: Dependence on spike timing, synaptic strength and postsynaptic cell type. J Neurosci 18:10464–10472

Bi Gq, Poo Mm (2001) Synaptic modification by correlated activity: Hebb's postulate revisited. Annu Rev Neurosci 24:139–166

Bliss TV, Lømo T (1973) Long-lasting potentiation of synaptic transmission in the dentate area of the anaesthetized rabbit following stimulation of the perforant path. J Physiol 232:331–356

Blossfeldt K (1994) Urformen der Kunst — Wundergarten der Natur. Schirmer-Mosel, München, Paris, London

Booth MCA, Rolls ET (1998) View-invariant representations of familiar objects by neurons in the inferior temporal visual cortex. Cereb Cortex 8:510–523

Bosking WH, Crowley JC, Fitzpatrick D (2002) Spatial coding of position and orientation in primary visual cortex. Nat Neurosci 5:874–882

Bosking WH, Zhang Y, Schofield B, Fitzpatrick D (1997) Orientation selectivity and the arrangement of horizontal connections in tree shrew striate cortex. J Neurosci 17:2112–2127

Braitenberg V, Schüz A (1991) Anatomy of the Cortex. Statistics and Geometry. Springer, Berlin

Bressloff PC (1999) Synaptically generated wave propagation in excitable neural media. Phys Rev Letters 82:2979–2982

Bressloff PC, Coombes S (1998) Traveling waves in a chain of pulse-coupled oscillators. Phys Rev Letters 80:4815–4818

Bringuier V, Chavane F, Glaeser L, Frégnac Y (1999) Horizontal propagation of visual activity in the synaptic integration field of area 17 neurons. Science 283:695–699

Brosch M, Bauer R, Eckhorn R (1995) Synchronous high-frequency oscillations in cat area 18. Eur J Neurosci 7:86–95

Brosch M, Bauer R, Eckhorn R (1997) Stimulus-dependent modulations of correlated high-frequency oscillations in cat visual cortex. Cereb Cortex 7:70–76

Bruns A, Eckhorn R (2004) Task-related coupling from high- to low-frequency signals among visual cortical areas in human subdural recordings. Int J Psychophysiol 51:97–116

Bush P, Sejnowski T (1996) Inhibition synchronizes sparsely connected cortical neurons within and between columns in realistic network models. J Comput Neurosci 3:91–110

Castelo-Branco M, Goebel R, Neuenschwander S, Singer W (2000) Neural synchrony correlates with surface segregation rules. Nature 405:685–689

Chapman B, Gödeke I, Bonhoeffer T (1999) Development of orientation preference in the mammalian visual cortex. J Neurobiol 41:18–24

Chisum HJ, Mooser F, Fitzpatrick D (2003) Emergent properties of layer 2/3 neurons reflect the collinear arrangement of horizontal connections in tree shrew visual cortex. J Neurosci 23:2947–2960

Condé F, Lund JS, Lewis DA (1996) The hierarchical development of monkey visual cortical regions as revealed by the maturation of parvalbumin-immunoreactive neurons. Dev Brain Res 96:261–276

Crair MC, Gillespie DC, Stryker MP (1998) The role of visual experience in the development of columns in cat visual cortex. Science 279:566–570

Cremers D, Herz AVM (2002) Traveling waves of excitation in neural field models: Equivalence of rate descriptions and integrate-and-fire dynamics. Neural Comput 14:1651–1667

Crook SM, Ermentrout GB, Vanier MC, Bower JM (1997) The role of axonal delay in the synchronization of networks of coupled coritcal oscillators. J Comput Neurosci 4:161–172

Dicke PW (1992) Simulation dynamischer Merkmalskopplungen in einem neuronalen Netzwerkmodell. Ph.D. thesis, Marburg

Eckhorn R (1994) Oscillatory and non-oscillatory synchronizations in the visual cortex and their possible roles in associations of visual features. In: van Pelt J, Corner MA, Uylings HBM, Lopes da Silva FH (eds.), *The Self-Organizing Brain*, vol. 102, pp. 405–426, Progress in Brain Research

Eckhorn R (1999) Neural mechanisms of scene segmentation: Recordings from the visual cortex suggest basic circuits for linking field models. IEEE Neural Networks 10:464–479

Eckhorn R, Bauer R, Jordan W, Brosch M, Kruse W, Munk M, Reitboeck H (1988) Coherent oscillations: A mechanism of feature linking in the visual cortex? Biol Cybern 60:121–130

Eckhorn R, Bruns A, Saam M, Gail A, Gabriel A, Brinksmeyer HJ (2001a) Flexible cortical gamma-band correlations suggest neural principles of visual processing. Vis Cog 8:519–530

Eckhorn R, Gail A, Al-Shaikhli B, Gabriel A, Brinksmeyer HJ, Saam M, Bruns A (2001b) Bindung und Trennung von Flächen — unterstützt durch Signal-Korrelation und -Entkopplung im primären Sehkortex wacher Affen: Physiologie und Modellierung. In: Bülthoff HH, Gegenfurtner KR, Mallot HA, Ulrich R (eds.), *TWK 2001, Beiträge zur 4. Tübinger Wahrnehmungskonferenz*, p. 44, Knirsch Verlag, Kirchentellinsfurt

Eckhorn R, Gail A, Bruns A, Gabriel A, Al-Shaikhli B, Saam M (2004a) Different types of signal coupling in the visual cortex. IEEE T Neural Networ 15:1039–1052

Eckhorn R, Gail A, Bruns A, Gabriel A, Al-Shaikhli B, Saam M (2004b) Neural mechanisms of visual associative processing. Acta Neurobiol Exp 64:239–252

Eckhorn R, Reitboeck H, Arndt M, Dicke P (1990) Feature linking via synchronization among distributed assemblies: Simulations of results from cat visual cortex. Neural Comput 2:293–307

Engel AK, König P, Kreiter AK, Singer W (1991a) Interhemispheric synchronization of oscillatory neuronal responses in cat visual cortex. Science 252:1177–1179

Engel AK, König P, Singer W (1991b) Direct physiological evidence for scene segmentation by temporal coding. P Natl Acad Sci USA 88:9136–9140

Ermentrout B (1998) The analysis of synaptically generated traveling waves. J Comput Neurosci 5:191–208

Ermentrout B, Pascal M, Gutkin B (2001) The effects of spike frequency adaptation and negative feedback on the synchronization of neural oscillators. Neural Comput 13:1285–1310

Ermentrout GB, Kleinfeld D (2001) Traveling electrical waves in cortex: Insights from phase dynamics and speculation on a computational role. Neuron 29:33–44

Ermentrout GB, Kopell N (1998) Fine structure of neural spiking and synchronization in the presence of conduction delays. P Natl Acad Sci USA 95:1259–1264

Ernst U, Pawelzik K, Geisel T (1995) Synchronization induced by temporal delays in pulse-coupled oscillators. Phys Rev Letters 74:1570–1573

Eurich CW, Pawelzik K, Ernst U, Cowan JD, Milton JG (1999) Dynamics of self-organized delay adaptation. Phys Rev Letters 82:1594–1597

Felleman DJ, van Essen DC (1991) Distributed hierarchical processing in the primate cerebral cortex. Cereb Cortex 1:1–47

Ferster D, Chung S, Wheat H (1996) Orientation selectivity of thalamic input to simple cells of cat visual cortex. Nature 380:249–252

Fox K, Daw N (1992) A model for the action of NMDA conductances in the visual cortex. Neural Comput 4:59–83

Fox K, Sato H, Daw NW (1989) The location and function of NMDA receptors in cat and kitten visual cortex. J Neurosci 9:2443–2454

Freeman WJ (1978) Spatial properties of an EEG event in the olfactory bulb and cortex. Electroencephalography and Clinical Neurophysiology 44:586–605

Frien A, Eckhorn R (2000a) Fast oscillations display sharper orientation tuning than slower components of the same recordings in striate cortex of awake monkey. Eur J Neurosci 12:1453–1465

Frien A, Eckhorn R (2000b) Functional coupling shows stronger stimulus dependency for fast oscillations than for low-frequency components in striate cortex of awake monkey. Eur J Neurosci 12:1466–1478

Frien A, Eckhorn R, Bauer R, Woelbern T, Kehr H (1994) Stimulus-specific fast oscillations at zero phase between visual areas V1 and V2 of awake monkey. NeuroReport 5:2273–2277

Gabriel A, Eckhorn R (2003) A multi-channel correlation method detects traveling γ-waves in monkey visual cortex. J Neurosci Methods 131:171–184

Gabriel A, Gail A, Eckhorn R (2004) Traveling γ-waves: New insights into coupling processes in visual texture coding. Ph.D. thesis, Philipps Universität, Marburg

Gail A, Brinksmeyer HJ, Eckhorn R (2000) Contour decouples gamma activity across texture representation in monkey striate cortex. Cereb Cortex 10:840–850

Gerstner W, Kempter R, van Hemmen JL, Wagner H (1996a) A neuronal learning rule for sub-millisecond temporal coding. Nature 383:76–78

Gerstner W, van Hemmen JL, Cowan JD (1996b) What matters in neural locking? Neural Comput 8:1653–1676

Gilbert CD (1983) Microcircuitry of the visual cortex. Annu Rev Neurosci 6:217–247

Gilbert CD, Wiesel TN (1979) Morphology and intracortical projections of functionally characterised neurones in the cat visual cortex. Nature 280:120–125

Gilbert CD, Wiesel TN (1983) Clustered intrinsic connections in cat visual cortex. J Neurosci 3:1116–1130

Gilbert CD, Wiesel TN (1989) Columnar specifity of intrinsic horizontal and corticocortical connections in cat visual cortex. J Neurosci 9:2432–2442

Girard P, Hupé JM, Bullier J (2001) Feedforward and feedback connections between areas V1 and V2 of the monkey have similar rapid conduction velocities. J Neurophysiol 85:1328–1331

Glaser EM, Ruchkin DS (1976) Principles of Neurobiological Signal Analysis. Academic Press

Godeke I, Bonhoeffer T (1996) Development of identical orientation maps for two eyes without common visual experience. Nature 379:251–254

Golledge HDR, Panzeri S, Zheng F, Pola G, Scannell JW, Giannikopoulos DV, Mason RJ, Tovée MJ, Young MP (2003) Correlations, feature-binding and population coding in primary visual cortex. NeuroReport 14:1045–1050

Golomb D, Amitai Y (1997) Propagating neuronal discharges in neocortical slices: Computational and experimental study. J Neurophysiol 78:1199–1211

Gray C, König P, Engel A, Singer W (1989) Oscillatory responses in cat visual cortex exhibit inter-columnar synchronization which reflects global stimulus properties. Nature 338:334–337

Gray CM (1999) The temporal correlation hypothesis of visual feature integration. Neuron 24:31–47

Gray CM, Maldonado PE, Wilson M, McNaughton B (1995) Tetrodes markedly improve the reliability and yield of multiple single-unit isolation from multi-unit recordings in cat striate cortex. J Neurosci Methods 63:43–54

Grinvald A, Lieke EE, Frostig RD, Hildesheim R (1994) Cortical point-spread function and long-range lateral interactions revealed by real-time optical imaging of macaque monkey primary visual cortex. J Neurosci 14:2545–2568

Grossberg S, Raizada RDS (2000) Contrast-sensitive perceptual grouping and object-based attention in the laminar circuits of primary visual cortex. Vision Res 40:1413–1432

Guillery RW (2005) Is postnatal neocortical maturation hierarchical? Trends Neurosci 28:512–517

Hebb DO (1949) The organization of behavior. Wiley, New York

Hirsch JA, Gilbert CD (1991) Synaptic physiology of horizontal connections in the cat's visual cortex. J Neurosci 11:1800–1809

Holmgren CD, Zilberter Y (2001) Coincident spiking activity induces long-term changes in inhibition of neocortical pyramidal cells. J Neurosci 21:8270–8277

Horton JC, Hocking DR (1996) An adult-like pattern of ocular dominance columns in striate cortex of newborn monkeys prior to visual experience. J Neurosci 16:1791–1807

Houzel JC, Milleret C, Innocenti G (1994) Morphology of callosal axons interconnecting areas 17 and 18 of the cat. Eur J Neurosci 6:898–917

Hubel D (1982) Exploration of the primary visual cortex, 1955-78. Nature 299:515–524

Hubel DH, Wiesel TN (1959) Receptive fields of single neurones in the cat's striate cortex. J Physiol 148:574–591

Hubel DH, Wiesel TN (1962) Receptive fields, binocular interaction, and functional architecture in the cat's visual cortex. J Physiol 160:106–123

Hubel DH, Wiesel TN (1965) Binocular interaction in striate cortex of kittens reared with artificiak squint. J Neurophysiol 28:1041–1059

Hubel DH, Wiesel TN (1970) The period of susceptibility to the physiological effects of unilateral eye closure in kittens. J Physiol 206:419–436

Hubel DH, Wiesel TN (1974) Uniformity of monkey striate cortex: A parallel relationship between field size, scatter and magnification factor. J Comput Neurosci 158:295–305

Hüning H, Glünder H, Palm G (1998) Synaptic delay learning in pulse-coupled neurons. Neural Comput 10:555–565

Hupé JM, James AC, Girard P, Bullier J (2001a) Response modulations by static texture surround in area V1 of the macaque monkey do not depend on feedback connections from V2. J Neurophysiol 85:146–163

Hupé JM, James AC, Girard P, Lomber SG, Payne BR, Bullier J (2001b) Feedback connections act on the early part of the responses in monkey visual cortex. J Neurophysiol 85:134–145

Hupé JM, James AC, Payne BR, Lomber SG, Girard P, Bullier J (1998) Cortical feedback improves discrimination between figure and background by V1, V2 and V3 neurons. Nature 394:784–787

Juergens E, Eckhorn R (1997) Parallel processing by a homogenous group of coupled model neurons can enhance, reduce and generate signal correlations. Biol Cybern 76:202–208

Katz LC, Shatz CJ (1996) Synaptic activity and the construction of cortical circuits. Science 274:1133–1138

Kempter R, Gerstner W, van Hemmen JL (1999) Hebbian learning and spiking neurons. Phys Rev E 59:4498–4514

Khazipov R, Esclapez M, Caillard O, Bernard C, Khalilov I, Tyzio R, Hirsch J, Dzhala V, Berger B, Ben-Ari Y (2001) Early development of neuronal activity in the primate hippocampus in utero. J Neurosci 21:9770–9781

Kistler WM (2000) Stability properties of solitary waves and periodic wave trains in a two-dimensional network of spiking neurons. Phys Rev E 62:8834–8837

Kistler WM, Seitz R, van Hemmen JL (1997) Modelling collective excitations in cortical tissue. Physica D 114:273–295

Kisvàrday ZF, Beaulieu C, Eysel UT (1993) Network of GABAergic large basket cells in cat visual cortex (area 18): Implication for lateral disinhibition. J Comp Neurol 327:398–415

Kisvarday ZF, Eysel UT (1993) Functional and structural topography of horizontal inhibitory connections in cat visual cortex. Eur J Neurosci 5:1558–1572

Kisvàrday ZF, Martin KAC, Freund TF, Maglóczky Z, Whitteridge D, Somogyi P (1986) Synaptic targets of HRP-filled layer III pyramidal cells in the cat striate cortex. Exp Brain Res 64:541–552

Kisvàrday ZF, Tóth E, Rausch M, Eysel UT (1997) Orientation-specific relationship between populations of excitatory and inhibitory lateral connections in the visual cortex of the cat. Cereb Cortex 7:605–618

Koffka K (1935) Principles of Gestalt Psychology. Lund Humphries, London

Kohonen T (1984) Self-organization and associative memory. Springer, Berlin

Komatsu Y, Iwakiri M (1993) Long-term modification of inhibitory synaptic transmission in developing visual cortex. NeuroReport 4:907–910

Komatsu Y, Nakajima S, Toyama K, Fetz EE (1988) Intracortical connectivity revealed by spike-triggered averaging in slice preparations of cat visual cortex. Brain Res 442:359–362

König P, Engel A, Roelfsema P, Singer W (1995) How precise is neuronal synchronization? Neural Comput 7:469–485

Kopell N, Ermentrout GB, Whittington MA, Traub RD (2000) Gamma rhythms and beta rhythms have different synchronization properties. P Natl Acad Sci USA 97:1867–1872

Kreiter A, Singer W (1992) Oscillatory neuronal responses in the visual cortex of the awake macaque monkey. Eur J Neurosci 4:369–375

Kreiter AK, Singer W (1996) Stimulus dependent synchronization of neuronal responses in the visual cortex of the awake macaque monkey. J Neurosci 16:2381–2396

Krüger J, Aiple F (1988) Multimicroelectrode investigation of monkey striate cortex: spike train correlations in the infragranular layers. J Neurophysiol 60:798–828

Kuramato Y (1984) Chemical Oscillations, Waves and Turbulence. Springer, New York

Kuramato Y (1991) Collective synchronization of pulse-coupled oscillators and excitable units. Physica D 50:15–30

Liu GB, Zhang Y, Pettigrew JD, Xu WF, Lib CY (2003) Spreading and synchronization of intrinsic signals in visual cortex of macaque monkey evoked by a localized visual stimulus. Brain Res 985:13–20

Livingstone MS (1996) Oscillatory firing and interneuronal correlations in squirrel monkey striate cortex. J Neurophysiol 75:2467–2485

Llampl I, Reichova I, Ferster D (1999) Synchronous membrane potential fluctuations in neurons of the cat visual cortex. Neuron 22:361–374

Magee J, Johnston D (1997) A synaptically controlled, associative signal for hebbian plasticity in hippocampal neurons. Science 275:209–212

Malach R, Amir Y, Harel M, Grinvald A (1993) Relationship between intrinsic connections and functional architecture revealed by optical imaging and in vivo targeted biocytin injections in primate striate cortex. P Natl Acad Sci USA 90:10469–10473

Margulis M, Tang CM (1998) Temporal integration can readily switch between sublinear and supralinear summation. J Neurophysiol 79:2809–2813

Markram H, Lübke J, Frotscher M, Sakmann B (1997) Regulation of synaptic efficiacy by coincidence of postsynaptic APs and EPSPs. Science 275:213–215

Markram H, Tsodyks M (1996) Redistribution of synaptic efficacy between neocortical pyramidal neurons. Nature 382:807–810

Martin KA, Whitteridge D (1984) Form, function and intracortical projections of spiny neurones in the striate cortex of the cat. J Physiol 353:463–504

Martin KAC, Somogyi P, Whitteridge D (1983) Physiological and morphological properties of identified basket cells in the cat's visual cortex. Exp Brain Res 50:193–200

McGuire BA, Gilbert CD, Rivlin PK, Wiesel TN (1991) Targets of horizontal connections in macaque primary visual cortex. J Comp Neurol 305:370–392

Meister M, Wong ROL, Baylor DA, Shatz CJ (1991) Synchronous bursts of action potentials in ganglion cells of the developing mammalian retina. Science 17:939–943

Michalski A, Gerstein GL, Czarkowska J, Tarneki R (1983) Interactions between cat striate cortex neurons. Exp Brain Res 51:97–107

Mignard M, Malpeli JG (1991) Paths of information flow through visual cortex. Science 251:1249–1251

Miller KD (1994) A model for the development of simple cell receptive fields and the ordered arrangement of orientation columns through activity-dependent competition between ON- and OFF-center inputs. J Neurosci 14:409–441

Milner PM (1974) A model for visual shape recognition. Psychol Rev 81:521–535

Mirollo RE, Strogatz SH (1990) Synchronization of pulse-coupled biological oscillators. SIAM J Appl Math 50:1645–1662

Mitzdorf U (1985) Current source-density method and application in cat cerebral cortex: Investigation of evoked potentials and EEG phenomena. Physiological Reviews 65

Miyashita M, Kim D, Tanaka S (1997) Cortical direction selectivity without directional experience. NeuroReport 8:1187–1191

Murakoshi T, Guo JZ, Ichinose T (1993) Electrophysiological identification of horizontal synaptic connections in rat visual cortex in vitro. Neurosci Lett 163:211–214

Nelson JI, Frost BJ (1985) Intracortical facilitation among co-orientated co-axially aligned simple cells in cat striate cortex. Exp Brain Res 61:54–61

Nischwitz A, Glünder H (1995) Local lateral inhibition: a key to spike synchronization? Biol Cybern 73:389–400

Nowak LG, Bullier J (1997) The timing of information in the visual system. In: Rockland, et al. (eds.), *Cerebral Cortex*, vol. 12, pp. 205–243, Plenum Press, New York

Nowak LG, Bullier J (1998) Axons, but not cell bodies, are activated by electrical stimulation in cortical gray matter: I. Evidence from chronaxie measurements. Exp Brain Res 118:477–488

Palanca BJA, DeAngelis GC (2005) Does neuronal synchrony underlie visual feature grouping? Neuron 46:333–346

Penn AA, Shatz CJ (1999) Brain waves and brain wiring: the role of endogenous and sensory-driven neural activity in development. Pediatr Res 45:447–458

Penn AA, Wong ROL, Shatz CJ (1994) Neuronal coupling in the developing mammalian retina. J Neurosci 14:3805–3815

Perez Y, Morin F, Lacaille JC (2001) A hebbian form of long-term potentiation dependent on mGluR1a in hippocampal inhibitory interneurons. P Natl Acad Sci USA 98:9401–9406

Phillips WA, Singer W (1997) In search of common foundations for cortical computation. Behav Brain Sci 20:657–722

Polsky A, Mel BW, Schiller J (2004) Computational subunits in thin dendrites of pyramidal cells. Nat Neurosci 7:621–627

Prechtl JC, Cohen LB, Mitra PP, Pesaran B, Kleinfeld D (1997) Visual stimuli induce waves of electrical activity in turtle cortex. P Natl Acad Sci USA 94:7621–7626

Rall W (1962) Electrophysiology of a dendritic neuron model. Biophys J 2:145–167

Reid RC, Alonso JM (1995) Specifity of monosynaptic connections from thalamus to visual cortex. Nature 378:281–284

Reitboeck HJ (1983) A multi-electrode matrix for studies of temporal signal correlations within neural assemblies. In: Basar E (ed.), *Synergetics of the Brain*, pp. 174–182, Springer, Berlin

Riesenhuber M, Poggio T (1999) Are cortical models really bound by the "binding problem"? Neuron 24:87–93

Ritz R, Gerstner W, Fuentes U, van Hemmen JL (1994) A biologically motivated and analytically soluble model of collective oscillations in the cortex, II. Application to binding and pattern segmentation. Biol Cybern 71:349–358

Rockland KS, Lund JS (1982) Widespread periodic intrinsic connections in the tree shrew visual cortex. Science 215:1532–1534

Roelfsema PR, Lamme VAF, Spekreijse H (2004) Synchrony and covariation of firing rates in the primary visual cortex during contour grouping. Nat Neurosci 7:982–991

Roerig B, Chen B (2002) Relationships of local inhibitory and excitatory circuits to orientation preference maps in ferret visual cortex. Cereb Cortex 12:178–198

Rushton WA (1951) A theory of the effects of fibre size in medullated nerve. J Physiol 115:101–122

Saam M, Eckhorn R (1998a) Width of association field in topographic neural map depends on lateral spike velocity and temporal dispersion of correlated input: A learning model with spiking neurons. In: Elsner N, Wehner R (eds.), *Proceedings of the 26th Göttingen Neurobiology Conference*, vol. 2, p. 767, Georg Thieme Verlag

Saam M, Eckhorn R (1998b) Width of association fields in visual cortex is influenced during hebbian learning by signal correlation among inputs and lateral spike velocity: A network model with spiking neurons. In: Lachnit H, Jacobs A, Roesler F (eds.), *Experimentelle Psychologie*, p. 298, Pabst Science Publishers

Saam M, Eckhorn R (1999) Spatial range of synchronization determines width of classical receptive field at next level of visual processing: A model with hebbian learning and spiking neurons. In: Elsner N, Eysel U (eds.), *Proceedings of the 27th Göttingen Neurobiology Conference*, vol. 2, p. 484, Georg Thieme Verlag

Saam M, Eckhorn R (2000) Lateral spike conduction velocity in the visual cortex affects spatial range of synchronization and receptive field size without visual experience: A learning model with spiking neurons. Biological Cybernetics 83:L1–L9

Saam M, Eckhorn R, Schanze T (1999) Spatial range of synchronization in visual cortex is determined by lateral conduction velocity and determines RF-Size at next processing level. In: *Society for Neuroscience, Abstracts*, vol. 25, part 1, p. 678

Saam M, Gabriel A, Al-Shaikhli B, Eckhorn R (2000) Neural mechanisms of figure-ground segregation: Recordings from awake monkey and a model with spiking neurons. In: Freska C (ed.), *Dynamische Perzeption*, vol. 9 of *Proceedings in Artificial Intelligence*, pp. 27–32, Baratoff G, Neumann H, infix, Berlin

Salin PA, Bullier J (1995) Corticocortical connections in the visual system: Structure and function. Physiological Reviews 75:107–154

Salin PA, Prince DA (1996) Electrophysiological mapping of GABAA receptor-mediated inhibition in adult rat somatosensory cortex. J Neurophysiol 75:1589–1600

Schillen T, König P (1991) Stimulus-dependent assembly formation of oscillatory responses: II. Desynchronization. Neural Comput 3:167–178

Schmidt KE, Kim DS, Singer W, Bonhoeffer T, Löwel S (1997) Functional specificity of long-range intrinsic and interhemispheric connections in the visual cortex of strabismic cats. J Neurosci 17:5480–5492

Schmolesky MT, Wang Y, Hanes DP, Thompson KG, Leutgeb S, Schall JD, Leventhal AG (1998) Signal timing across the macaque visual system. J Neurophysiol 79:3272 – 3278

Shadlen MN, Movshon JA (1999) Synchrony unbound: A critical evaluation of the temporal binding hypothesis. Neuron 24:67–77

Siegel M, Körding KP, König P (2000) Integrating top-down and bottom-up sensory processing by somato-dendritic interactions. J Comput Neurosci 8:161–173

Sincich LC, Blasdel GB (2001) Oriented axon projections in primary visual cortex of the monkey. J Neurosci 21:4416–4426

Singer W (1999) Neuronal synchrony: A versatile code for the definition of relations? Neuron 24:49–65

Softky W, Koch C (1993) The highly irregular firing of cortical cells is inconsistent with temporal integration of random EPSPs. J Neurosci 13:334–350

Spitzner L (2004) Coincidence detection enhances appropriate wiring of the nervous system. P Natl Acad Sci USA 101:5311–5312

Steriade M, Amzica F, Contreras D (1996) Synchronization of fast (30-40 Hz) spontaneous cortical rhythms during brain activation. J Neurosci 16:392–417

Stetter M, Lang EW, Obermayer K (1997) Synapse clustering can drive simultaneous ON-OFF and ocular-dominance segregation in a model of area 17. In: *Artificial Neural Networks ICANN '97*, pp. 189–194, Springer Verlag

Stettler DD, Das A, Bennett J, Gilbert CD (2002) Lateral connectivity and contextual interactions in macaque primary visual cortex. Neuron 36:739–750

Stoecker M, Eckhorn R, Reitboeck HJ (1997) Size and position invariant visual representation supports retinotopic maps via selective backward paths: A dynamic second order neural network model for a possible functional role of recurrent connections in the visual cortex. Neurocomputing 17:111–132

Stoecker M, Reitboeck HJ, Eckhorn R (1996) A neural network for scene segmentation by temporal coding. Neurocomputing 11:123–134

Stuart GJ, Sakmann B (1994) Active propagation of somatic action potentials into neocortical pyramidal cell dendrites. Nature 367:69–72

Sur M, Leamey CA (2001) Development and plasticity of cortical areas and networks. Nat Rev Neurosci 2:251–262

Tovee MJ, Rolls ET, Azzopardi P (1994) Translation invariance in the responses to faces of single neurons in the temporal visual cortical areas of the alert macaque. J Neurophysiol 72:1049–1060

Traub R, Whittington M, Stanford I, Jefferys J (1996) A mechanism for generation of long-range synchronous fast oscillations in the cortex. Nature 383:621–624

Traub RD, Jeffreys JGR, Miles R (1993) Analysis of propagation of disinhibition-induced after-discharges along the guinea-pig hippocampal slice in vitro. Journal of Physiology London 472:267–287

Ts'o DY, Gilbert CD, Wiesel TN (1986) Relationships between horizontal interactions and functional architecture in cat striate cortex as revealed by cross-correlation analysis. J Neurosci 6:1160–1170

Tucker TR, Katz LC (2003) Spatiotemporal patterns of excitation and inhibition evoked by the horizontal network in layer 2/3 of ferret visual cortex. J Neurophysiol 89:488–500

Tyzio R, Represa A, Jorquera I, Ben-Ari Y, Gozlan H, Aniksztejn L (1999) The establishment of GABAergic and glutamatergic synapses on CA1 pyramidal neurons is sequential and correlates with the development of the apical dendrite. J Neurosci 19:10372–10382

Ungerleider LG, Haxby JV (1994) 'What' and 'where' in the human brain. Curr Opin Neurobiol 4:157–165

Ungerleider LG, Mishkin M (1982) Two cortical visual systems. MIT Press, Cambridge, MA

Ursino M, La Cara GE, Sarti A (2003) Binding and segmentation of multiple objects through neural oscillators inhibited by contour information. Biol Cybern 89:56–70

Usrey WM, Alonso JM, Reid RC (2000) Synaptic interactions between thalamic inputs to simple cells in cat visual cortex. J Neurosci 20:5461–5467

van Vreeswijk C, Abbott LF, Ermentrout G (1994) When inhibition not excitation synchronizes neural firing. J Comput Neurosci 1:313–321

von der Malsburg C (1999) The what and why of binding: The modeler's perspective. Neuron 24:95–104

von der Malsburg C, Schneider W (1986) A neural cocktail-party processor. Biol Cybern 54:29–40

von Stein A, Sarnthein J (2000) Different frequencies for different scales of cortical integration: from local gamma to long range alpha/theta synchronization. Int J Psychophysiol 38:301–313

Waxman SG, Bennett MV (1972) Relative conduction velocities of small myelinated and non-myelinated firbres in the central nervous system. Nature 238:217–219

Weliky M, Kandler K, Fitzpatrick D, Katz LC (1995) Patterns of excitation and inhibition evoked by horizontal connections in visual cortex share a common relationship to orientation columns. Neuron 15:541–552

Weliky M, Katz LC (1997) Disruption of orientation tuning in visual cortex by artificially correlated neuronal activity. Nature 386:680–685

Weliky M, Katz LC (1999) Correlational structure of spontaneous neuronal activity in the developing lateral geniculate nucleus in vivo. Science 285:599–604

Whittington M, Traub R, Jefferys J (1995) Synchronized oscillations in interneuron networks driven by metabotropic glutatmate receptor activation. Nature 373:612–615

Wiemer J, Spengler F, Joublin F, Stagge P, Wacquant S (2000) Learning cortical topography from spatiotemporal stimuli. Biol Cybern 82:173–187

Wiesel TN, Hubel DH (1963) Single-cell responses in striate cortex of kittens deprived of vision in one eye. J Neurophysiol 26:1003–1017

Wiesel TN, Hubel DH (1974) Ordered arrangement of orientation columns in monkeys lacking visual experience. J Comp Neurol 158

Wilson HR, Cowan JD (1972) Excitatory and inhibitory interactions in localized populations of model neurons. Biophysical Journal 12:1–24

Wilson M, Bower J (1991) A computer simulation of oscillatory behavior in primary visual cortex. Neural Comput 3:498–503

Wong ROL, Chernjavsky A, Smith SJ, Shatz CJ (1995) Early functional neural networks in the developing retina. Nature 374:716–718

Wong ROL, Oakley DM (1996) Changing patterns of spontaneous bursting activity of on and off retinal ganglion cells during development. Neuron 16:1087–1095

Yoshimura Y, Sato H, Imamura K, Watanabe Y (2000) Properties of horizontal and vertical inputs to pyramidal cells in the superficial layers of the cat visual cortex. J Neurosci 20:1931–1940

Zeki SM (1991) Cerebral akinetopsia (visual motion blindness). Brain 114:811–824

Zhang LI, Poo Mm (2001) Electrical activity and development of neural circuits. Nat Neurosci 4:1207–1214

Zhang LI, Tao HW, Holt CE, Harris WA, Poo M (1998) A critical window for cooperation and competition among developing retinotectal synapses. Nature 395:37–44

Glossary

Action potential A large electrical signal (≈ 100 mV, ≈ 1 ms) that is initiated at the initial segment or *axon* hillock of the *neuron* and propagated without failure, in an all-or-none fashion, along an *axon* to its presynaptic terminal.

Axon A cable-like structure which conducts electrical impulses away from the *neuron's soma*. *Neurons* have only one axon, but this will usually undergo extensive branching, enabling communication with many target cells.

Coherence Linear, spectral selective coupling measure for pairwise signals, here exclusively used for time series. At each frequency coherence is independently normalized, and is sensitive to covariation of amplitude densities and constancy of relative phase at this frequency.

Depolarization A decrease in the *membrane potential* of a *neuron* that increases the likelihood of this neuron to generate an *action potential* and is therefore excitatory.

Dendrite A short, branching arbour of cellular extensions that conducts the electrical stimulation received from other cells to the soma. Each *neuron* has numerous dendrites with profuse dendritic branches. These structures form the main information receiving network for the *neuron*.

Excitation The *depolarization* of a postsynaptic *neuron*, increasing the likelihood that an *action potential* will be generated.

Figure-ground segregation Segregation of a visual pattern into an object (figure) seen in front of a background. The background is assumed to extend behind the object.

Hyperpolarization An increase in the *membrane potential* of a *neuron* that decreases the likelihood of this neuron to generate an *action potential* and is therefore inhibitory.

Inhibition, postsynaptic The *hyperpolarization* of a postsynaptic *neuron*, reducing the likelihood of or preventing an *action potential* in the postsynaptic *neuron*.

Local field potential, LFP Local superposition of *postsynaptic potentials* of a group of *neurons*. Captured by extracellular micro-electrode recordings after low-pass filtering (1–140 Hz; 18 dB/oct). Estimated radius of support: ≈ 0.5 mm (half-height decline, Mitzdorf, 1985).

Long-term depression, LTD weakening of a *synapse* that last from hours up to years. LTD and *long-term potentiation* (LTP) are regarded as the cellular basis for learning.

Long-term potentiation, LTP A long-lasting strengthening (from hours up to years) of the connection between two nerve cells. This form of synaptic plasticity is regarded as the cellular basis for learning.

Membrane potential the electrical potential difference (voltage) across a *neuron's* membrane.

Multiple unit activity, MUA Local *action potential* density of a group of neurons. Captured by extracellular micro-electrode recordings after band-pass filtering (1–10 kHz, 18 dB/oct), full-wave rectification, and subsequent low-pass filtering (140 Hz, 18 dB/oct). Estimated radius of support: ≈ 0.05 mm (half-height decline, Mitzdorf, 1985).

Neuron The fundamental signaling unit of the nervous system. The human brain contains about 10^{11} neurons, each forming about 1000 *synapses*. A typical neuron constists of *dendrites*, a *soma* and an *axon*.

Peri-stimulus time histogram, PSTH Neuronal response time signals averaged over repetitions of identical stimulus presentations and triggered with respect to the time of the stimulus onsets.

Postsynaptic potential, PSP a graded change in the *membrane potential* of a *neuron* produced by a *synaptic* input. A postsynaptic potential can either be excitatory (EPSP) or inhibitory (IPSP).

Primary visual cortex, V1 First cortical area to receive input via the main visual sensory pathway.

Receptive field, RF Concept that refers to the spatial area of photoreceptors activating a certain neuron when elicited. The term is synonymously used for the corresponding area of the visual field, and is mostly defined as a minimum response field determined with a small test stimulus. The concept can also be extended by its dynamic properties, or by the definition of additional regions of modulatory influence.

Soma The cell-body of the *neuron*. The relatively large central part of the cell between the *dendrites* and the *axon*.

Spike cf. *action potential*

Single unit activity, SUA *Action potential* output of a single *neuron*.

Synapse, chemical A specialized junction through which two *neurons* signal to one another. The two *neurons* are separated by the synaptic cleft. The presynatic *neuron* releases a neurotransmitter that binds receptors on the postsynaptic neuron and in this way influences the excitability in the postsynaptic *neuron*. Synapses can mediate either *excitatory* or *inhibitory* actions.

Threshold critical level of depolarization of the *neuron's* membrane at which the *neuron* can actively generate an *action potential*.

Acknowledgements

There are many people to thank for their expertise, assistance and friendship, without whom this thesis would not have been possible. First and foremost, I gladly acknowledge my debt to Prof. Dr. Reinhard Eckhorn for his motivating enthusiasm on brain functions and his encouragement and advice for my work over many years. Prof. Dr. Frank Roesler critically reviewed my dissertation and kindly served as co-chairman for my committee.

Dr. Andreas Gabriel was not only an inspiring room mate, but is also a valuable research fellow and a longtime friend. Dr. Alexander Gail introduced me into the mysteries of experimental recording procedures, critically reviewed previous versions of this thesis and was a willing companion for various sporting activities. Basim Al-Shaikhli contributed with his diploma thesis a complementary view for the decoupling processes shown in Chapter 3. Dr. Andreas Bruns generously assisted me with his sound knowledge in data analysis.

I'm grateful to all members of the NASE team (Neural Assembly Simulation Environment), in particular Dr. Andreas Thiel and Dr. Rüdiger Kupper, for many helpful plotting and simulation routines that eased up my programming work. Thanks to Sigrid Thomas for her dedicated help in all administrative tasks.

All members of the Neurophysics Group contributed to a pleasant, motivating athmosphere that gave me the feeling of being at home at work.

Last but not least, I am especially grateful to Kristina, for her love and patience during this long period and to my parents for their enduring support.

This work was funded by the Deutsche Forschungsgemeinschaft to R.E. in the context of the research group 'Dynamics of Cognitive Representation' (DFG Ro529/12-1).